



Calhoun: The NPS Institutional Archive DSpace Repository

Theses and Dissertations

1. Thesis and Dissertation Collection, all items

1976

A comparative evaluation of two acoustic signal dereverberation techniques.

Gallemore, James B.

<http://hdl.handle.net/10945/17691>

Downloaded from NPS Archive: Calhoun



<http://www.nps.edu/library>

Calhoun is the Naval Postgraduate School's public access digital repository for research materials and institutional publications created by the NPS community.

Calhoun is named for Professor of Mathematics Guy K. Calhoun, NPS's first appointed -- and published -- scholarly author.

Dudley Knox Library / Naval Postgraduate School
411 Dyer Road / 1 University Circle
Monterey, California USA 93943

A COMPARATIVE EVALUATION OF TWO
ACOUSTIC SIGNAL DEREVERBERATION
TECHNIQUES

James B. Gallemore

DUDLEY KNOX LIBRARY
NAVAL POSTGRADUATE SCHOOL
MONTEREY, CALIFORNIA 93940

A COMPARATIVE EVALUATION OF TWO ACOUSTIC
SIGNAL DEREVERBERATION TECHNIQUES

by

James B. Gallemore

B.S. United States Naval Academy
(1971)

SUBMITTED IN PARTIAL FULFILLMENT OF THE REQUIREMENTS
FOR THE DEGREES OF

MASTER OF SCIENCE IN OCEAN ENGINEERING,
MASTER OF SCIENCE IN ELECTRICAL ENGINEERING

and
ELECTRICAL ENGINEER

at the

MASSACHUSETTS INSTITUTE OF TECHNOLOGY

June 1976

A COMPARATIVE EVALUATION OF TWO ACOUSTIC
SIGNAL DEREVERBERATION TECHNIQUES

by

James B. Gallemore

Submitted to the Departments of Ocean Engineering and Electrical Engineering and Computer Science on May 7, 1976 in partial fulfillment of the requirements for the Degrees of Master of Science in Ocean Engineering, Master of Science in Electrical Engineering and Electrical Engineer.

ABSTRACT

Two dereverberation techniques are applied to synthetic seismic data and their performance in removing water column multiples is evaluated and compared. One method is an application of homomorphic deconvolution and the other utilizes linear estimation based on a minimum mean square error criterion. The analytical formulations of both methods are discussed. Performance is evaluated in terms of three criteria: percent of multiple energy removed, percent of signal (reflector) distortion, and visual improvement of the data. Results are presented which represent the performance of both algorithms for a range of environmental and signal processing parameters including white noise level, multiple coherence, reflector/multiple overlap, filter parameters and water column travel time estimate. The techniques are found to have comparable effectiveness on the synthetic data; however, indications are that homomorphic dereverberation has greater potential in shallow water applications while the linear technique appears to be more efficient for deep water data.

THESIS SUPERVISOR: Arthur B. Baggeroer

TITLE: Associate Professor of Electrical Engineering and
Associate Professor of Ocean Engineering

ACKNOWLEDGEMENTS

The assistance I have received from several of my friends has been generously given and is very gratefully appreciated.

I would especially like to thank Professor Arthur Baggeroer for guiding me toward an interesting topic and freely sharing his knowledge and experience throughout this endeavor.

Ken Theriault has helped me from the beginning of this project in more ways than I can name. His advice and encouragement have contributed tangibly to the quality of my work and the enjoyment I have derived from it.

I would not have completed the homomorphic analysis without the frequent assistance of José Tribolet, who supplied me with his phase unwrapping algorithm and several of his other computational routines. He has also shared much of his time with me in tutorials and discussions which I have enjoyed and appreciated.

Ken Prada, Tom O'Brien and Steve Leverette of the Woods Hole Oceanographic Institution have assisted me in learning to use the data processing equipment and allowed me time in their busy computer schedule to complete this project. I appreciate their support and cooperation very much.

I would like to thank my fellow students, Dick Kline and Tom Marzetta, for their frequent advice and discussions and moral support.

TABLE OF CONTENTS

CHAPTER I	INTRODUCTION AND PROBLEM STATEMENT.....	5
CHAPTER II	ANALYTICAL FORMULATION AND IMPLEMENTATION.....	13
	A. Analytical Formulation of the TDL Filter.....	13
	B. Implementation of the TDL Algorithm.....	23
	C. Analytical Formulation of Homomorphic Deconvolution.....	26
	D. Implementation of Homomorphic Deconvolution...	37
CHAPTER III	DESCRIPTION OF THE PERFORMANCE ANALYSIS.....	42
CHAPTER IV	RESULTS.....	52
	A. Introduction.....	52
	B. Results of TDL Dereverberation Performance....	53
	1. Operator Length, Multiple Distortion and Multiple-to-Signal Ratio.....	53
	2. Water Travel Time Estimate.....	68
	3. Multiple Periodicity.....	77
	4. Reflector/Multiple Overlap.....	81
	5. Additive White Noise and Filtering.....	89
	C. Results of Homomorphic Dereverberation Performance.....	102
	1. Introduction.....	102
	2. Multiple Periodicity.....	103
	3. Multiple-to-Signal Ratio.....	108
	4. Multiple Distortion.....	110
	5. Water Travel Time Estimate.....	115
	6. Reflector/Multiple Overlap.....	117
	7. Additive White Noise and Filtering.....	126

D. Comparative Examples of Processing Results....	143
CHAPTER V SUMMARY AND DISCUSSION.....	155
REFERENCES.....	162
APPENDIX A COMPUTATION OF THE PHASE DERIVATIVE OF THE Z-TRANSFORM.....	163

CHAPTER I

INTRODUCTION AND PROBLEM STATEMENT

The geologic structure of the earth beneath the seafloor is most often determined by seismic profiling. The procedure generally involves excitation of an impulsive acoustic source near the sea surface and recording of the reflected earth response with a hydrophone array. Low frequency sound penetrates the bottom and propagates in the substrata with reflections occurring at discontinuities in the acoustic impedance of the earth. The thickness and density of sub-bottom layers may be estimated from the reflected acoustic signal, or seismogram.

The earth is modelled as a discrete layered medium with distinct interfaces for most seismic applications. This assumed structure, while not strictly accurate, has led to good processing results in practical seismic work and has the additional advantage of being analytically tractable. We shall employ this assumption throughout the present analysis. A detailed description of the earth model used is given in Chapter III.

The amount of energy reflected at a discontinuity is ideally measured by the reflection coefficient,

$$R = \frac{r_2 c_2 - r_1 c_1}{r_2 c_2 + r_1 c_1} ,$$

where r_1 , r_2 and c_1 , c_2 are the densities and acoustic velocities in media 1 and 2. Here the sound propagates from medium 1 to medium 2 and normal incidence has been assumed. The assumption of normally incident plane waves is generally made in single channel (one receiver) seismology since it leads to analytical simplicity and appears to be reasonably accurate. In utilizing this simplified model we have ignored near field effects and spreading losses. These are not of major importance in single channel dereverberation and their inclusion would unnecessarily complicate the earth model.

It is evident from the reflection coefficient expression that large reflections occur at points of significant change in impedance. The largest impedance discontinuity encountered by seismic signals occurs at the water-air interface where R is nearly -1. The water-bottom interface is also a strong reflector in most cases. Thus, the water column becomes a reverberating channel wherein a significant portion of the source energy is trapped. Repeated reflections from the bottom, or multiples, are received at intervals corresponding to the two-way travel time of sound in the water column. Deeper reflections from the substrata are masked by multiples when their arrivals are nearly coincident in time. Since propagation losses are much smaller in water, the energy in the multiples is usually large compared to that in the deeper reflectors. Thus, water column multiples form an unwanted

component of the seismogram.

The reflection coefficient expression indicates that all earth layers also introduce reverberation. Except in some shallow water situations, internal multiples are generally not a serious problem for two major reasons. Most importantly the acoustic attenuation in the earth is much greater than that in water so that very little internal multiple energy is actually returned to the receiver. Secondly, the reflection coefficients at earth layer boundaries are usually small compared to those at the surface and seafloor so that a relatively small part of the incident energy is actually trapped.

Figure 1 shows a synthetic seismogram with strong multiples. Response amplitude is measured on the ordinate and travel time in seconds on the abscissa. The first large signal component is the bottom reflection at one second of travel time or about 750 meters water depth. The first multiple is an attenuated, phase-inverted replica of this reflection at two seconds. Note that the return from a reflection horizon at two seconds travel time would coincide with this multiple and be obscured. The overall periodicity of the multiples is apparent in this plot. Actual reflectors occur at 1.5, 2.2 and 2.9 seconds. Figure 2 shows the seismic environment which would produce such a seismogram.

The first practical multiple analysis and dereverberation

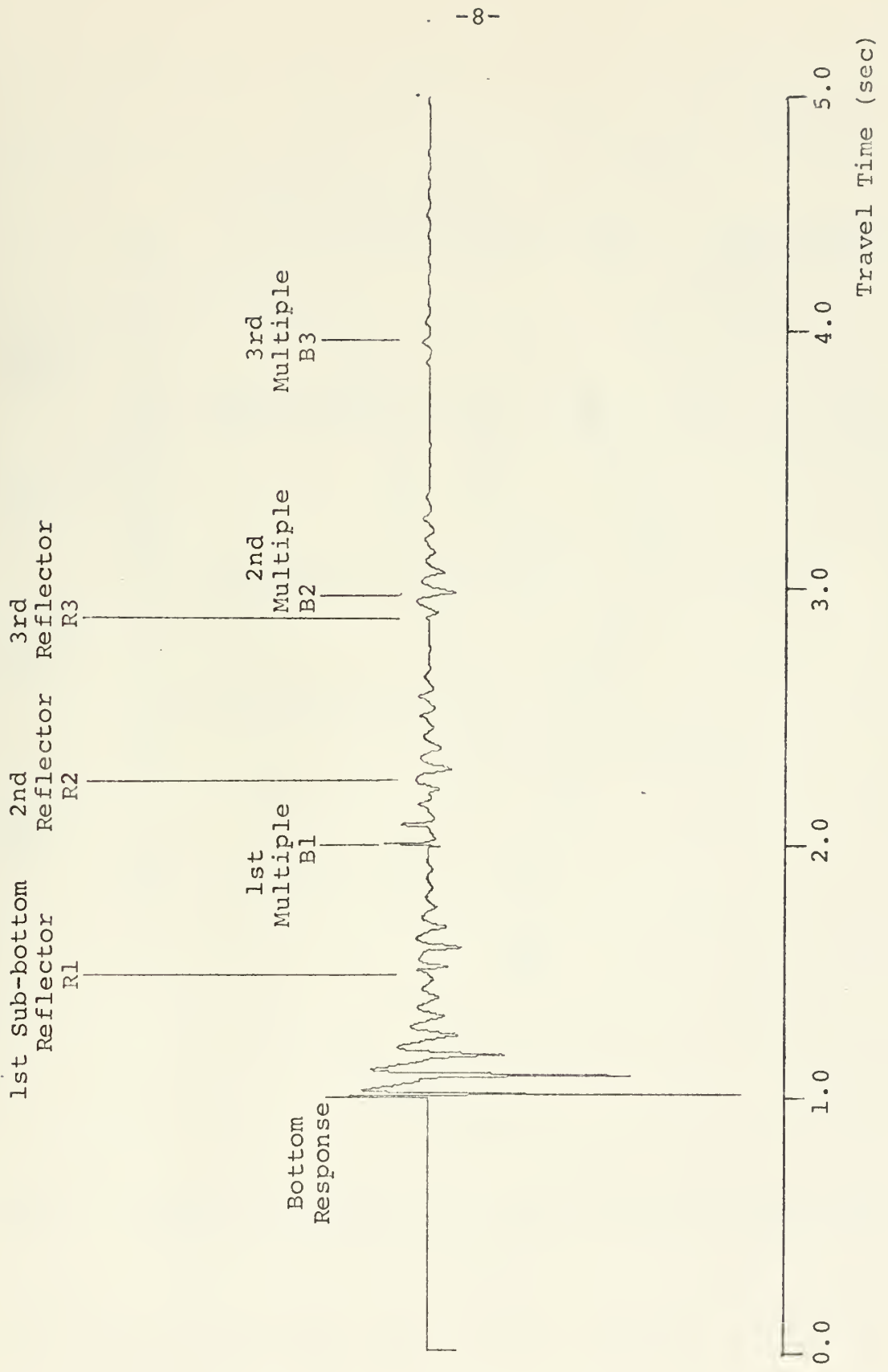


Figure 1 Synthetic seismogram including three multiples. Reflectors are designated R_i and multiples by B_i .

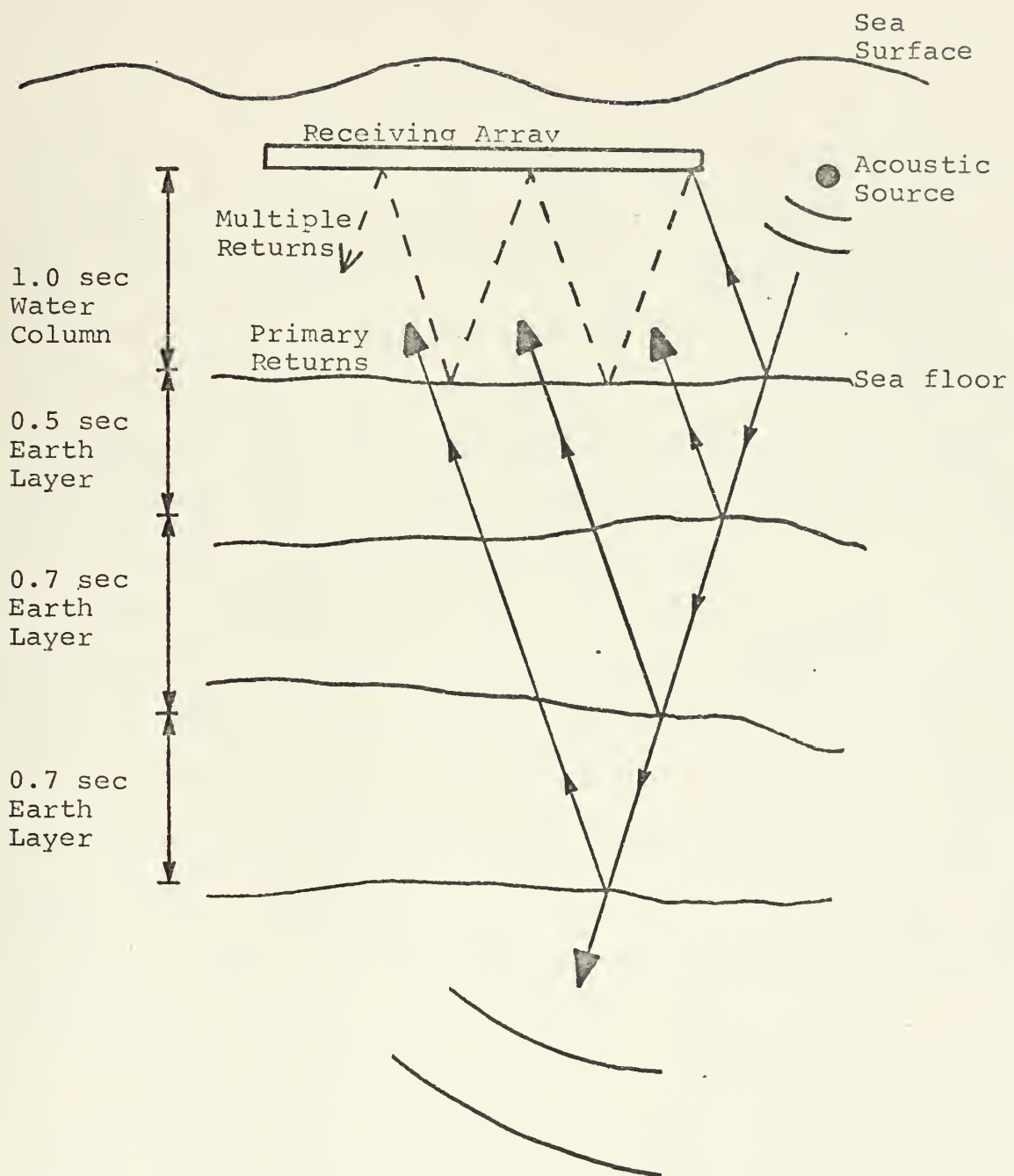


Figure 2 Earth structure which would produce seismogram like that shown in Figure 1.

algorithm was proposed by Backus [1]. His approach was to characterize the water column as a sharp, ringing filter with an impulse response composed of a weighted sum of delayed impulses. The weights and delays are determined by the bottom reflection coefficient and the water column travel time respectively. This model leads to a three-point operator with elements spaced at intervals corresponding to the two-way water travel time. Implementation of the Backus filter requires estimation of the bottom reflection coefficient and water column travel time. Several aspects of the performance of this method are discussed in Chapter II.

Spatial processing has also been used to reduce multiples [2]. Spatial schemes normally require multichannel arrays of large physical extent which can be effectively focused to discriminate against reverberation. Such systems are widely used and quite effective in shallow water but their costs, both for hardware and data processing, are very high. Hence, there is still a need for time domain multiple removal techniques in deep water situations and for single channel systems.

Two techniques have recently been applied to seismic multiple removal with demonstrated success. The first, an inverse filter algorithm based on a tapped delay line model, is due to Baggeroer [3], and is referred to hereafter as the TDL filter. A tapped delay line is simply a realization of the time domain convolution of a signal and a gapped operator [4].

Results of this method have proven superior to those of three-point filtering, at least in some deep water situations.

A nonlinear filtering scheme using homomorphic deconvolution has been applied to several aspects of seismic signal processing. The use of this method for dereverberation has been demonstrated by Stoffa, Buhl and Bryan [5]. The homomorphic transformation is essentially a mapping from convolution to addition so that, after transforming, deconvolution can be accomplished by simple linear filtering. Seismic dereverberation appears theoretically to be a very promising application of homomorphic deconvolution because of the distinct properties of seismic signal components. The method has not, however, been fully evaluated or widely used in practice.

The motivation for this study arises from the disparate theoretical mechanisms by which these techniques operate to perform the same function. Since analytical comparison is not feasible, this functional, comparative approach is thought to be the best means of gaining insight into this interesting problem.

The purpose of the analysis is twofold. First, it is intended to indicate those factors which have significant effects on the performance of each algorithm. The factors to be considered are environmental variables and processing parameters. These are discussed in Chapter III. Secondly, the analysis is intended to point out the relative strengths

and weaknesses of the methods by comparison of results on similar data.

Each algorithm is evaluated for a range of simulated processing conditions. Quantitative and qualitative criteria are specified which provide a comprehensive description of the manner in which each signal is affected by processing for multiple removal. These criteria also serve as a basis for comparison of results. The scope of the analysis and the specific performance criteria are discussed thoroughly in Chapter III.

CHAPTER II

ANALYTICAL FORMULATION AND IMPLEMENTATION

A. Analytical Formulation of the TDL Filter

A simple feedback model for the propagation of reverberating seismic signals is given by Baggeroer [3]. Multiple removal based on this model is then formulated as an inverse filtering problem. The dereverberation filter is designed using a least squared error criterion and the constraint that the filter have a tapped delay line structure.

The formulation will be developed here from a different point of view using Baggeroer's feedback model as a starting point. A summary of the feedback model is included for clarity.

Figure 3 shows the Laplace transform representation of a propagating seismic signal. $S(s)$ is the transform of the source signature. The signal first encounters the downward travel time delay which corresponds to a phase shift in this domain. $H_b(s)$ represents the transfer function of the earth beneath the water column including the reflections from layer boundaries which comprise the desired information. Internal multiples or reverberations between the various earth layers are also included in $H_b(s)$. Another phase shift corresponds to the return of the reflected signal through the water column. $P(s)$ is the feedback gain representing the water column multiple mechanism. In most cases this is well approximated by -1, which corresponds to the nearly perfect pressure release

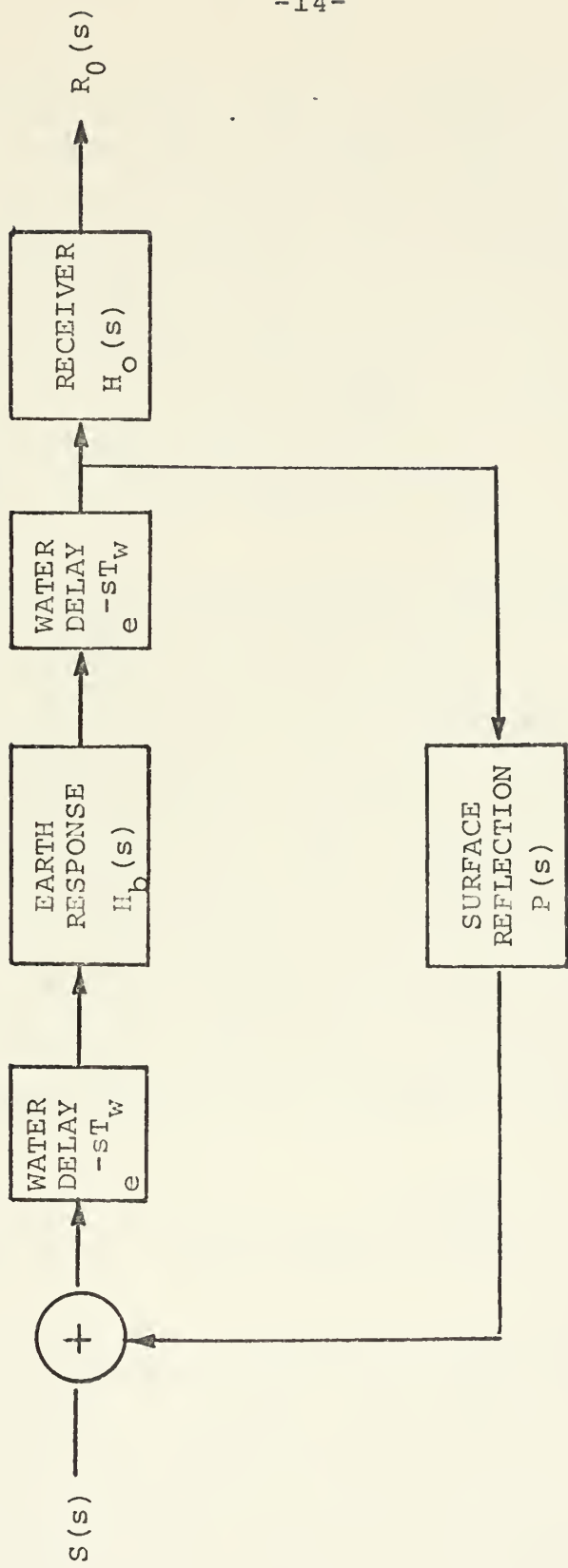


Figure 3 Laplace transform model of propagating seismic signal

reflection at the surface. $H_o(s)$ includes the observation effects such as hydrophone bandwidth and array tow depth. Ambient noise and receiver front end noise are modelled as additive white Gaussian noise.

The overall transfer function is

$$\frac{R_o(s)}{S(s)} = \frac{H_o(s) H_b(s) e^{-2sT_w}}{1 - P(s) H_b(s) e^{-2sT_w}} \quad (1)$$

where T_w is the one-way water travel time and $R_o(s)$ is the received signal without additive noise.

It is apparent that the presence of multiples is due only to the denominator of this expression. Thusfar we have assumed implicitly that the earth response can be modelled accurately as a linear system and that the multiples are exactly periodic. The validity of these assumptions will become apparent in the discussion of performance in Chapter IV.

The obvious task is now to design an inverse filter having the form

$$F(s) = [1 - P(s) H_b(s) e^{-2sT_w}] .$$

Hence, we are required to estimate T_w and the impulse response, $h_b(t)$, corresponding to $H_b(s)$. The earth response need not be estimated precisely for its entire duration. Estimating the dominant energy part of $h_b(t)$ is adequate to produce an effective dereverberation filter. A typical deep water

seismogram has the great majority of its energy concentrated in the first 200-300 msec of its duration. Effective representation of this portion of the signal requires about 10-20 filter coefficients, depending on the bottom and source characteristics.

The transfer function of equation (1) can be re-written in series form as

$$\frac{R_O(s)}{S(s)} = H_O(s) \sum_{n=1}^{\infty} (-1)^{n+1} H_b(s) e^{-2nsT_w}$$

The received signal then has the time domain representation

$$r_O(t) = s(t) * [h_O(t) * \sum_{n=1}^{\infty} (-1)^{n+1} h_b(t - 2nT_w)]$$

where * represents convolution. This can be rewritten as the sum of the primary return and the multiple signal.

$$r_O(t) = [s(t) * h_O(t)] * \left[h_b(t - 2T_w) + \sum_{n=2}^{\infty} (-1)^{n+1} h_b(t - 2nT_w) \right]$$

$$r_O(t) = b(t) + m(t)$$

where

$$b(t) = s(t) * h_O(t) * h_b(t - 2T_w)$$

is the received primary and

$$m(t) = s(t) * h_O(t) * \sum_{n=2}^{\infty} h_b(t - 2nT_w)$$

is the received multiple signal.

The estimation problem, given the feedback model of figure 3, is to determine $b(t)$ in the presence of $m(t)$ and white noise, $w(t)$. It is convenient to group the unwanted signal components.

$$n(t) = m(t) + w(t) \quad (2)$$

Since the unwanted component is an additive one, we can consider estimating $n(t)$ and subtracting the result from the received signal. We then have the filtering problem depicted in figure 4.

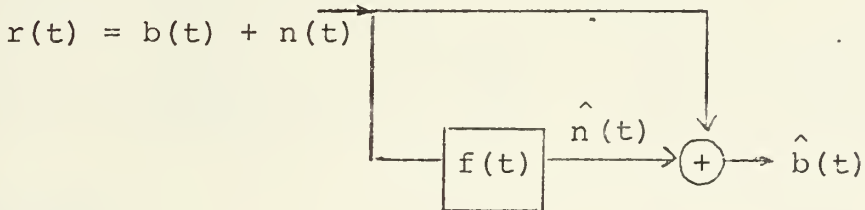


Figure 4

Here $f(t)$ is the filter impulse response and $\hat{n}(t)$ is the minimum mean square error (MMSE) estimate of $n(t)$, given the received signal $r(t)$.

The number of digital filter coefficients to be estimated is $2TW+1$, where T is the effective duration (portion containing about 80% or more of the signal energy) of $h_b(t)$ and W is the signal bandwidth. The coefficients will then be spaced at the Nyquist sampling interval of $1/2W$ seconds.

The optimum digital filter for $n(t)$ will have coefficients, f_k , which minimize

$$e = E \left\{ \sum_{i=i_0}^{i_f} \left[\hat{n}(i/2W) - n(i/2W) \right]^2 \right\} \quad (3a)$$

where

$$\hat{n}(i/2W) = \sum_{k=i_0}^{i_f} f_k \cdot r \left(\frac{(i-k)}{2W} - 2T_w \right). \quad (3b)$$

The input in (3b) is shifted by the two-way travel time to avoid useless filtering of the signal prior to the bottom reflection. $[i_0/2W, i_f/2W]$ is the time interval over which $n(t)$ is observed.

Substituting (3b) into (3a) yields

$$e = E \left\{ \sum_{i=i_0}^{i_f} \left[\sum_{k=i_0}^{i_f} f_k \cdot r \left(\frac{(i-k)}{2W} - 2T_w \right) - n(i/2W) \right]^2 \right\}.$$

Minimizing,

$$\begin{aligned} \frac{\partial e}{\partial f} &= E \left\{ \left[2 \sum_{i=i_0}^{i_f} f_k \cdot r \left(\frac{(i-k)}{2W} - 2T_w \right) - n(i/2W) \right] \left[-r \left(\frac{(i-k)}{2W} - 2T_w \right) \right] \right\} \\ 0 &= \sum_{k=i_0}^{i_f} f_k R_{rr} \left(\frac{(i-k)}{2W} \right) - R_{nr} \left(\frac{(i-k)}{2W} + 2T_w \right). \end{aligned} \quad (4)$$

Here we have assumed stationarity over the duration of the multiple period. This assumption has led to effective processing of both real and synthetic data. From (2)

$$R_{nr} \left(\frac{(i-k)}{2W} + 2T_w \right) = R_{mr} \left(\frac{(i-k)}{2W} + 2T_w \right) + R_{wr} \left(\frac{(i-k)}{2W} + 2T_w \right)$$

Here it is useful to assume (see ref.[3], p.15) that for shifts close to $2T_w$ the cross-correlation of $w(t)$ and $r(t)$ is very small compared to $R_{mr}(\tau)$ which will generally have a peak in this region. This is equivalent to assuming that the white noise has a very short correlation time compared to $2T_w$. We then have

$$R_{nr}(k/2W+2T_w) \approx R_{mr}(k/2W+2T_w)$$

so that (4) becomes

$$\sum_{k=i_0}^{i_f} f_k R_{rr}((i-k)/2W) = R_{mr}(k/2W+2T_w) \quad (4a)$$

Baggeroer has derived equation (4a) by designing the Wiener filter for $b(t)$ with the constraint that the filter have a tapped delay line structure, i.e.

$$f(t) = \delta(t) - \sum_{k=0}^{2TW} f_k \delta(t-k/2W-2T_w) \quad (5)$$

When our estimate, $\hat{n}(t)$, is subtracted from the unshifted, received signal, the resulting overall filter operation has exactly the form of (5). This indirect approach yields the estimator equations of reference [3] without imposing the TDL structure directly.

The above derivation also emphasizes the estimator-subtractor or prediction error structure of this filter. The entire impulse response may be written as follows:

$$1, \underbrace{0, 0, \dots, 0}_{2T_w \text{ zeros}}, -f_1, -f_2, \dots, -f_k.$$

This is the prediction error structure for a prediction distance of $2T_w$. Equation (4a), however, which generates the $\{f_i\}$ differs from the prediction equations in that the right hand side vector is $R_{mr}(\tau+2T_w)$ rather than $R_{rr}(\tau+2T_w)$. As written, equation (4a) corresponds to the Wiener filter which produces the MMSE estimate of $m(t)$ with $r(t-2T_w)$ as an input. Subtraction of this estimate from $r(t)$ whitens only those spectral components which are due to the multiple.

It is simply proved that the magnitude of the error in $\hat{b}(t)$ is equal to that in the prediction operator.

$$\hat{b}(t) = r(t) - \hat{n}(t)$$

$$\hat{b}(t) = b(t) + (\hat{n}(t) - \hat{n}(t))$$

$$|\hat{b}(t) - b(t)| = |\hat{n}(t) - \hat{n}(t)|$$

Thus far the only departures from optimum estimation have been the two assumptions of stationarity and the relative insignificance of $R_{wr}(\tau+2T_w)$. One further assumption is required for actual implementation of the filter. Note that $R_{mr}(\tau+2T_w)$ is a required input which is apparently not measurable from the given data. Baggeroer has observed that for the deep water case, which is of primary interest for this method,

$$R_{mr}(\tau+2T_w) \approx R_{rr}(\tau+2T_w) .$$

That is, for shifts of nearly twice the water travel time, the great majority of the crosscorrelation energy is due to $m(t)$. Hence, the equations used for data processing are given by

$$\sum_{k=i_0}^{i_f} f_k R_{rr}((j-k)/2w) = R_{rr}(j/2w+2T_w) \quad j=0, 1, \dots, 2Tw$$

Having seen the analytical formulation of this inverse filtering procedure it is instructive to compare it with the Backus three-point method. Processing actual data with both filters (ref.[3]) has shown the Backus filter to be significantly less effective. Some reasons for this are apparent from the foregoing analysis.

The Backus filter is rigidly dependent on the accuracy of two assumptions. The first, the assumption of strictly periodic multiples, is violated due to the horizontal separation of source and receiver. This effect becomes more severe as water depth decreases. Since the Backus filter is implemented as only three, equidistant operator coefficients it is very sensitive to this lack of periodicity. Even if the statistics of the signal generate very accurate estimates of the bottom reflection coefficient the filter structure is so simple and rigid that proper cancellation will not occur if the multiples are significantly aperiodic.

A second restrictive assumption of the Backus filter is that the bottom reflection should be accurately characterized by a single reflection coefficient. All of the statistical information available is forced into a single parameter estimation scheme. It is apparent that such a filter lacks flexibility for dealing with more complicated bottom interaction mechanisms.

The relatively better performance of the TDL filter on real data is apparently due to its greater inherent flexibility. That is, the finite length impulse response, or prediction operator, gives the filter a capability for removing reverberation effectively in cases where the bottom response is not accurately modelled as a weighted impulse. If the bottom has a ringing or smearing effect on the incident signal then the deconvolution operator must be extended in time. The Backus filter, because of its rigid structure, cannot accomodate these situations. The TDL structure provides $2TW+1$ (usually 10-20) parameters which can be varied in the design procedure to optimize dereverberation of each seismogram. The special case of an ideal bottom will generate a filter response which is essentially a single spike proportional to the bottom reflection coefficient. This result has been confirmed in the analysis of synthetic data. In such a case the TDL filter consists basically of the first two points of the Backus three-point filter. Performance (multiple energy removed) in these cases

was found to be essentially independent of operator length.

The structural flexibility of the TDL filter also gives it some potential for dealing with aperiodic multiples. It should be noted, however, that the TDL algorithm, like the Backus and other classical dereverberation techniques, is essentially a correlation-cancellation operation. Consequently, increased aperiodicity of multiples can be expected to degrade performance in all cases.

B. Implementation of the TDL Algorithm

Figure 5 shows a flow diagram of the filter implementation used for this analysis. Actual programming was done in Fortran IV for use on a 32K computer. Referring to figure 5, the correlation function is computed by the standard shift-and-add operation with no windowing applied. Results of windowing are included in reference [3]. Correlation time is variable and may be specified by the operator. The crosscorrelation function is approximated by the correlation function as discussed in the previous section.

Solution of the filter equations is accomplished by conventional matrix inversion. The Toeplitz symmetry can be exploited for computational savings. Spacing of the operator elements is determined by the estimated signal bandwidth which is specified as an input parameter.

Actual deconvolution is implemented exactly as shown in

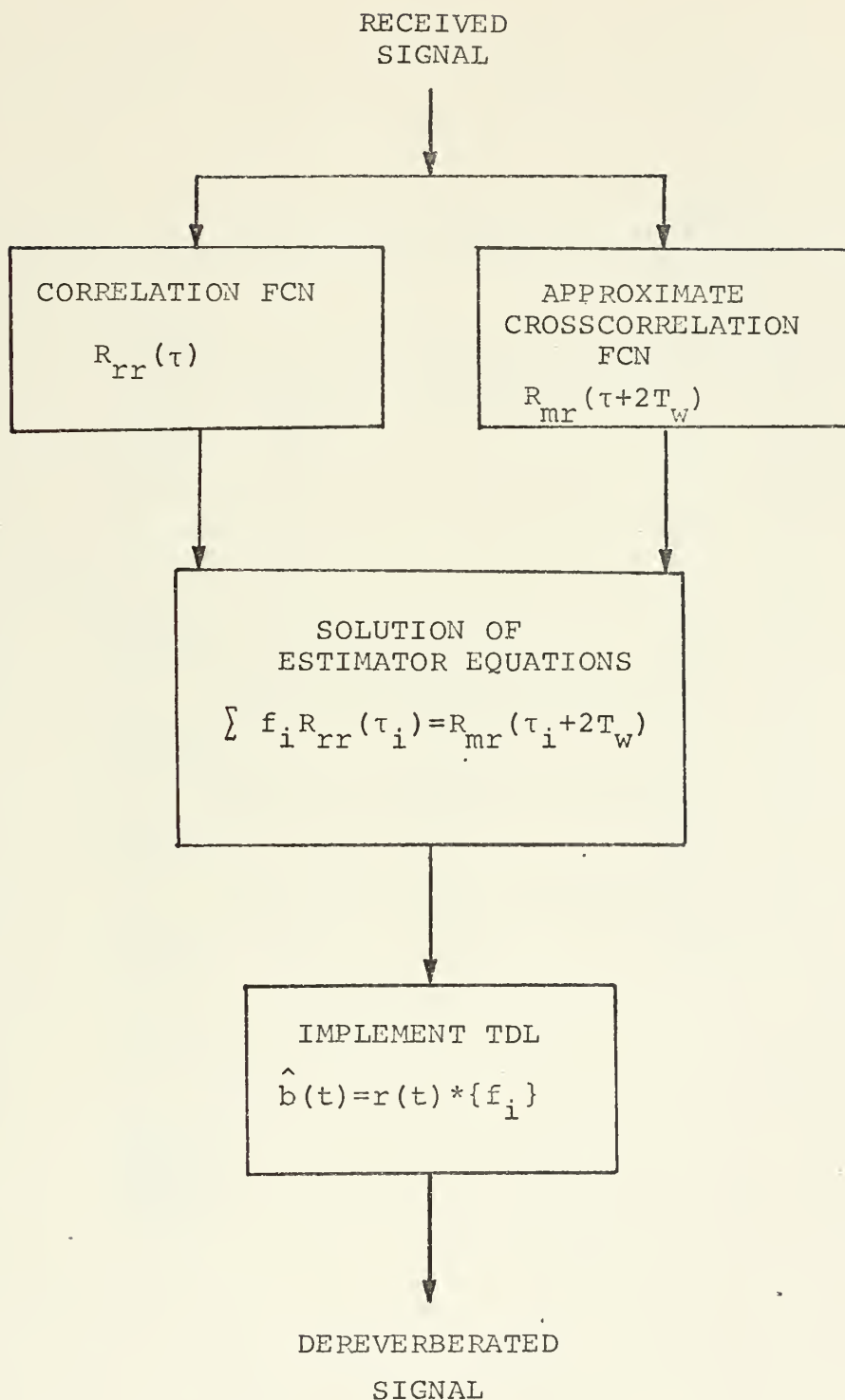


Figure 5 Flow chart of TDL algorithm.

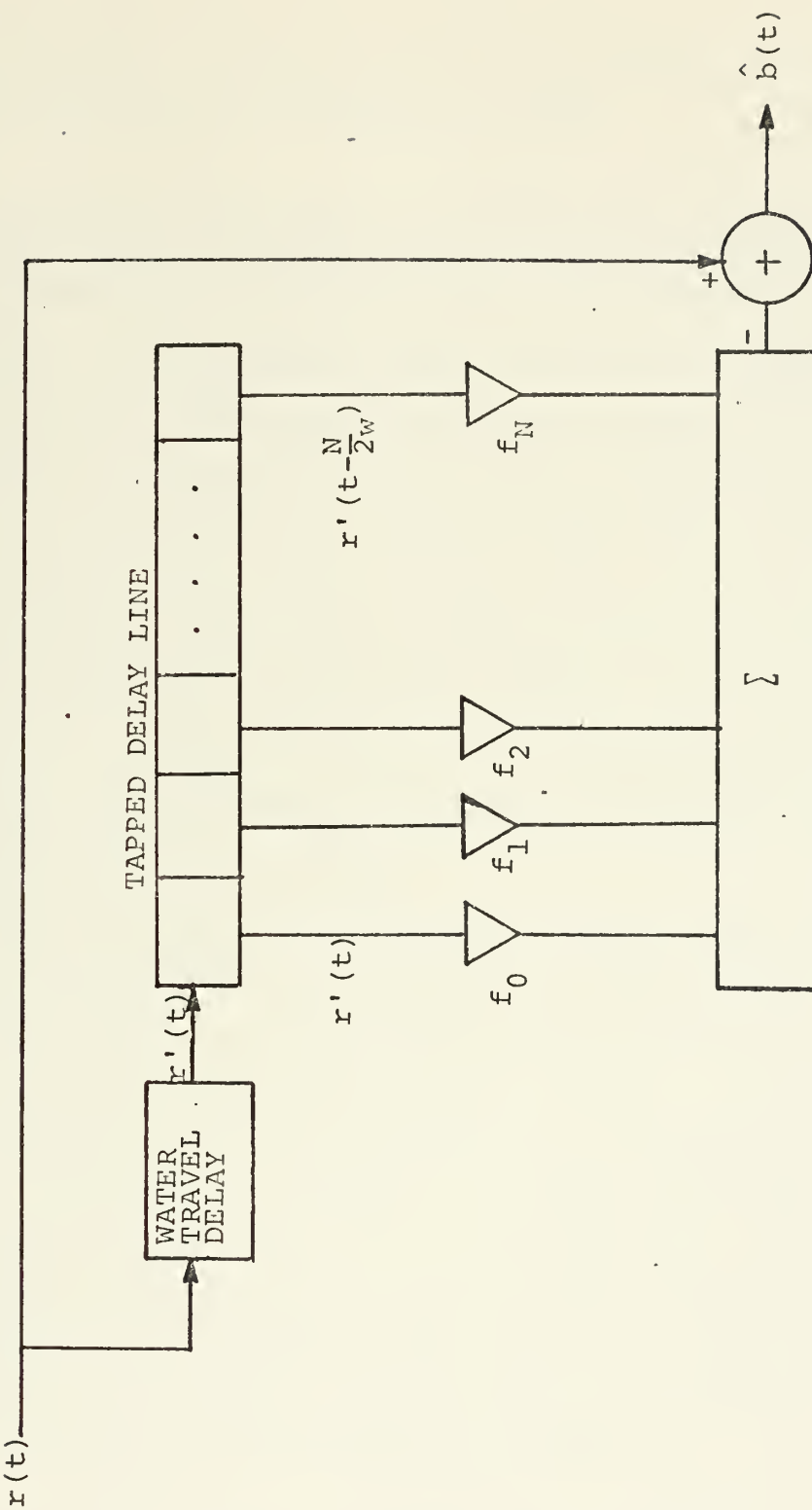


Figure 6 Tapped delay line model of convolution with a gapped operator.

figure 6, i.e., by means of a tapped delay line or, equivalently, convolution with the gapped operator.

C. Analytical Formulation of Homomorphic Deconvolution

A homomorphic system is one which obeys a generalized principle of superposition and which can be represented as an algebraically linear transformation between two vector spaces. A detailed description of the theory of homomorphic systems is given by Oppenheim and Schafer [6]. This material will not be repeated in depth here; rather, we shall discuss the basic characteristics of homomorphic systems for convolution with emphasis on those properties which facilitate dereverberation. Additional discussions of these properties are found in references [5], [7] and [8].

The usefulness of linear systems for separating additively combined signals is due primarily to superposition. Signals which are added and happen to be disjoint in the frequency domain can be separated by means of an appropriate bandpass filter. Homomorphic systems for convolution have a similar effect on signals which have been convolved. That is, a homomorphic transformation maps the input signal to a domain in which the convolved components may be disjoint. Such a transformation is illustrated in figure 7.



Figure 7

The mapping characteristic of this system is intuitively apparent. Suppose $x(n)$ is composed of two components which have been convolved.

$$x(n) = x_1(n) * x_2(n)$$

The z-transform operation yields a signal with multiplied components, $X_1(z)$ and $X_2(z)$. The logarithm output is

$$\hat{x}(z) = \log[X_1(z)] + \log[X_2(z)].$$

The inverse z-transform,

$$\hat{x}(n) = \hat{x}_1(n) + \hat{x}_2(n),$$

preserves the additive combination of the components and yields a sequence which is real and stable for a real and stable $x(n)$.

The sequence $\hat{x}(n)$ is called the complex cepstrum of $x(n)$.

Although it is real for real inputs, the "complex" is retained to emphasize that it contains both the magnitude and phase information from $X(z)$. Hence the complex logarithm is required even for real $x(n)$. (We shall omit the modifier here for brevity.)

The cepstrum variable, n , is normally called the quefrency (a paraphrase of frequency) or period variable. Filter operations in this domain are generally similar to those encountered in the frequency domain. Exact subtraction of $\hat{x}_1(n)$ from $\hat{x}(n)$ followed by computation of the inverse cepstrum (figure 8) yields the sequence $x_2(n)$, exactly, in the time domain.

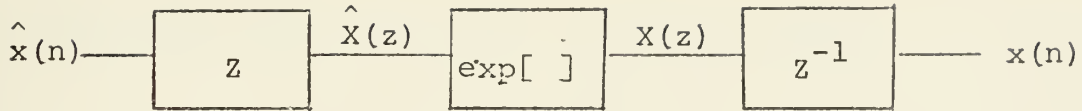


Figure 8

It is this property which renders homomorphic processing valuable for deconvolution.

As an example of complex cepstrum transformation consider a signal composed of a short pulse (2 samples) convolved with a decaying, periodic impulse train.



$$x(n) = s(n) * p(n)$$

$$x(n) = (\delta(n) + \frac{1}{2} \delta(n+1)) * \sum_{k=0}^{\infty} (-1)^k R^k \delta(n-kT)$$

where

$$|R| < 1 \text{ and } T > 2$$

Taking the z -transform,

$$X(z) = (1 + z/2) \cdot \sum_{k=0}^{\infty} (-1)^k R^k z^{-kT}$$

$$X(z) = (1 + z/2) \cdot (1 + Rz^{-T})^{-1}.$$

The logarithm then produces a sum

$$\hat{X}(z) = \log(1 + z/2) - \log(1 + Rz^{-T}).$$

Both terms are simply expanded in Laurent series.

$$\log(1 + z/2) = \sum_{n=-1}^{-\infty} \frac{(-1)^n}{n2^{-n}} z^{-n}, \quad |z| < 2$$

$$\log(1 + Rz^{-T}) = \sum_{n=1}^{\infty} \frac{(-1)^n R^n}{n} z^{-nT}, \quad |Rz^{-T}| < 1$$

The z -transforms are easily recognized.

$$\hat{s}(n) = \frac{(-1)^n}{n2^{-n}}, \quad n = -1, -2, \dots, -\infty$$

$$\hat{p}(n) = \frac{(-1)^k R^k}{k} \delta(n-kT), \quad k = 1, 2, \dots, \infty$$

$$\hat{x}(n) = \hat{s}(n) + \hat{p}(n)$$

We see that $\hat{s}(n)$ occupies only the negative quefrency region and $\hat{p}(n)$ only the positive quefrency region. Exact deconvolution can be accomplished in this case by zeroing the desired half of the cepstrum.

The canonic form of homomorphic systems for convolution is shown in figure 9.

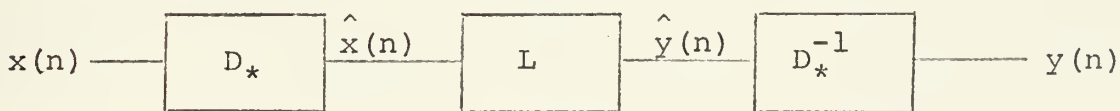


Figure 9

The characteristic systems D_* and D_*^{-1} are shown in figures 7 and 8 respectively. The system L is a conventional linear system. When L has a transfer function of 1, then $x(n)$ is recovered exactly at the output of D_*^{-1} . The choice of L will determine the effectiveness of deconvolution for a given input sequence.

Two further specifications are required to ensure the validity and uniqueness of the transformation. The complex logarithm is a multivalued function with an infinite number of branches.

$$\log[X(z)] = \log|X(z)| + j(\text{Arg}[X(z)] \pm 2\pi k) \quad \text{for all } k$$

where Arg specifies the principal value of the phase. This ambiguity must be resolved while simultaneously satisfying the requirement that $\hat{X}(z)$ be a valid z-transform. Note that if $\hat{x}(n)$ is to be real and stable, $\hat{X}(z)$ must be conjugate symmetric and analytic in an annulus of the z-plane containing the unit circle. That is, the real and imaginary parts of $\hat{X}(z)$ must be continuous functions of z in the region including the unit circle. The imaginary part, $\text{arg}[X(z)]$, can only be made continuous by "unwrapping" $\text{Arg}[X(z)]$ in such a way that all jumps of $\pm 2\pi k$ are removed. This unique unwrapping leads to a unique, valid $\hat{X}(z)$ which transforms to a stable, real $\hat{x}(n)$. The requirement of a continuous phase curve poses some computational difficulties which will be discussed in the following

section.

It is apparent from the foregoing description that homomorphic systems have the potential for separating convolved signals. One might expect, however, by analogy with linear systems that deconvolution is most effective for signals with certain cepstral properties. This is, in fact, the case and, fortunately, seismic signal components are generally amenable to deconvolution. Recall that a seismogram is modelled as a convolution of a source signature and an impulsive reflector series. Reverberation appears as a minimum phase, periodic addition to the reflector series. Thus, we have

$$r_0(n) = p(n) * (b(n) + m(n))$$

where $p(n)$ is the source signature, $b(n)$ is the desired signal and $m(n)$ is reverberation. Generalizations can be made concerning the cepstral properties of each component.

The source signature is, in general, a mixed phase, short duration time sequence. It is clear from the definition of the z-transform that any such finite sequence transforms to a rational function of z with no poles except at the origin. In general

$$P(z) = C z^{-k} \prod_{i=1}^m (1-a_i z^{-1}) \prod_{j=1}^l (1-b_j z) \quad |a_i|, |b_j| < 1$$

The a_i and b_j represent zeros inside and outside the unit circle respectively. z^{-k} corresponds to a linear phase shift.

$$\begin{aligned}\hat{P}(z) &= \log C + \sum_{i=1}^m \log(1-a_i z^{-1}) + \sum_{j=1}^l \log(1-b_j z) \\ \log C &\quad n=0 \\ \hat{p}(n) &= \sum_{i=1}^m \frac{a_i^n}{n} \quad n>0 \\ &\quad \sum_{j=1}^l \frac{b_j^n}{n} \quad n<0\end{aligned}\tag{6}$$

Here it has been assumed that the linear phase term is removed before computation. $\hat{p}(n)$ is a two-sided sequence which is always of infinite duration but decays faster than $1/n$. Hence, most of the cepstral energy is concentrated near the quefrency origin.

The reflector sequence is modelled as a train of randomly spaced impulses which may be mixed phase. Stoffa, Buhl and Bryan [5] give a general, but very complicated expression for the complex cepstrum of such a sequence. Some specific examples are given by Schafer [7]. The resulting cepstrum is an impulse train with impulses at the time domain impulse locations, at all their multiples, and at various other locations, both positive and negative on the quefrency axis. Three important observations can be made.

The cepstrum of a minimum phase reflector train contains no contributions for negative quefrency. Consider the special case of equation (6) in which all the b_j are zero. This

corresponds to all zeros being inside the unit circle, i.e., a minimum phase sequence. Note that $p(n)$ and $s(n)$ in the example are minimum and maximum phase respectively, leading to causal and anticausal cepstra.

Secondly, it happens that no non-zero cepstral contributions occur between the origin (first impulse) and the location of the second impulse in time, if the time series is minimum phase. Therefore, the cepstrum of a minimum phase impulse train, unlike that of a general sequence does not have its contributions concentrated near the origin. The cepstrum of a minimum phase impulse train will always contain a gap equal to that between the first two time domain contributions.

Finally, we observe (see Schafer [7]) that a reflector series can easily be made minimum phase by exponential weighting.

$$r'(n) = w^n r(n) \quad |w| < 1$$

$$R'(z) = C z^{-k} \prod_{i=1}^m \left(1 - (a_i w) z^{-1} \right) \left(1 - (b_j / w) z \right)$$

The value of w is chosen so that

$$|b_j w^{-1}| > 1 \quad \text{for all } b_j.$$

Weighting of the impulse train is effected by weighting of the entire signal since, if

$$s(n) = p(n) * b(n),$$

then

$$w^n s(n) = (w^n p(n)) * (w^n b(n)).$$

Note that the reflector series may be made minimum phase without making the entire signal minimum phase. Very little weighting is normally required in practice.

The remaining contribution to the seismic signal is reverberation. This component is merely a special case of a minimum phase impulse train in which the impulses are periodic. It is easily verified that if

$$m(n) = \sum_{k=1}^{\ell} y(n) \delta(n - kn_0)$$

then

$$\hat{m}(n) = \hat{y}(n/n_0).$$

The cepstrum is, therefore, periodic with the same period as the reverberation.

A useful property for deverboration is derived by Stoffa, et al.[5]. The derivation is summarized here because of its direct pertinence to seismic processing.

Consider a normalized multiple signal,

$$m(n) = \sum_{i=0}^{\infty} (-1)^i R^i \delta(n - i2T_w) \quad (7)$$

where R is the bottom reflection coefficient. Then, as we have seen

$$\hat{m}(n) = \sum_{i=1}^{\infty} \frac{(-1)^i R^i}{i} \delta(n - 2iT_w).$$

Subtracting the first j cepstral contributions and transforming,

$$\hat{m}_j(n) = \hat{m}(n) - \sum_{i=1}^j \frac{(-1)^i R}{i} \delta(n-2iT_w)$$

$$\hat{M}_j(z) = \sum_{i=j+1}^{\infty} -\frac{Rz^{-2iT_w}}{i}$$

$$\hat{M}_j(z) = \prod_{i=j+1}^{\infty} \exp \left[-\frac{R}{i} z^{-2iT_w} \right] .$$

Expanding in a power series

$$M_j(z) = \prod_{i=j+1}^{\infty} \sum_{k=0}^{\infty} -\frac{R^{ik} z^{-2ikT_w}}{k! i^k}$$

$$M_j(z) = 1 + \sum_{k=1}^{\infty} \frac{(-Rz^{-2T_w})^{j+k}}{j+k} + \sum_{k=3}^{\infty} \sum_{i=1}^{\infty} \frac{(-Rz^{-2T_w})^{2j+k}}{2(i+j)(j+k-i)} + \dots$$

(8)

Comparing (7) and (8), the first j time domain multiples have been removed completely and the $(j+1)$ st multiple is reduced by $1/(j+1)$. All succeeding multiples are also reduced. Thus, removal of only the first cepstrum multiple would remove the first time domain multiple and reduce the second by $1/2$, the third by $1/3$, etc..

Having seen the cepstral properties of each seismic signal component the advantages of homomorphic deconvolution are apparent. The source signature and reflector series have their cepstral energy concentrated in different regions of the quefrency

axis, thus facilitating removal of the source. The cepstral contributions of the reverberation occur at predictable locations so that multiple removal is possible.

Due to the nature of the homomorphic transformation, linear filtering of the cepstrum is not the normal convolution operation but a simple zeroing of the unwanted contributions. That is, the linear filter is generally frequency invariant rather than time or quefrency invariant. The name "quefrency" was adopted to reflect this reversal of the customary time and frequency filtering roles.

The foregoing analysis is based on assumptions similar to those employed in classical seismic processing. Namely, we have assumed that the seismogram consists of a source signature convolved with distinct, impulsive reflectors and periodic multiples. It is difficult to predict the sensitivity of the overall processing scheme to these assumptions because of its complex analytical structure. Hence, various parameters have been varied in the performance analysis to obtain an empirical measure of this sensitivity.

Finally, we note that the additive noise was not included in the analytical formulation of the homomorphic processing scheme. The algorithm is designed to separate convolved components and, unfortunately, no effective processing gain is achieved over added noise. In practice, additive noise has been dealt with through classical bandpass filtering. This

performance analysis includes a description of the effects of additive noise on homomorphic deconvolution.

D. Implementation of Homomorphic Deconvolution

Figures 7, 8 and 9 show the sequence of operations required for homomorphic deconvolution. A processing scheme was designed to implement this algorithm in Fortran IV on a 32K digital computer. A flow diagram of the scheme is shown in figure 10. Some aspects of the computation are noteworthy.

All z-transforms in the algorithm are implemented via FFT. Recall from the analytical formulations that z-transforms involved in the processing of a real, stable sequence are required to have regions of convergence which include the unit circle. The discrete Fourier transform is simply a sampling of the z-transform on the unit circle which, for properly band-limited signals, is sufficient to specify the signal completely. Data sequences are normally padded with zeros to reduce cepstral aliasing, e.g., 2048-point cepstra are computed for 1024-point seismograms. Since the cepstrum is always of infinite extent, a truncated version always results in some aliasing when computation is not done recursively.

The major difficulty in computing an accurate cepstrum is the computation of a continuous phase curve. The data sequences are normally sampled at a rate based on the frequency content. There is no assurance, however, that this sampling rate is adequate to uniquely specify $\hat{x}(z) = \log[X(z)]$.

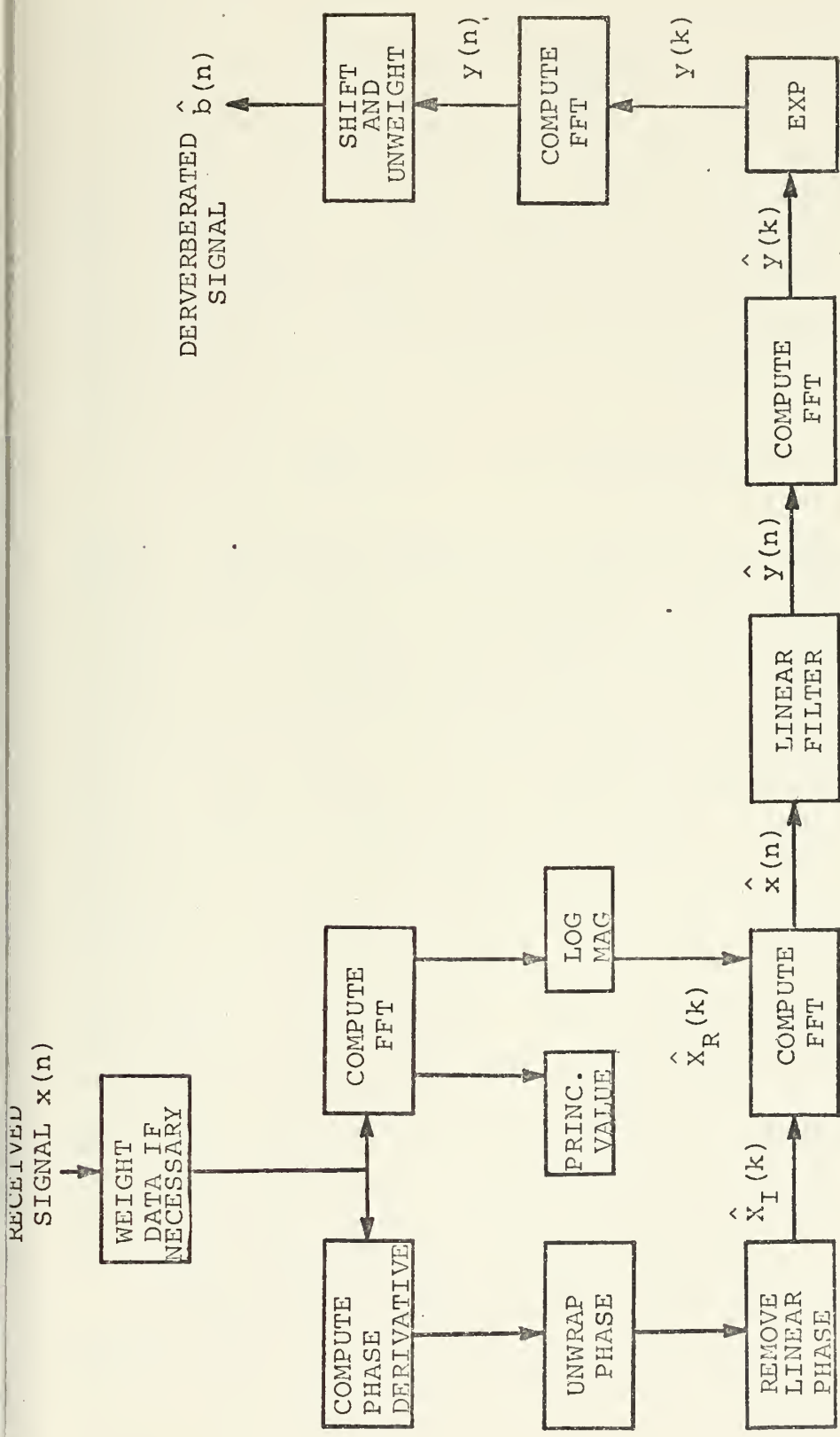


Figure 10 Flow chart of homomorphic deverbberation algorithm.

The method used for this analysis is due to Tribolet [9] and is thought to be quite accurate and efficient. The flow diagram for this algorithm is shown in figure 11.

The phase derivative, $\frac{d\hat{X}_R(z)}{dz}$ and principal value, $\text{Arg}[X(z)]$, are easily computed from the transforms of $x(n)$ and $n x(n)$ (see appendix A). The values of the derivative are integrated using the trapezoidal rule and the integral output is compared with $\text{Arg } X(z)$ at each step. If the two values do not agree within

$$2n\pi \pm \epsilon \quad n = 0, \pm 1, \pm 2, \dots$$

where ϵ is a small positive number, the latest computed value of $\arg X(z)$, say a_i , is discarded. The routine then returns to the last correct integration value, computes an intermediate derivative value, and begins integrating with a step size half that of the original grid. The integrate-and-compare process is continued at this step size until a_i has been computed correctly or until a comparison fails. Integration is resumed at the initial step size in the former case or, in the latter, step size is again halved. The number of possible step sizes is theoretically unlimited. The value of ϵ may be adjusted by trial-and-error for most efficient integration. The adaptive step feature compensates for the undersampling problem in a very efficient and accurate manner.

Linear phase contributions are easily identified and removed from the computed continuous phase curve. Having

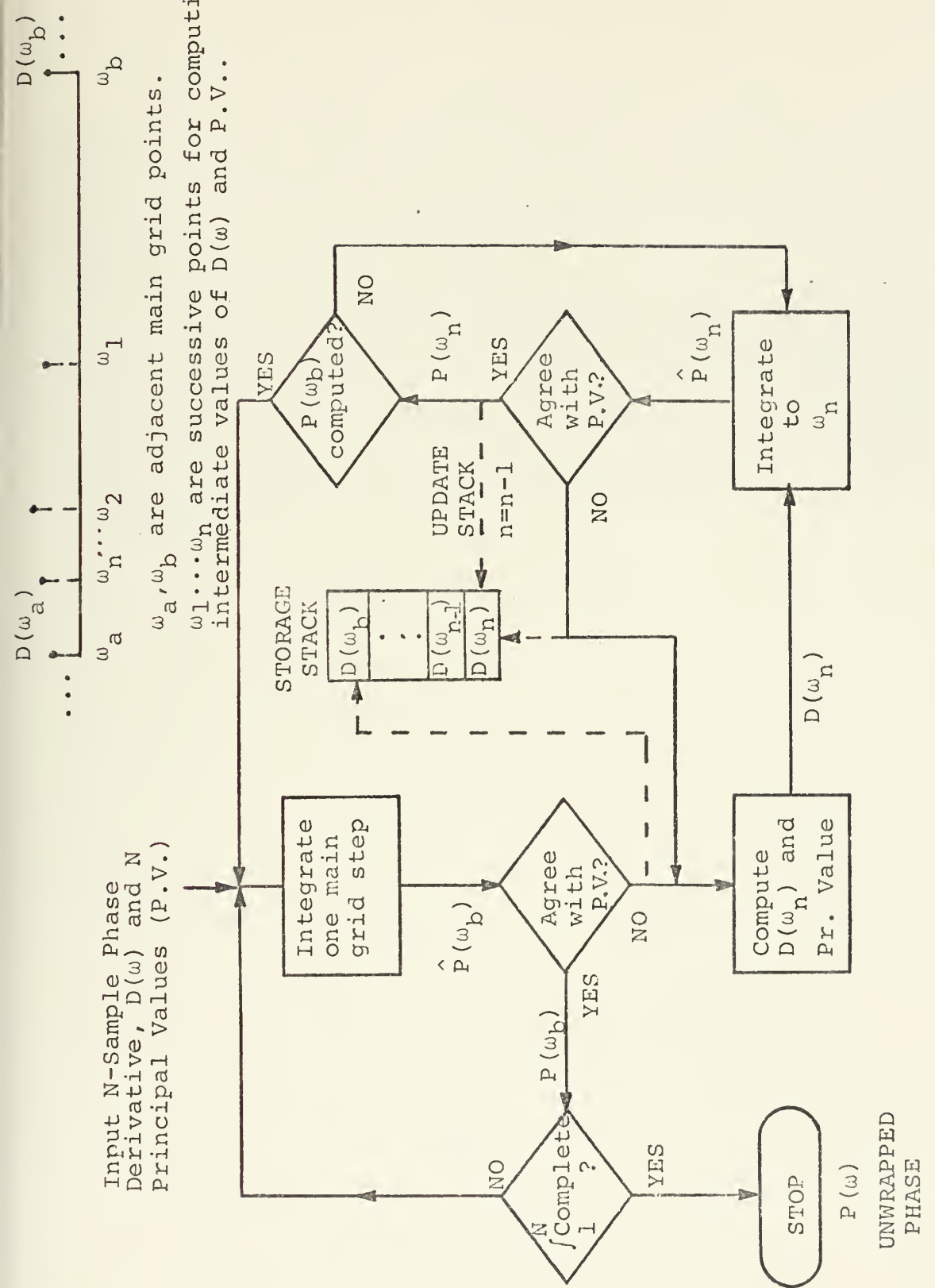


Figure 11 Flow chart of Tribolet phase unwrapping algorithm

computed the log magnitude and phase, the inverse z-transform is straightforward.

Linear filtering is accomplished by zeroing the unwanted cepstrum values. One might consider windowing procedures which are common in linear filtering, but these were not employed in the present analysis.

The inverse cepstrum computation is completely straightforward since no ambiguities arise in the exponentiation process. The final steps are shifting the output sequence by the linear phase value and unweighting the shifted sequence, if necessary.

CHAPTER III
DESCRIPTION OF THE PERFORMANCE ANALYSIS

The purpose of this analysis is to evaluate, both quantitatively and qualitatively, the performance of the TDL and homomorphic dereverberation techniques. Each method is to be evaluated for a variety of simulated seismic conditions in order to determine those factors which significantly influence performance. The comparative nature of the analysis is intended to emphasize the relative strengths and weaknesses of each technique.

It should be noted that absolute performance figures are not inherently valuable, especially when obtained from synthetic data. The diverse geological and oceanographic conditions encountered in marine seismology coupled with the many different processing systems currently employed may be expected to yield a range of absolute results. The greater value of this analysis is to indicate the parameters, environmental and mathematical, which can be expected to affect significantly the performance of these algorithms. The numbers obtained provide a measure of the relative performance of the two methods under similar conditions and, in some cases, provide asymptotic performance criteria. Synthetic data were chosen so that signal parameters could be accurately controlled.

Three criteria are specified for comprehensive evaluation of performance. The first, most direct, measure of effectiveness

is the percentage of multiple energy removed from the signal. This is easily measured by calculating the zero-lag correlation of the signal, in time windows spanning only the multiple locations, before and after processing. That is, the squared amplitude (energy) of the signal in the multiple region is computed after processing and subtracted from the squared amplitude of the original signal in that region. This difference is divided by the original energy of the multiple to yield the fraction of energy removed by processing. The use of synthetic data facilitates this method of analysis since reflectors and multiples can be placed in disjoint regions to avoid ambiguity.

The second criterion is the amount of signal distortion introduced by dereverberation. This is measured by comparing reflector energy before and after processing. As before, reflectors and multiples must be disjoint for meaningful results.

Although these two criteria provide an accurate quantitative measure of performance they are restricted to situations in which reflectors and multiples do not overlap. The overlap case is most important in processing real data since the multiples then obscure the reflectors most severely. In order to judge performance in these situations we must evaluate qualitatively the improvement of visual interpretability. This visual enhancement of reflector-to-multiple ratio is our third criterion. It is an important measure in spite of its

subjective nature since the primary means of seismogram analysis is visual interpretation.

The analysis is limited in scope to the single channel processing configuration. Although both techniques are applicable, in principle, to multichannel processing, the many additional variables involved and unavailability of appropriate synthetic data would lead to a complicated extension of this analysis. A single channel treatment is adequate to identify the important performance traits of both methods.

Parameters to be varied fall into two general categories; environmental and operational. The environmental parameters include noise level, multiple periodicity, multiple-to-signal level and multiple/reflector separation or overlap. These are varied within ranges which are thought to be representative of ambient conditions normally encountered in marine seismology. Effects of noise level are considered only for the case of white Gaussian noise. The effects of aperiodicity have not been evaluated for the TDL algorithm because it is intended primarily for deep water use where only the first multiple is usually of interest. Operational parameters refer to those which can be controlled during processing. These include filter cutoff frequencies, operator lengths, travel time estimates, cepstral stopbands, and weighting. Windowing of the correlation function is not evaluated although a discussion of this subject is contained in reference [3].

The algorithm used in generating simulated earth impulse responses is due to Theriault [10]. A brief description of Theriault's earth model is given here.

The model is based on the following assumptions:

- (1) An air gun source generates longitudinal pressure waves which impinge upon all earth layers as normally incident plane waves.
- (2) All earth layers are horizontally infinite, parallel and homogeneous.
- (3) Abrupt changes in acoustic impedance occur at each layer interface and these boundaries are characterized by the customary acoustic reflection and transmission coefficients.
- (4) The earth has a uniform density.
- (5) The water column is a non-attenuating fluid with a perfect pressure release interface at its surface.
- (6) Each layer is characterized by a transfer function, $F(\omega)$ which represents the attenuation and travel time delay for that layer.

These assumptions are incorporated into a lumped parameter model. Figure 12 shows a frequency domain model of a two layer earth. The $F_i(\omega)$ have the functional form

$$\left(\frac{1}{j\omega\alpha_i + 1} \right)^3 \exp\left(-j\omega x_i/c_i\right) \quad (9)$$

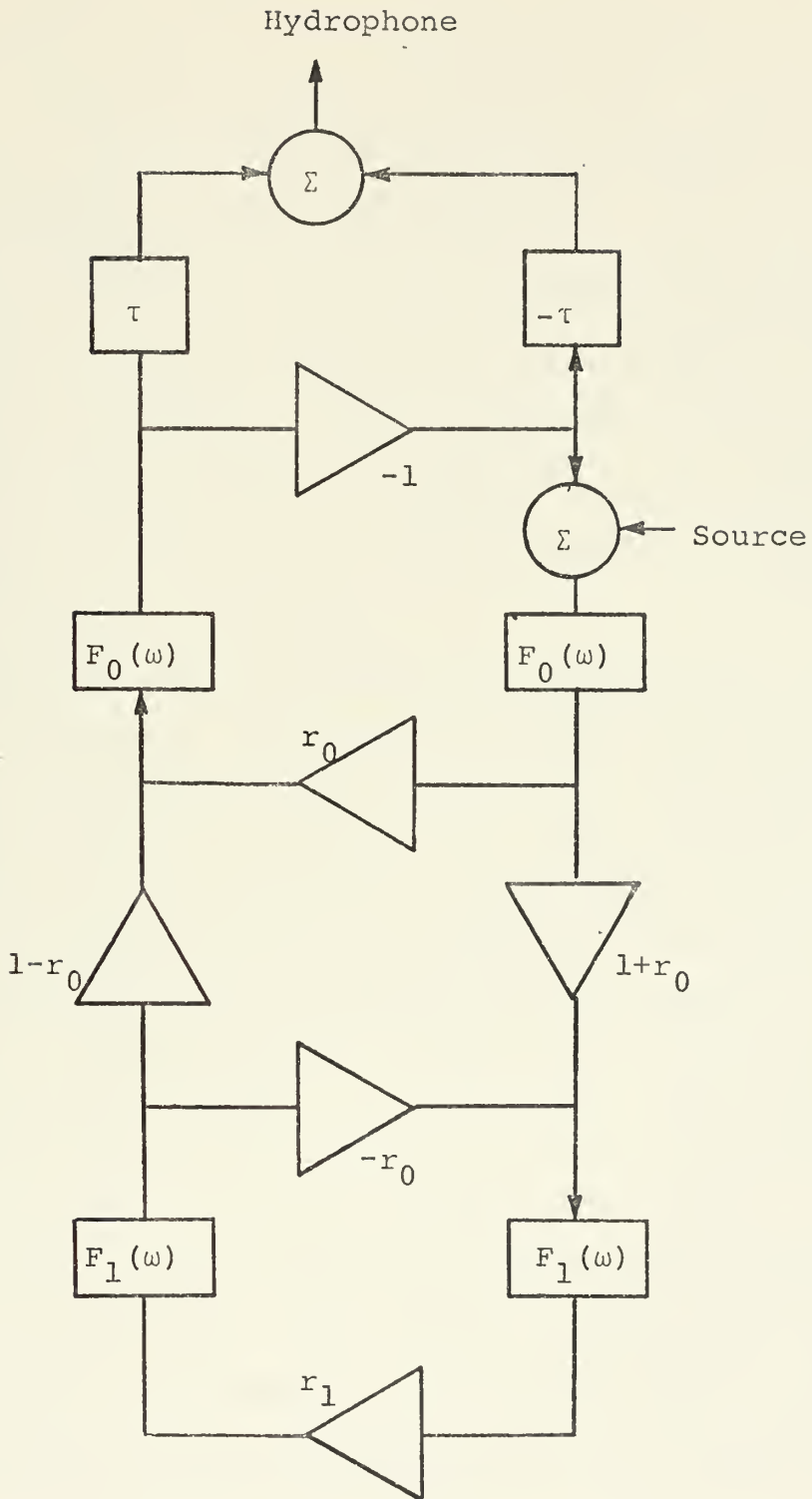


Figure 12 Two layer earth transfer function schematic
(after Theriault).

where x_i , c_i and α_i are the i th layer thickness, sound speed and layer attenuation parameter respectively. These transfer functions are combined using a semi-group property rather than the usual frequency domain multiplication.

The -1 multiplier completes a feedback loop around the source which generates the water column multiples. Since the water column is assumed to have no attenuation the multiples appear in the earth response as impulses, and in the resulting seismogram as replicas of the source signature reduced by the bottom reflection coefficient.

The above multiple mechanism is inadequate for representing effects of incoherent (distorted) multiples and varying bottom interaction mechanisms. These effects are introduced by insertion of water column attenuation which causes the bottom response and multiple responses to be of exponential form given by the Fourier transform of (9). Thus the bottom response is extended in time and each multiple is a distorted version of the previous one. Examples of multiple appearance with and without water column attenuation are shown in figure 13a and b.

The topmost loop of figure 12 simulates the effects of finite receiver depth τ . Any number of layers with the desired parameters can be combined into an overall earth transfer function which is easily transformed to yield the earth impulse response.

Synthetic seismograms for this analysis were generated by

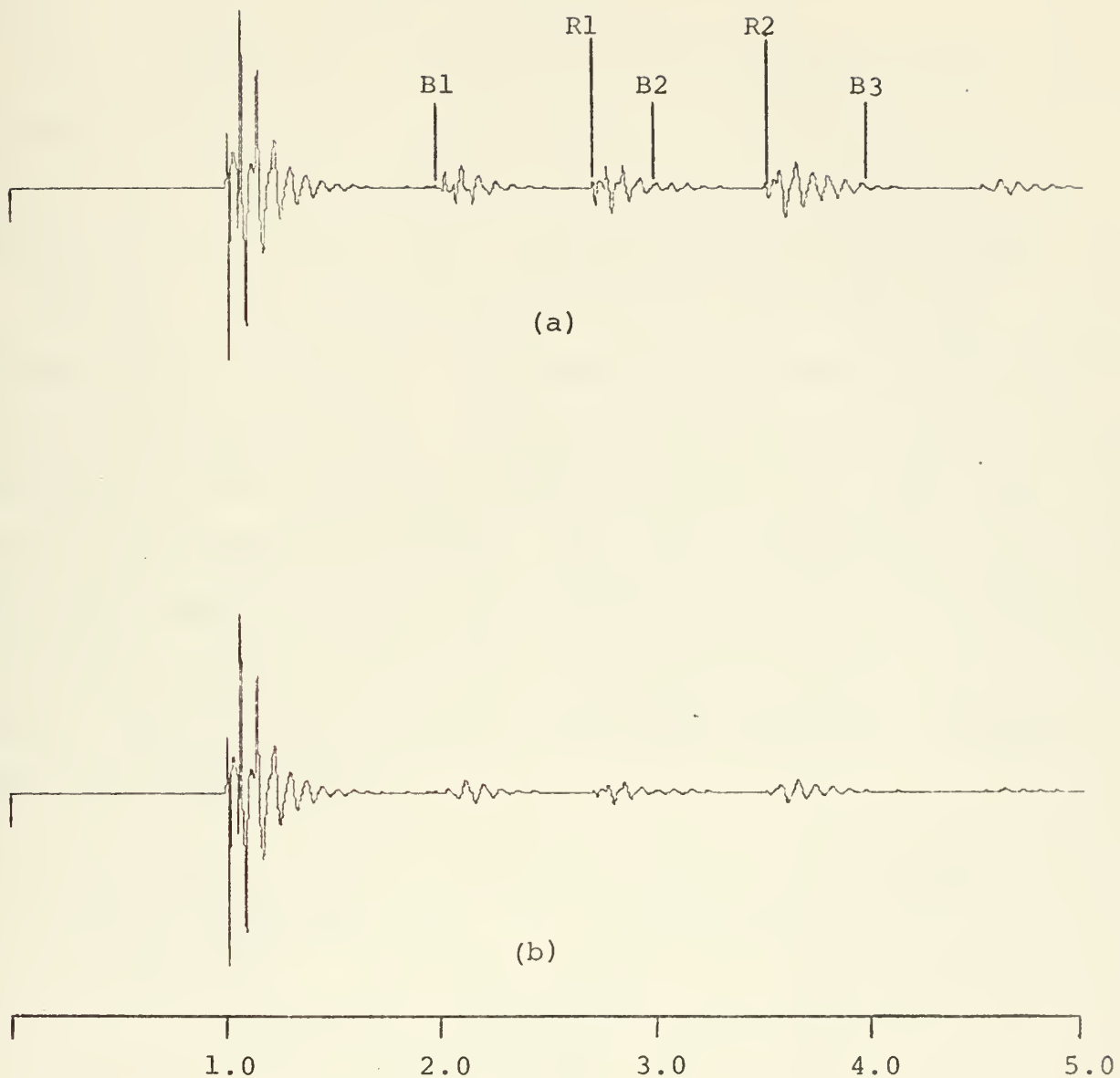
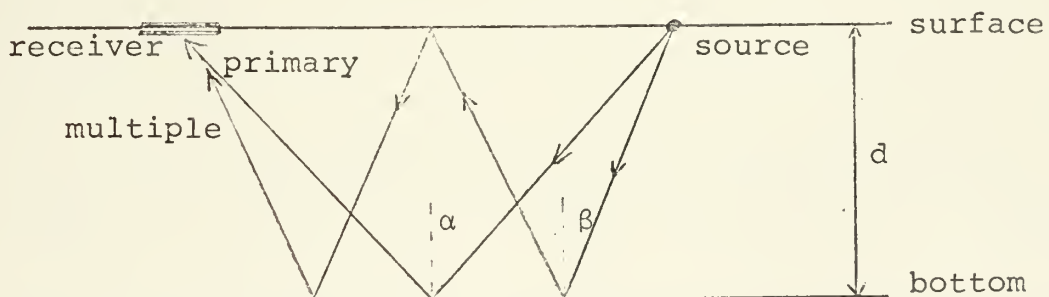


Figure 13 (a) Synthetic seismogram with coherent multiples.
(b) Synthetic seismogram with distorted multiples
due to water column attenuation.

convolution of various Theriault impulse responses with air gun signatures obtained from actual at-sea recordings. A typical signature is shown in figure 14.

It is important to note that these seismograms contain all water column multiples and internal multiples of all orders. For realistic parameter values earth attenuation characteristics usually render internal multiples negligible.

Finally, we note one drawback of using this model for multiple removal analysis. The algorithm produces multiples which are exactly periodic. This periodicity gives these seismograms strong correlation characteristics which are not usually encountered in practice. The lack of periodicity in actual seismograms is due to the horizontal separation of the source and receiving array. The difference in travel paths arising from this separation is illustrated below for a primary return and first multiple.



$$\text{primary path length} = \frac{2d}{\cos \alpha}$$

$$\alpha > \beta$$

$$\text{multiple path length} = \frac{4d}{\cos \beta}$$

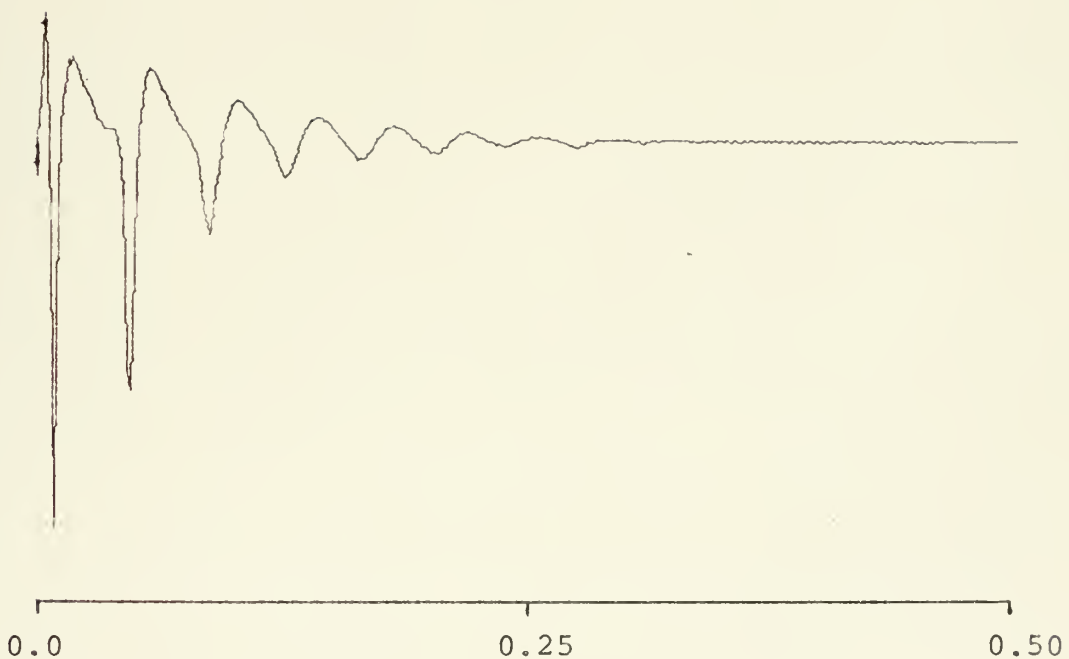


Figure 14 Air gun signature (obtained by at-sea recordings) convolved with synthetic earth response functions to form seismograms.

For a known separation and water depth the travel time difference can be easily calculated. This effect becomes minimal in deep water where $\cos \alpha$ and $\cos \beta$ are approximately equal to one.

CHAPTER IV

RESULTS

A. Introduction

The results of applying the multiple removal methods described in Chapter II to synthetic data are described here in terms of the criteria of Chapter III. Performance based on the first two criteria is emphasized because it can be quantified much more accurately. Specifically, the reflectors and multiples have been positioned at distinct locations in most cases so that the amount of energy removed from reflectors and multiples can be measured without ambiguity. This emphasis leads, however, to a certain lack of realism in several of the synthetic data plots. Separation of this kind in an actual seismogram would, of course, eliminate the necessity for multiple removal. Hence, several cases of interfering reflectors and multiples are also shown. Although these are not amenable to quantitative analysis they can be judged on the basis of the third criterion, viz., improvement of visual record quality.

A second deviation from normal processing conditions has been required to compare effectively the performance of the two methods. Homomorphic dereverberation is accomplished in practice (see [5]) concurrently with source deconvolution, where practical, since both operations are simply performed after the cepstrum has been computed. This leads to a considerable amount of energy removal at each multiple and

reflector location which is due to source deconvolution alone. Although this may lead to improvement of the record, the criterion of energy removed does not accurately measure dereverberation performance in the same way it does for the TDL results. For example, source deconvolution might typically lead to 90% reduction of multiples and 90% removal of reflector energy. This gross change in configuration cannot be effectively compared with TDL processing on the basis of energy removed. Hence, source removal has not been accomplished in most cases tested. The results of this "partial" processing can be quantitatively evaluated and easily compared with TDL results. Cepstral filtering which includes source removal, thus retaining only high quefrency energy, is referred to as "longpass filtering". Several examples of longpass filtering are included and interpreted in terms of the third criterion.

The performance of each method is discussed individually for various processing situations. A direct comparison of the performance of both methods for the same data is also included. The comparison is extended in Chapter V.

B. Results of TDL Dereverberation Performance

1. Operator Length, Multiple Distortion and Multiple-to-Signal Ratio

The number of tap gains required for optimum multiple removal was found to be highly signal-dependent. Recall from Chapter II that the tapped delay line is essentially an

estimate of the high energy portion of $h_b(t)$, the earth impulse response. In most applications the reflected bottom response is dominant. The time-bandwidth product of this response would then be expected to govern the filter length requirements. Measured results confirm this.

Seismograms containing exactly impulsive (one sample) bottom responses exhibited little or no variation of performance with filter length. Typical filter impulse responses for a seismogram of this type are shown in figure 15. The reflection coefficient in this case is 0.3. The first tap gain is close to -0.3 in each response, as would be expected from the Backus formulation in which the second operator point is an estimate of the bottom reflection coefficient. Increasing filter length can be seen to cause variation in the "estimation" of the reflection coefficient. Figure 16 shows energy removed vs. filter length for this seismogram. Multiple energy removed decreases slightly with increasing filter length. Reflector distortion is nearly constant at low values (6% for one and -2% for the other). The signal used in figure 16 is shown in figure 17a. The processed result shown was obtained using only one tap.

Introduction of a non-impulsive multiple mechanism was found to produce a marked dependence of performance on operator length. Synthetic seismograms were generated with finite length bottom responses, resulting in distorted multiples which are not simply weighted replicas of the source signature.

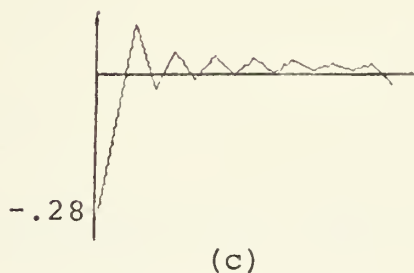
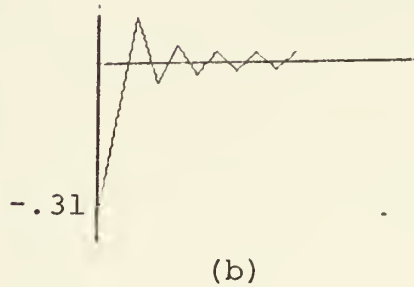
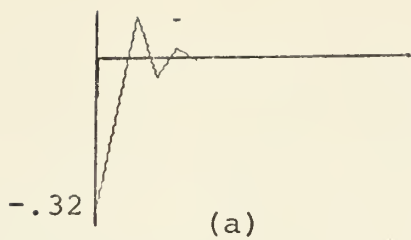


Figure 15 TDL impulse responses for three operator lengths.
(a) 5 taps (b) 10 taps (c) 15 taps

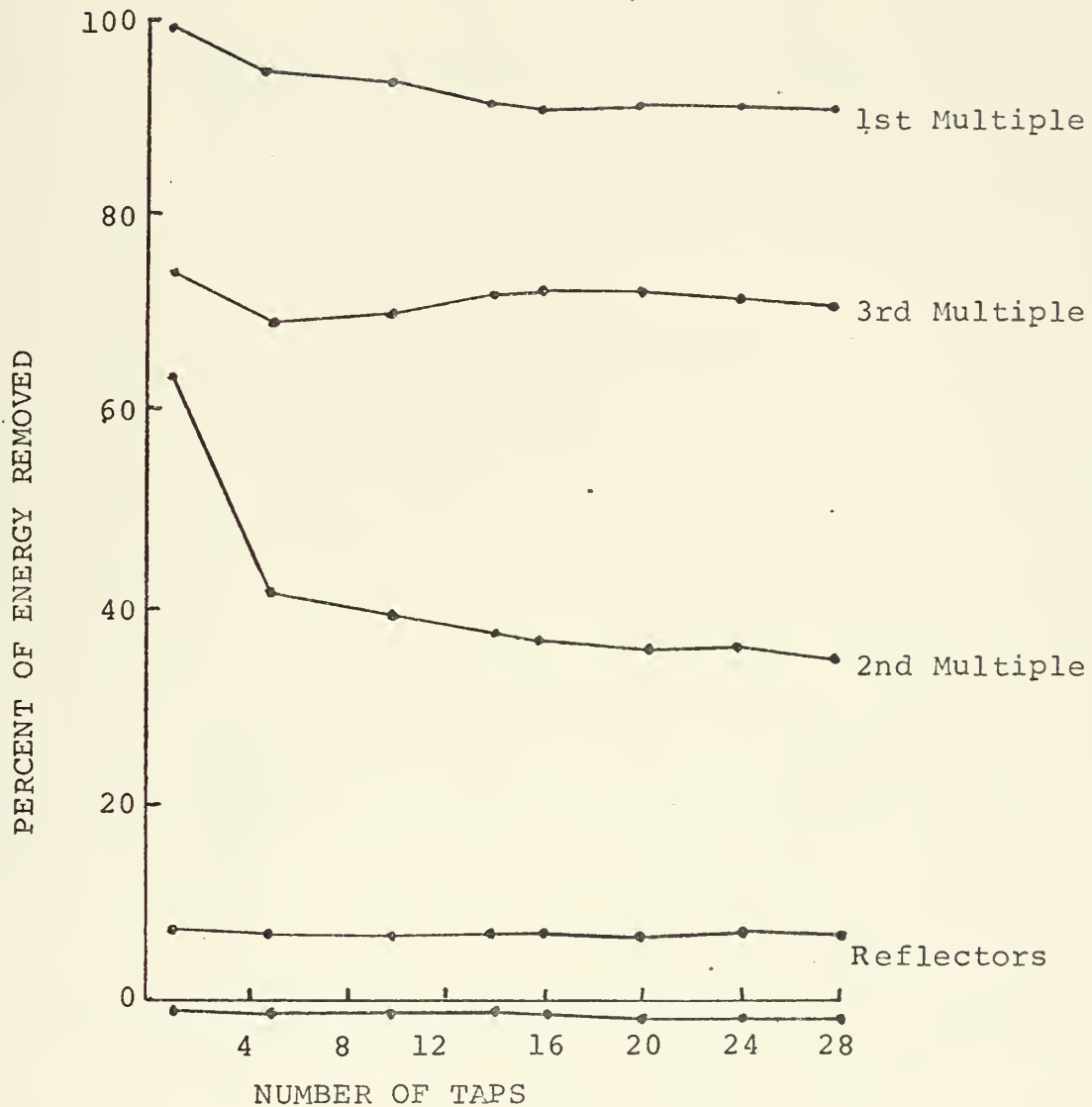


Figure 16 Operator length vs. performance for a signal with with impulsive multiples.

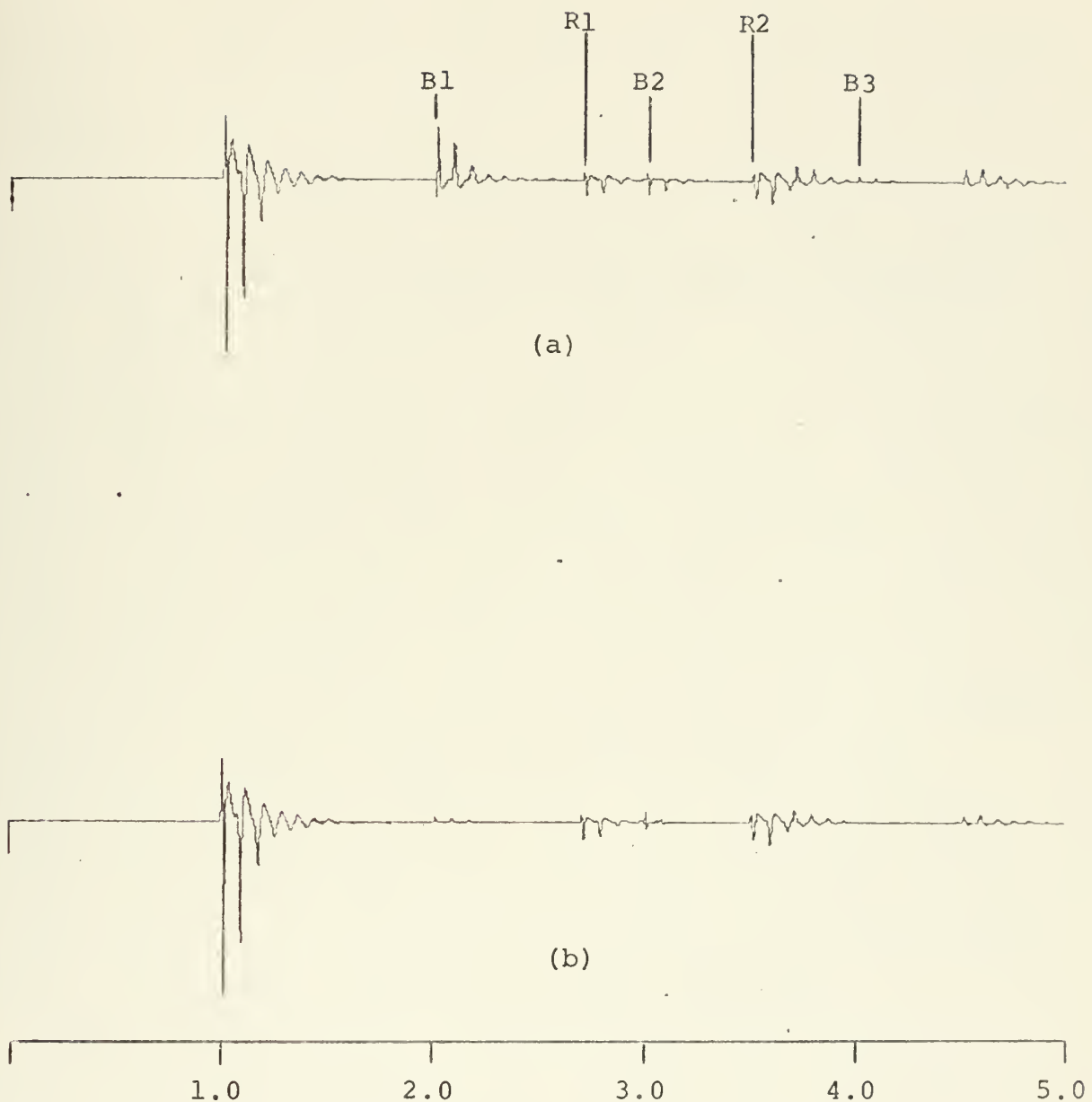


Figure 17 (a) Seismogram with coherent multiples.
(b) Result of TDL processing with a one point operator.

Figure 18 shows filter performance vs. operator length for three seismograms having different degrees of distortion in their bottom reflection mechanisms. This distortion is equivalent to extension of the bottom impulse response in time. The signals associated with curves (1), (2) and (3) are shown in figures 19a, 19b and 19c respectively. The increasing distortion of the multiple at 2.0 seconds is evident. Curve (1) corresponds to a signal with very slight multiple distortion. Operator length is seen to have no effect on performance. The seismogram corresponding to curve (2) has a bottom impulse response which is significant for $T = .03$ seconds. The tap spacing in this case is $1/2W = 4.88$ msec, so that $2TW = 6.1$, and six or seven tap gains should be adequate if the signal has been properly sampled. Reference to curve (2) confirms that increasing the filter length beyond seven does not improve performance. Filters of fewer than seven elements yield monotonically decreasing performance. The bottom response for curve (3) is significant for $.045$ seconds so that, for the same tap spacing, $2TW = 9.2$ and we anticipate that nine or ten taps will be adequate. This is, in fact, the case.

Figure 20 shows the 5, 9 and 15 point filter impulse responses associated with curve (3). There is an observable convergence to a $t^2 e^{-bt}$ shape which is the actual functional form of the synthetic bottom response. Figures 20a and 20b exhibit a "diverging tail" effect which was found to be common

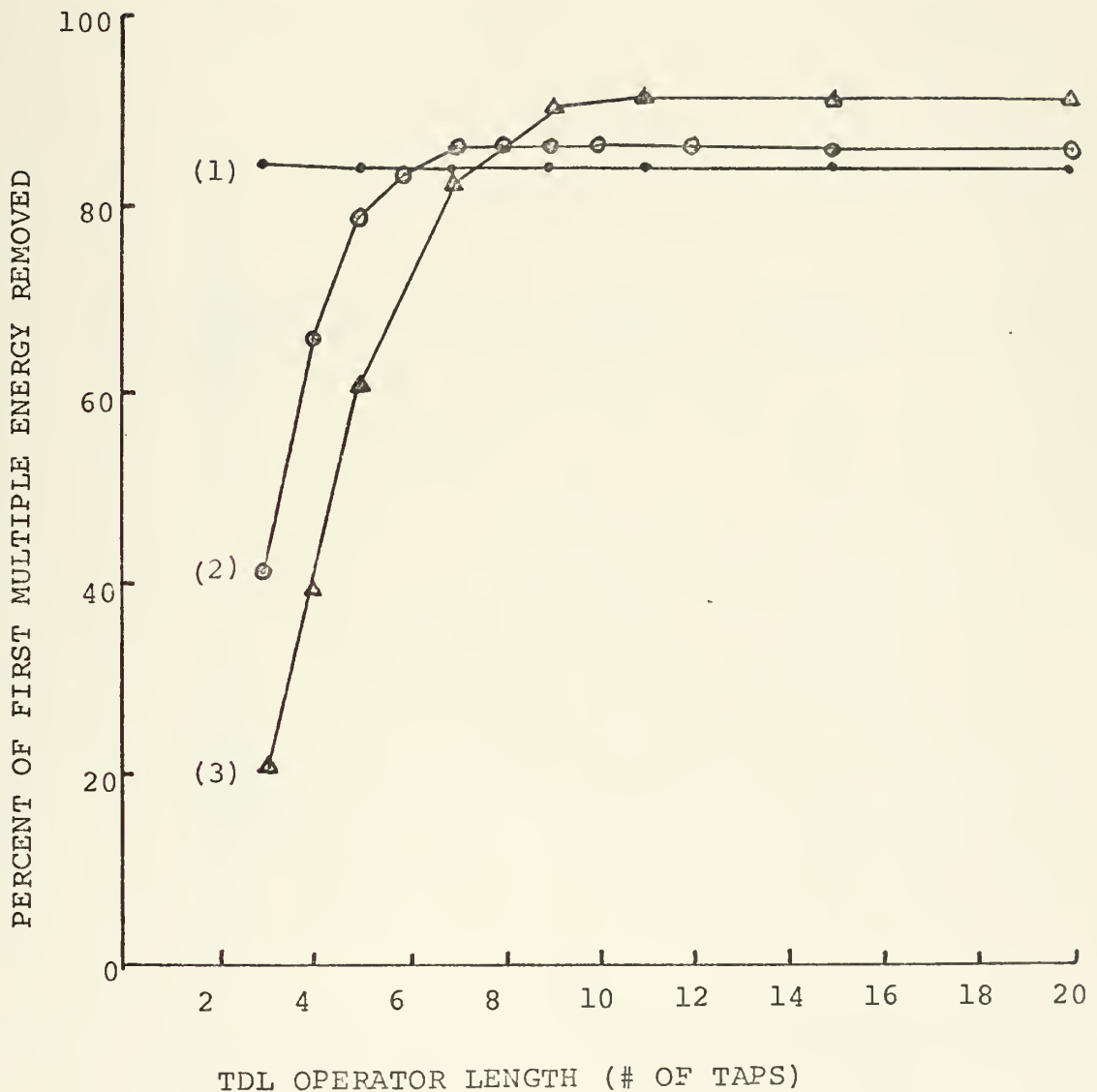
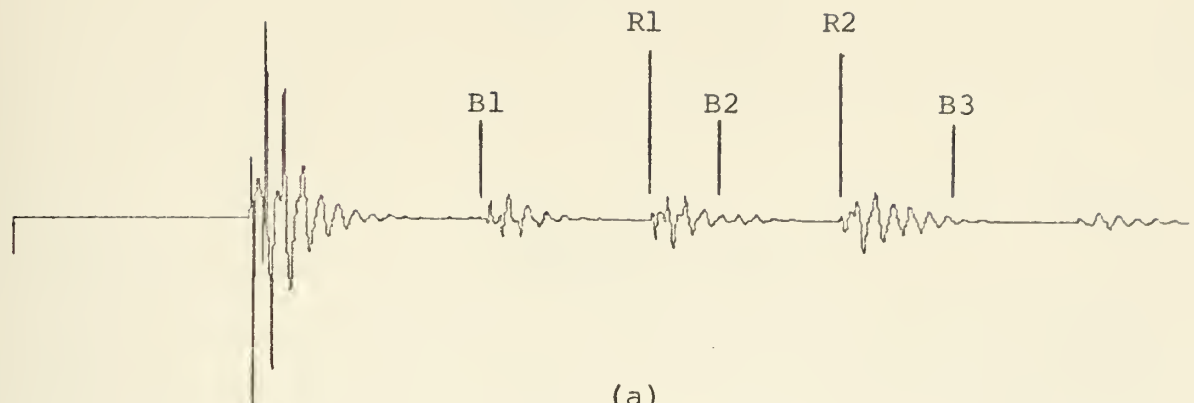
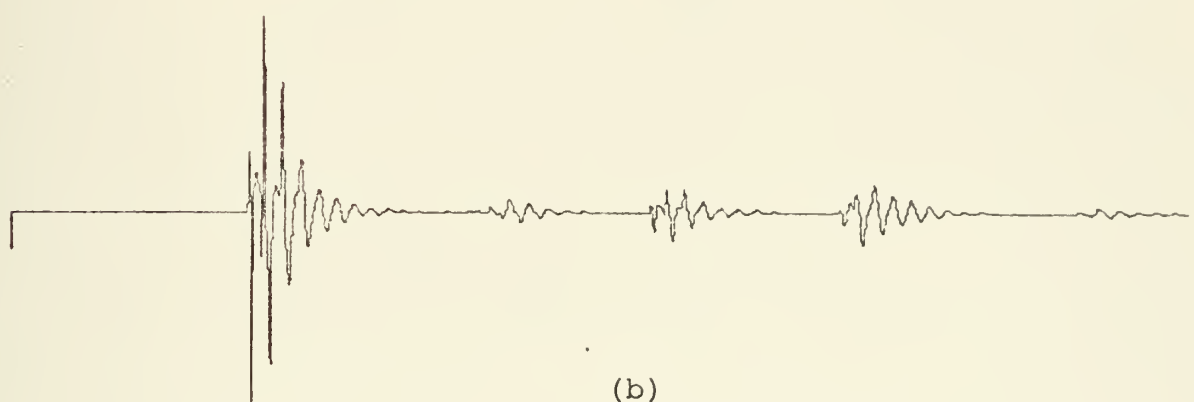


Figure 18 Performance vs. operator length for three signals with bottom interaction times varying from (1) impulsive to (3) .045 seconds.

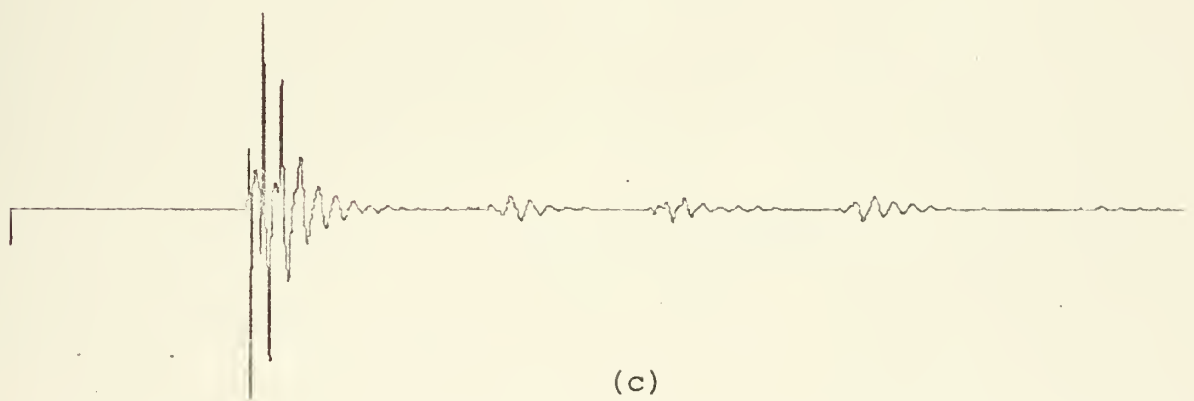
-60-



(a)



(b)



(c)

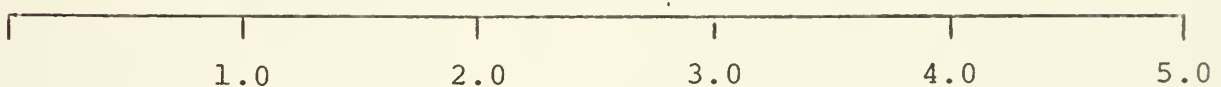
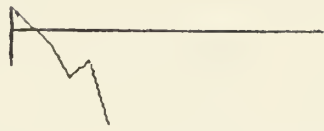
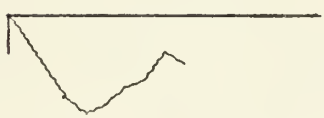


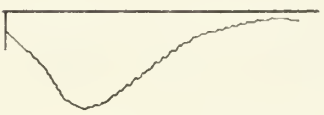
Figure 19 Seismograms associated with the curves of figure 18. (a) Curve (1). (b) Curve (2). (c) Curve (3).



(a)



(b)



(c)

Figure 20 Filter impulse responses associated with Curve (3) of figure 18. (a) 5 points (b) 9 points (c) 15 points.

when the specified filter length is too short. This type of phenomenon occurs in some numerical approximation methods when an inadequate number of terms is specified.

It is apparent from the above results that the effect of operator length is closely related to the bottom interaction mechanism. As discussed in Chapter II, the filter should be an estimated replica of the bottom impulse response when the interaction process can be accurately modelled as a convolution of the source signature with the bottom response. Figures 15 and 20 are good examples of this behavior.

In the cases summarized in figure 18 performance increases as multiple distortion increases. This need not be true in general since bottom interactions may become very complex.

The slowly varying $t^2 e^{-bt}$ responses lead to operators which have a greater cancellation effect as they are extended. A higher bandwidth bottom impulse response might not exhibit this behavior. As it was not possible to include more complicated bottom responses in the earth model used, these effects were not investigated further.

Reflector distortion was found to be nearly constant for all filter lengths tested. The reflector at 2.7 seconds was essentially undistorted in all cases. The 3.5 second reflector had an average distortion of 7%. Figures 21-24 show some processed results for the signals in figure 19. Each of the

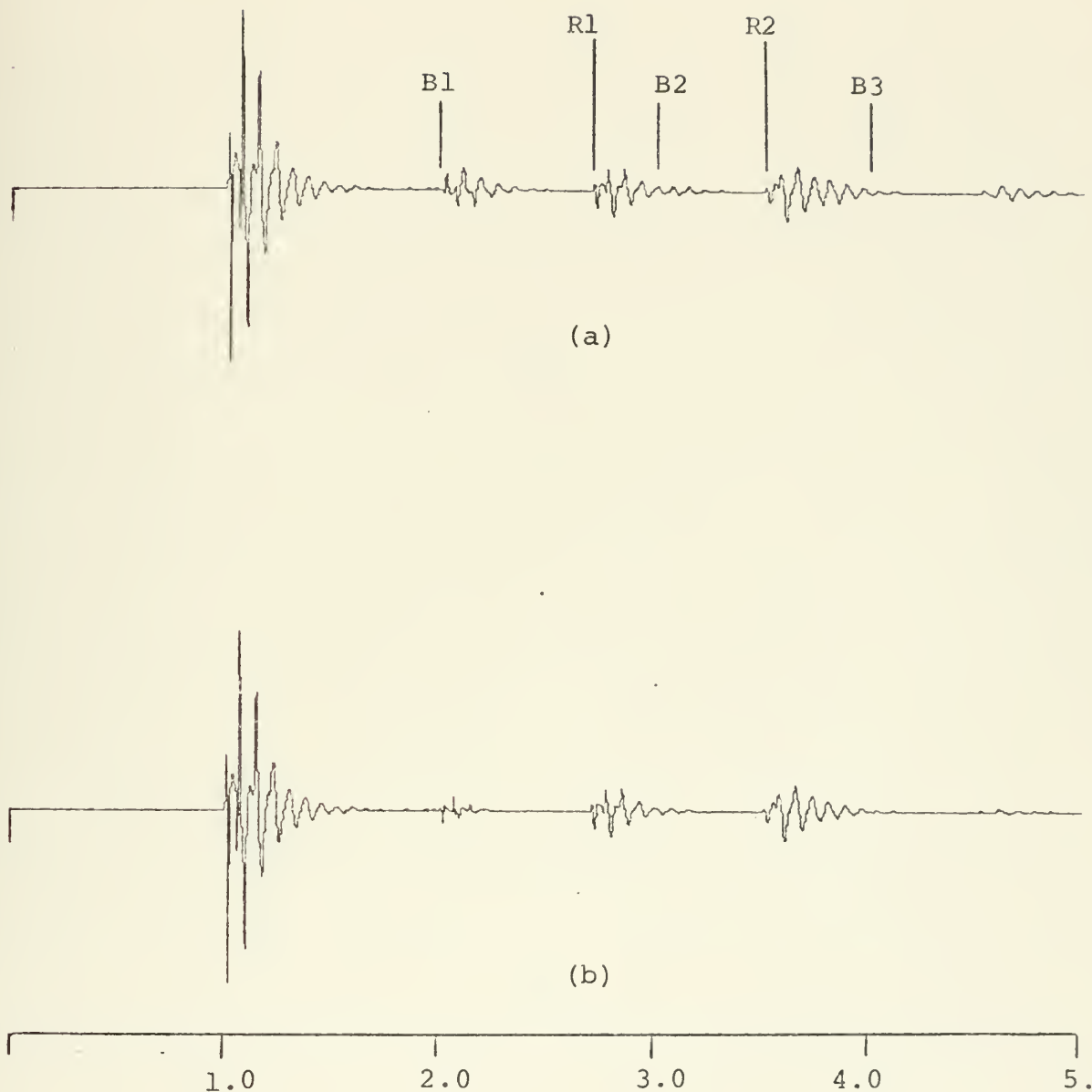
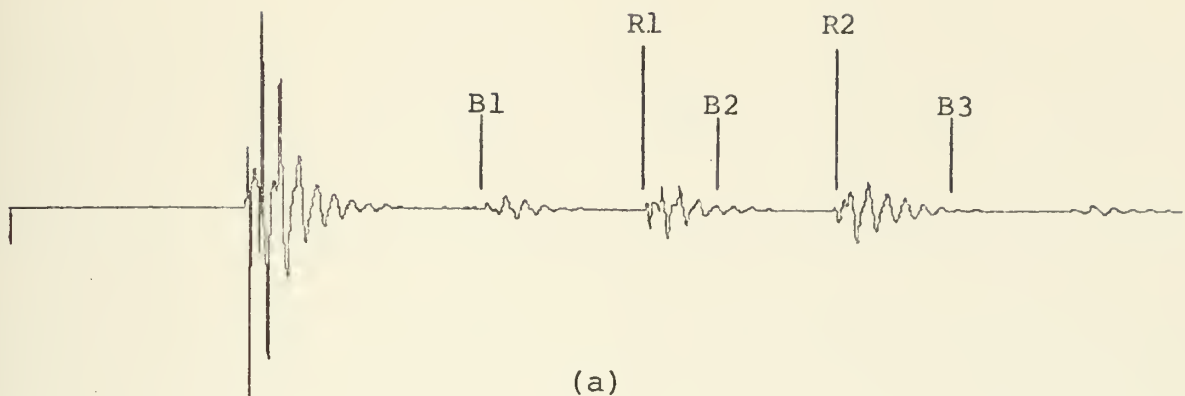
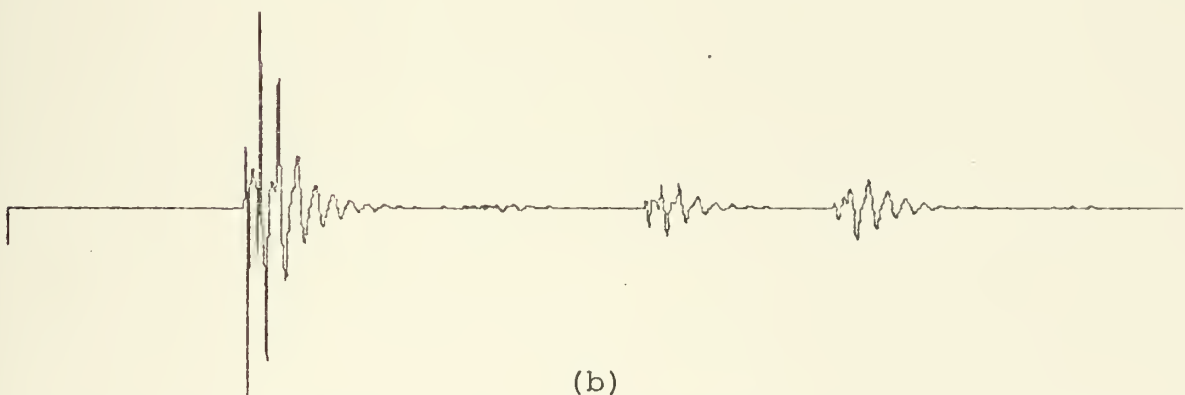


Figure 21 (a) Seismogram with very coherent multiples.
(b) Result of TDL processing with three taps.



(a)



(b)

1.0 2.0 3.0 4.0 5.0

Figure 22 (a) Seismogram with moderately distorted multiples;
bottom response is significant for .035 seconds.
(b) Result of processing with 7 taps.

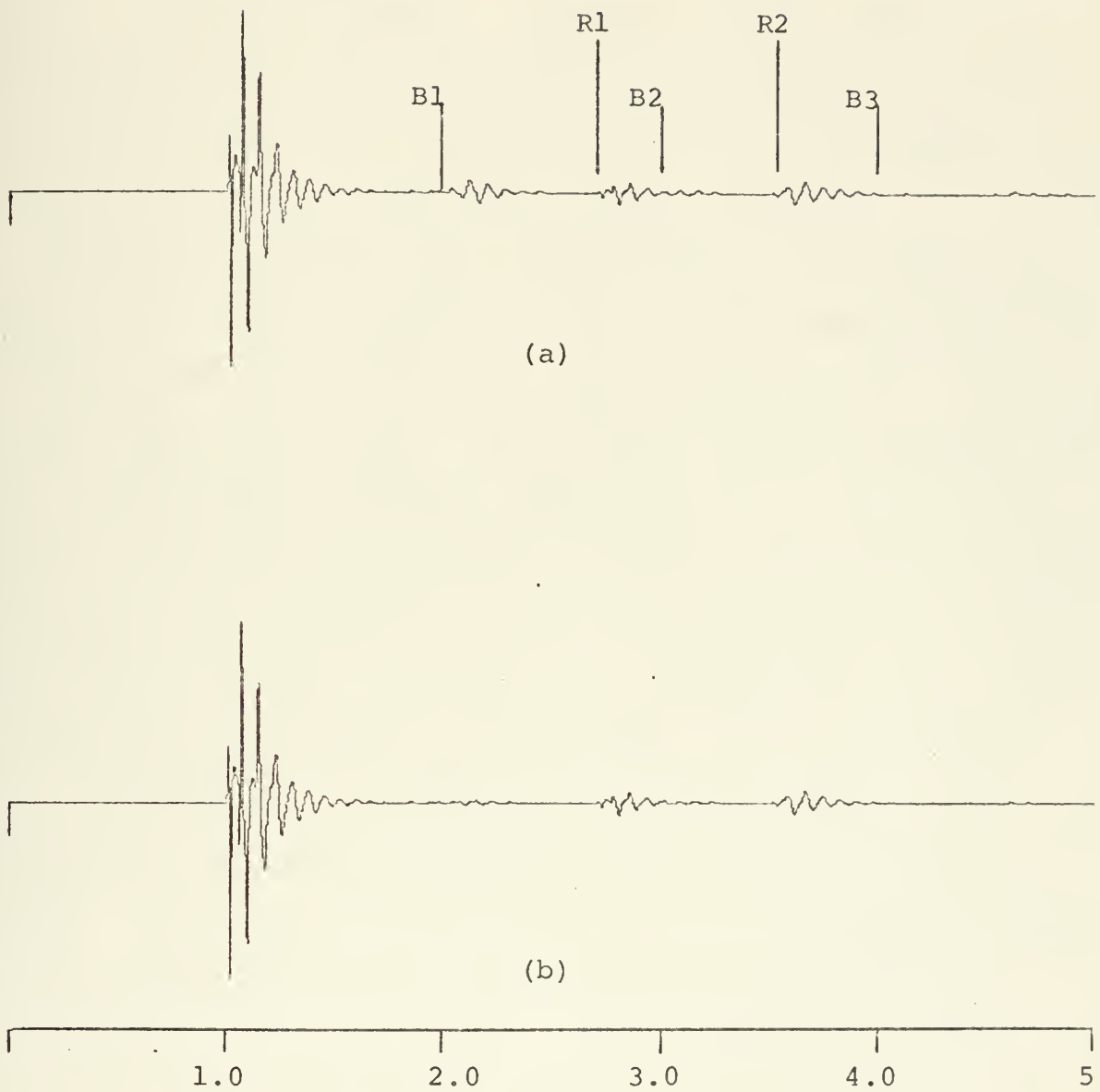
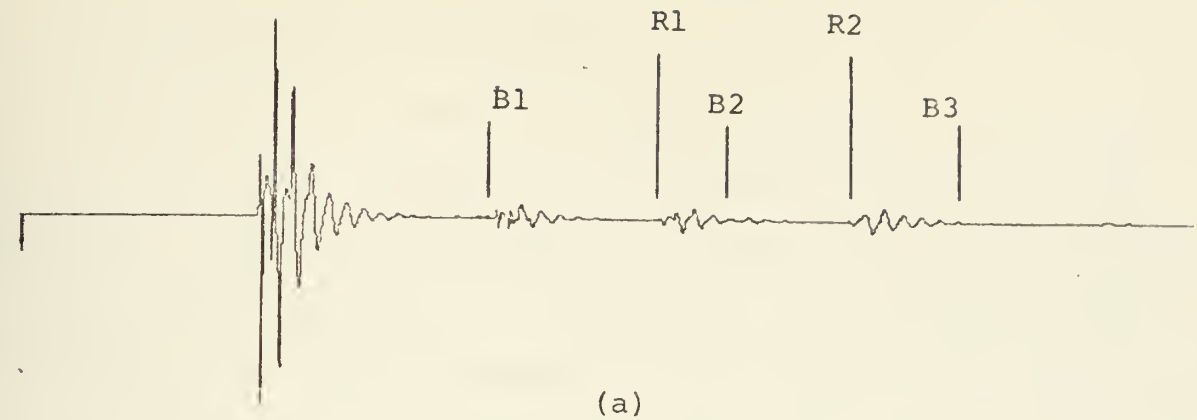


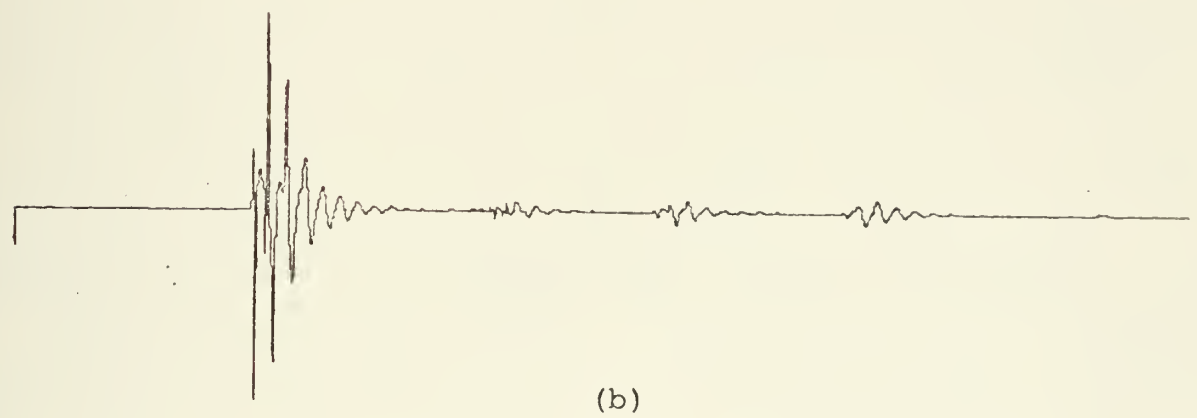
Figure 23 (a) Seismogram with considerable multiple distortion; bottom response is significant for .045 seconds.
(b) Result of TDL processing with 11 taps.

first three figures (21, 22 and 23) show signals before and after processing with the fewest number of taps required to achieve optimum performance. Visually, multiple removal is almost complete in each case. The signal of figure 23a is shown in figure 24 after processing with 3, 5 and 7 taps. The improvement from figure 24a to 24c is obvious.

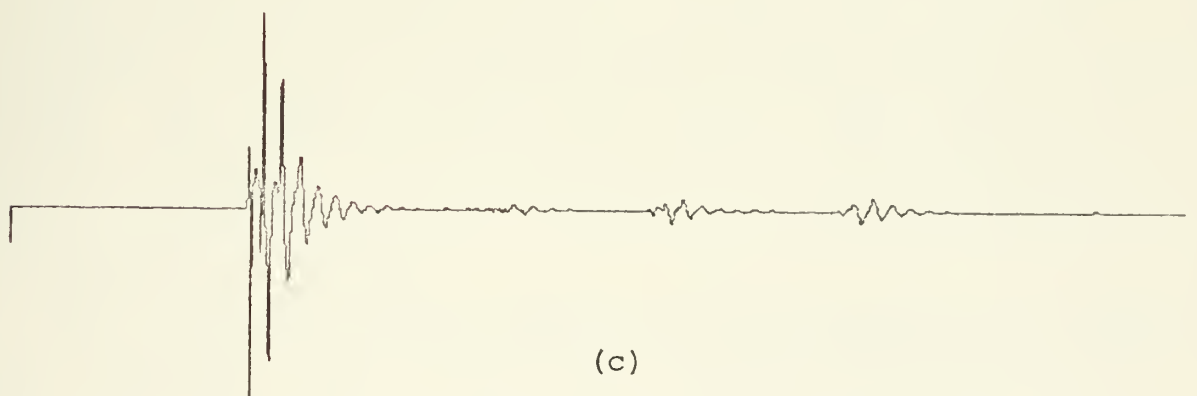
Multiple-to-signal ratio (defined here as the ratio of energy in the first multiple to that in the largest sub-bottom reflector, abbreviated MSR) was found to be of little importance in most cases of interest. For signals in which multiples are large enough to be a problem (comparable to, or larger than smaller reflectors), the multiple dominate the crosscorrelation function so that an effective filter is generated. For these cases the performance was found to be insensitive to the width of the time window used for correlation. In the relatively less interesting case of signals with small multiples, the performance is greatly dependent on the choice of correlation window. If large reflectors are included in the window, performance is adversely affected because of the large reflector contribution to the statistics. For some cases of interest this effect may be a consideration in choosing an appropriate correlation window. Inclusion of large reflectors should be avoided.



(a)



(b)



(c)



Figure 24 Results of processing seismogram of figure 23a with inadequate TDL lengths (a) 3 taps (b) 5 taps (c) 7 taps.

2. Water Travel Time Estimate

It was noted in Chapter II that an estimate of the water column travel time is required for implementation of the TDL algorithm. This is accomplished in practice by various methods including visual estimation, energy detection and correlation techniques. The estimate appears in the filter design equations as the minimum shift of the crosscorrelation function, R_{mr} . This estimate may also be identified as the prediction distance when the operator is interpreted as a prediction error filter.

The actual estimation of water column travel time was not investigated in this analysis. The effects of travel time estimation on filter performance were, however, considered.

Figure 25 shows the results of water travel time estimation errors for the ideal case of a signal with impulsive multiples. The unprocessed seismogram, shown in figure 26a, contains reflectors at 2.7 and 3.5 seconds and a strong multiple at 2.0 seconds. The actual two-way travel time in this case is 1.0 second. The strong similarity between the bottom reflection and multiple is apparent.

First multiple energy removed is very sensitive to travel time estimation, with an error of ± 10 msec resulting in a performance degradation of about 20%. This effect is analogous to that observed in matched filter receivers in that the coherent signal components exhibit very high correlation for a small range of lags. In this case the strong coherence and

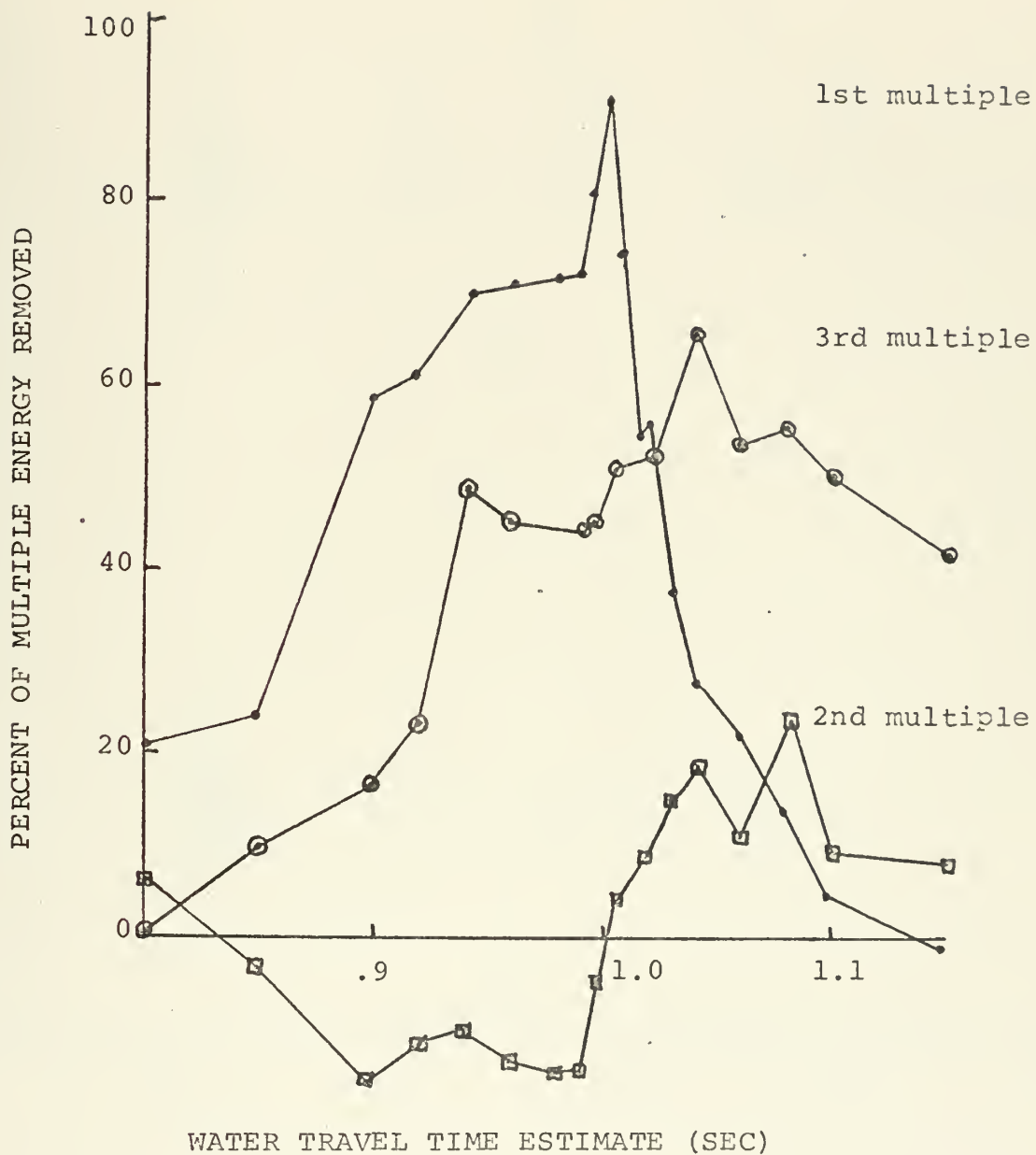


Figure 25 Effects of water column travel time estimate on multiple removed for a signal with coherent multiples.

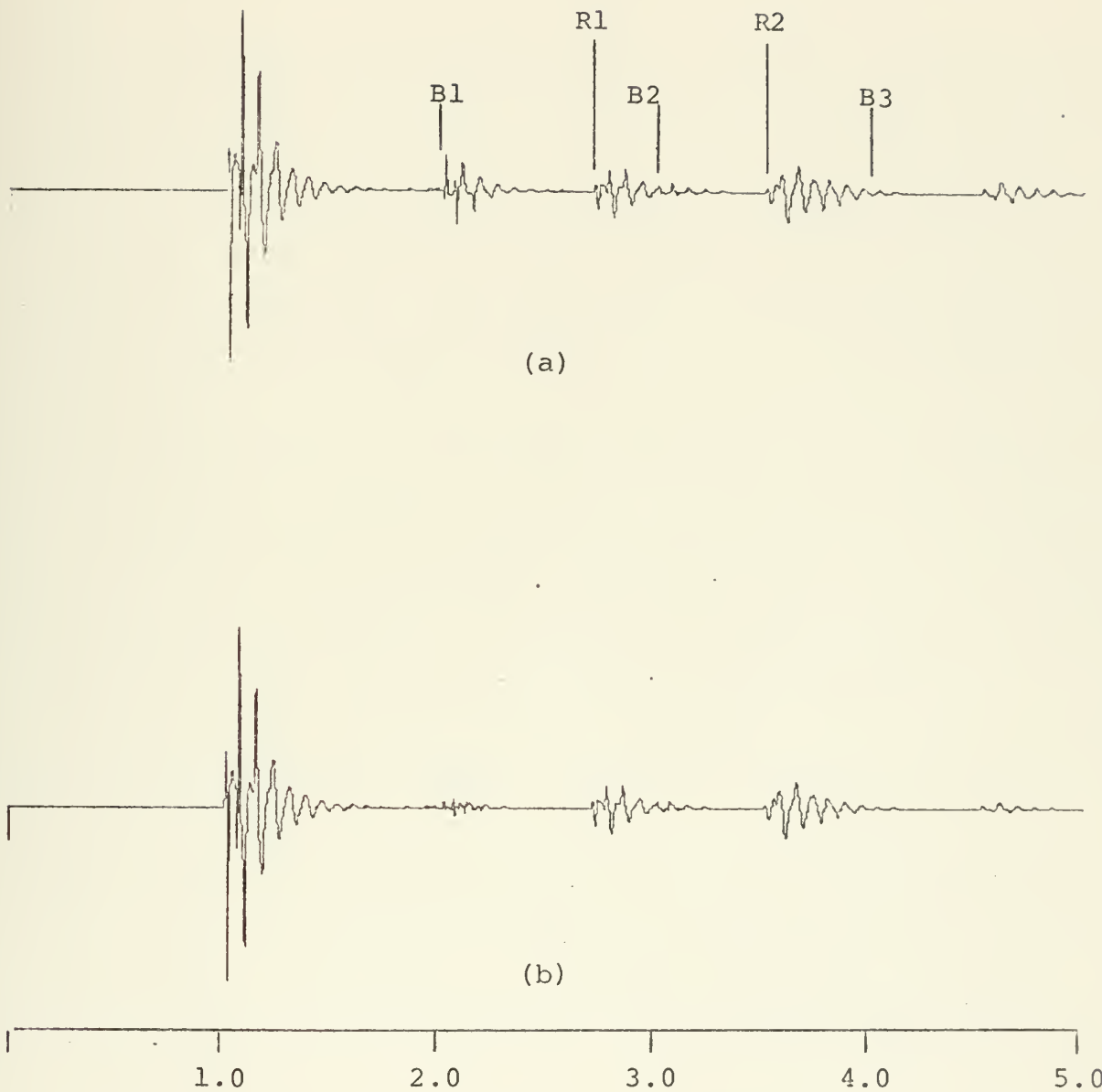


Figure 26 (a) Unprocessed seismogram with impulsive multiples.
(b) TDL result based on correct water travel time estimation.

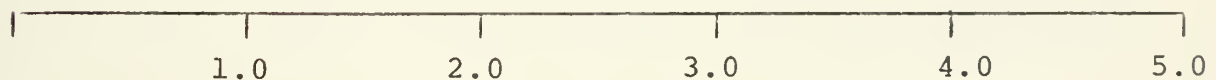
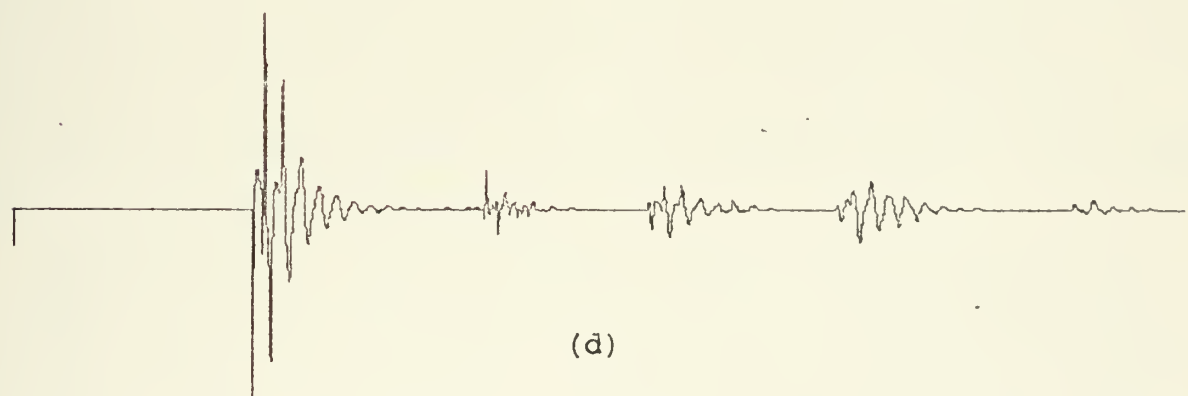
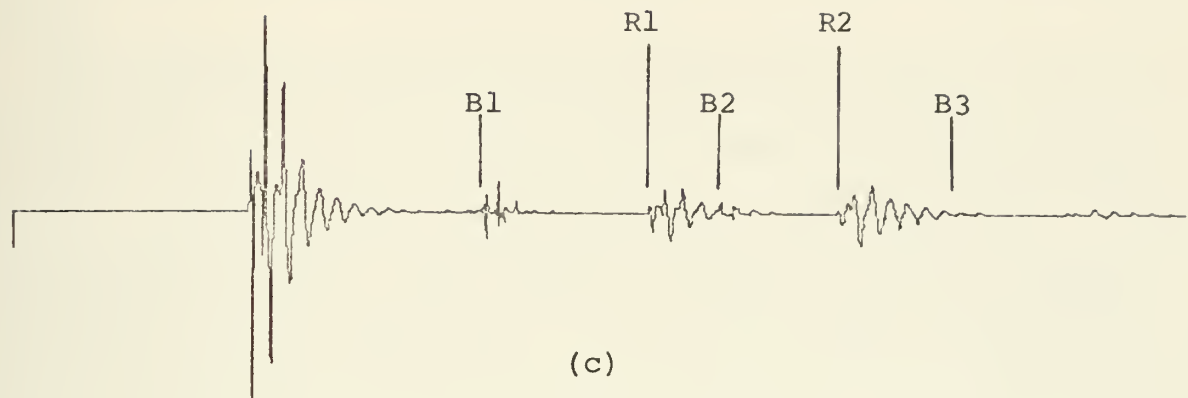


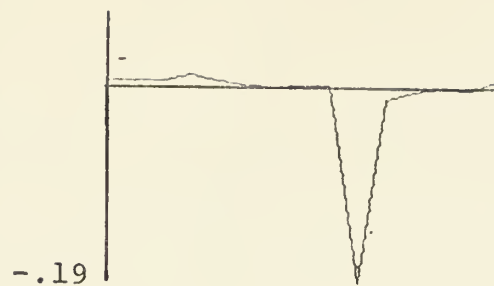
Figure 26 (cont'd) (c) Result of TDL processing based on an early water travel time estimate.
(c) Same processing based on a late estimate.

multiple periodicity yield the sharp correlation peak for lags near the water column travel time, which is also the multiple period.

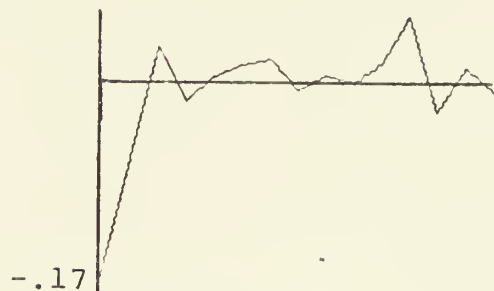
The second and third multiple performance peaks occur at 1.08 and 1.04 seconds respectively, and have values of 24% and 60%. These shifted and reduced peaks are caused by digitization effects. For such an extremely coherent signal, a multiple position deviation of one sample (due to sampling interval round-off) can cause the cancellation operation to be severely affected. In this case the second and third multiple performance maxima are due to secondary crosscorrelation peaks introduced by the periodic oscillations in the source signature. These peaks occur at intervals approximately equal to the period of the basic source (air gun) frequency. The three performance peak values correspond closely to the first three air gun pulse amplitudes.

Figures 26 b, c and d show the results of on-time, early and late travel time estimates respectively. In the first case the multiple has been effectively removed while the early and late estimates lead to multiples which are still significant after processing.

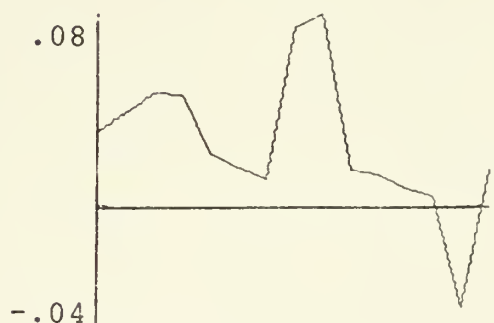
The effects of travel time estimation error on the operator impulse response are seen in figure 27. The optimum estimate yields an operator with a large peak at the origin, nearly equal to the bottom reflection coefficient (.2), and a



(a)



(b)



(c)

Figure 27 TDL filter impulse responses based on travel time estimates which are (a) 40 msec early, (b) correct, and (c) 20 msec late.

smaller peak at the source pulse oscillation interval. The initial spike is due to the largest peak in the crosscorrelation function (approximated here by the correlation function) which occurs at a shift equal to the two-way travel time. The smaller peak in the filter is introduced by an additional shift of one source period. The early (by 40 msec) estimate still allows observation of the crosscorrelation maximum and yields the shifted spike of figure 27a. It is evident in figure 25 that performance is reasonably good for estimation errors less than about .07 seconds, which is the length of the tapped delay line. For greater travel time errors the range of correlation lags computed does not include the peak; hence, the filter is ineffective. Late travel time always results in poor performance since the peak is not observed. Figure 27c shows a typical impulse response due to late travel time estimation.

The seismogram of figure 28a contains a small reflector at 2.2 seconds and a larger one at 3.0 seconds. The first multiple partially overlaps the smaller reflector and the second multiple coincides with the larger. Figures 28 b, c and d demonstrate how travel time estimation errors can lead to ambiguous results. Figure 28b was processed using the correct travel time, resulting in good resolution of both reflectors. The early and late estimates lead to the signals of figures 28c and d in which the smaller reflector cannot be clearly resolved.

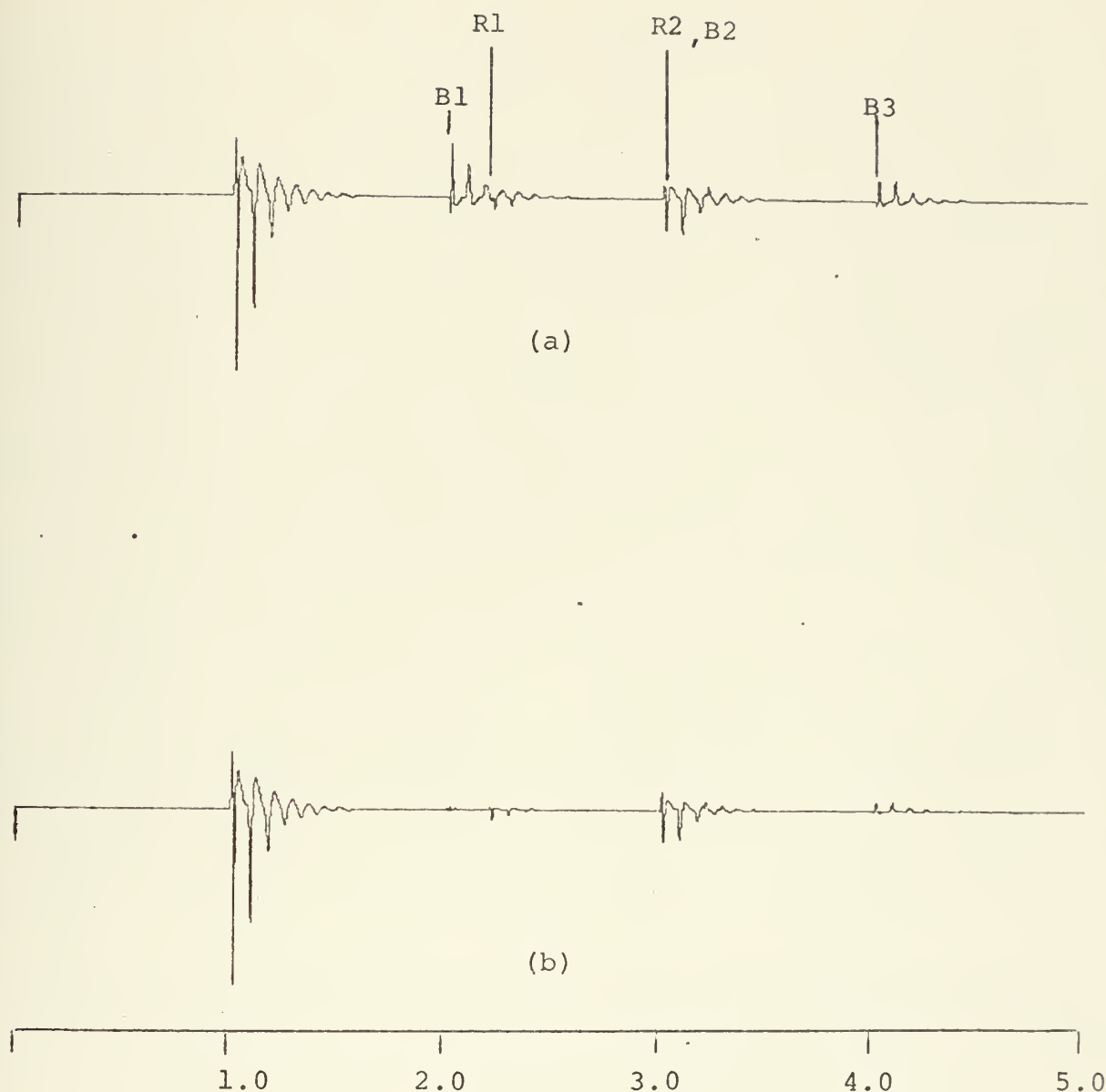
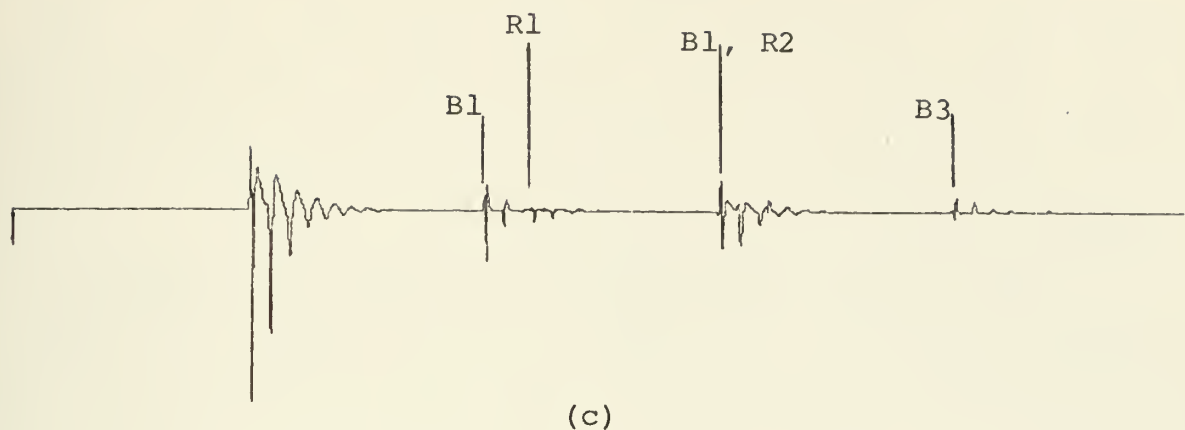
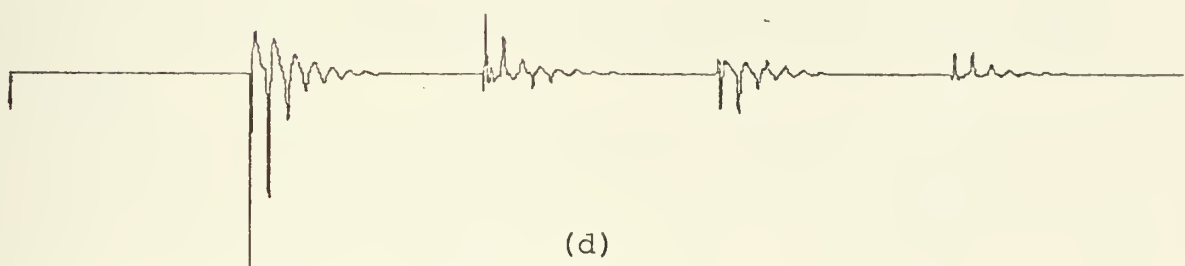


Figure 28 (a) Seismogram with overlapping reflectors and multiples.
(b) Result of TDL processing based on a correct travel time estimate.



(c)



1.0 2.0 3.0 4.0 5.0

Figure 28 (cont'd) (c) Result of TDL processing based on a 40 msec early travel time estimate.
(d) Same processing based on a 20 msec late estimate.

Less coherent seismograms exhibit less sensitivity to travel time estimation as shown in figure 29. Curves (1), (2) and (3) were generated using the seismograms of figure 19 a, b and c respectively, which contain increasing distortion in their multiples. The MSR is considerably lower than in figure 25 so that the later multiples are not clearly visible. The crosscorrelation peaks are considerably broader than in the impulsive multiple signals. Curve (3), the least coherent signal, exhibits the lowest sensitivity to travel time estimates. Increasingly sharper peaks are evident for curves (2) and (1). The performance degradation due to over-estimation is precipitous in all cases although the rate of fall-off is related to signal coherence.

Reflector distortion (not shown) was negligible in all cases for the first reflector and nearly constant at 7% for the second.

Examples of processed signals for curves (2) and (3) are shown in figures 30 and 31.

3. Multiple Periodicity

The effects of aperiodic multiples on TDL dereverberation performance were not investigated in this analysis since the algorithm is designed primarily for deep water use, where only one multiple is significant in most applications. Successful employment of this technique in shallow water is limited since

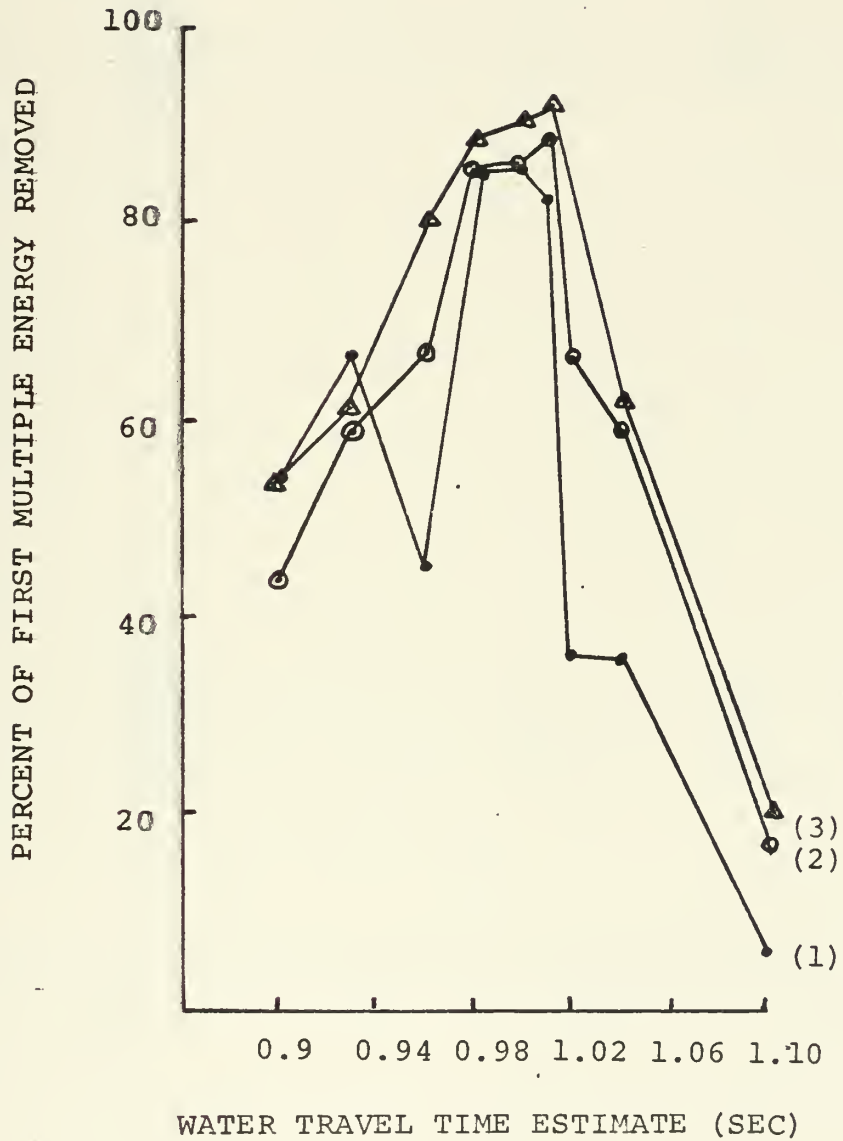


Figure 29 Effects of water column travel time on three signals with varying degrees of multiple distortion.

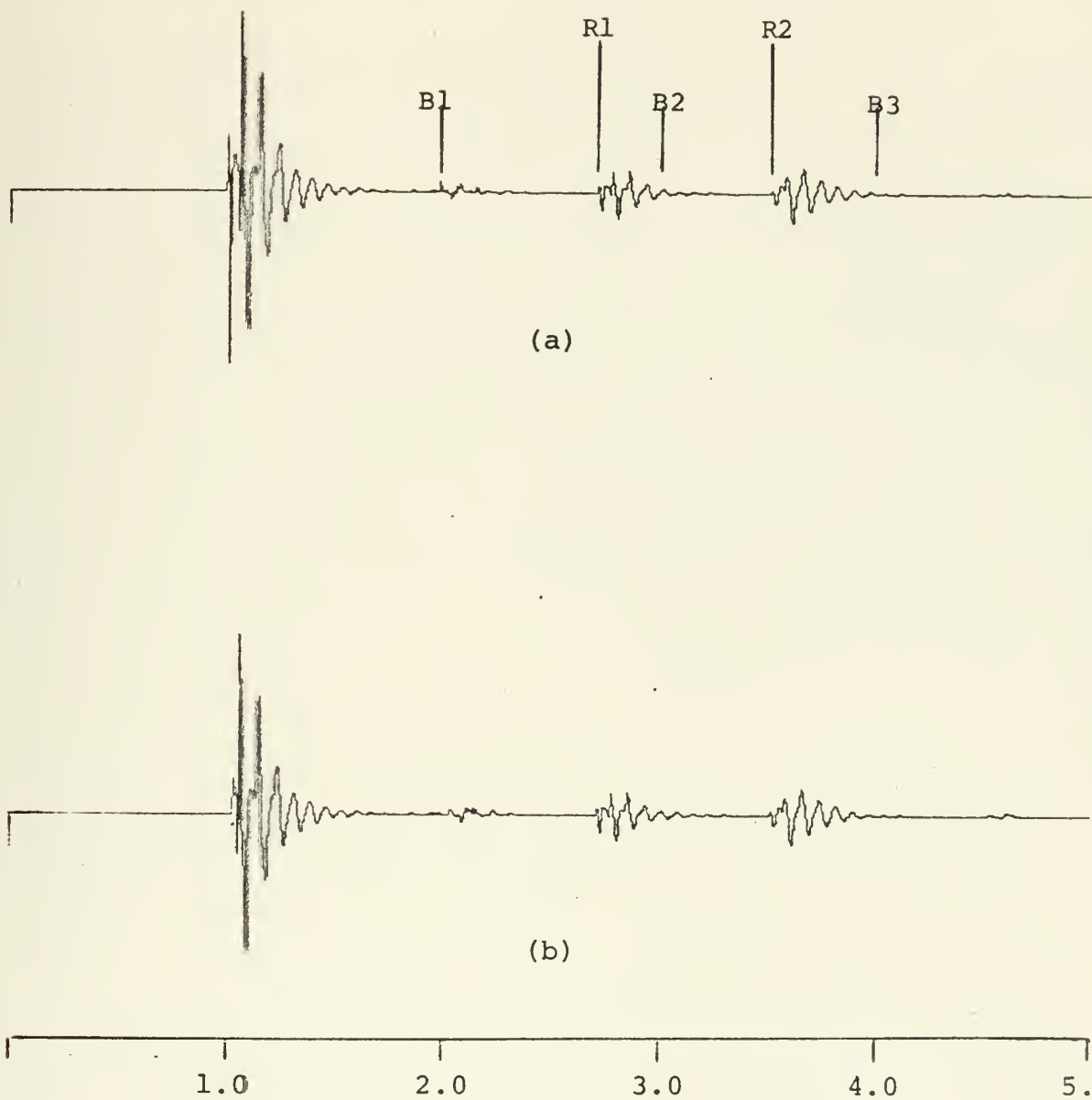


Figure 30 Processed seismograms associated with figure 19b and curve (2) of figure 29. (a) Travel time estimate 40 msec early (b) 40 msec late.

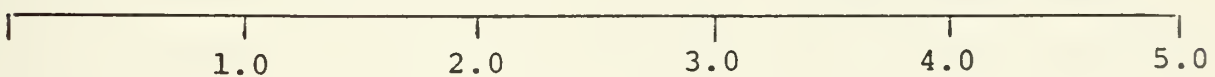
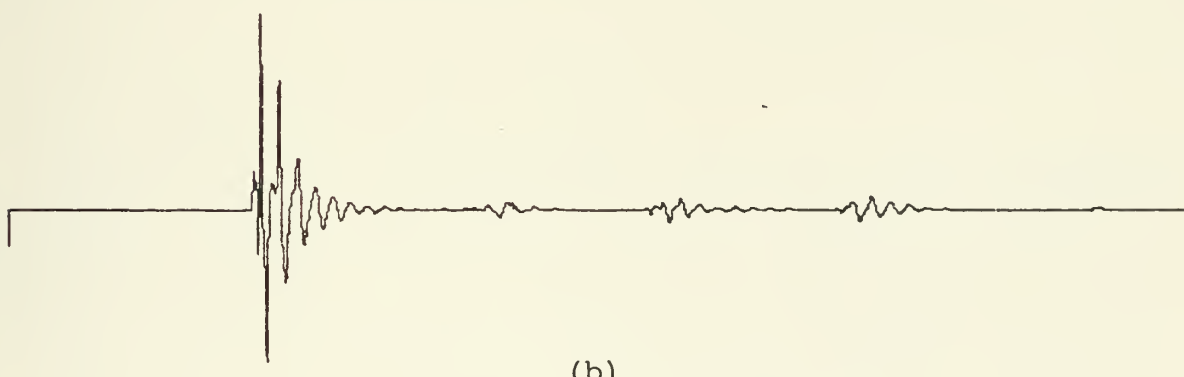
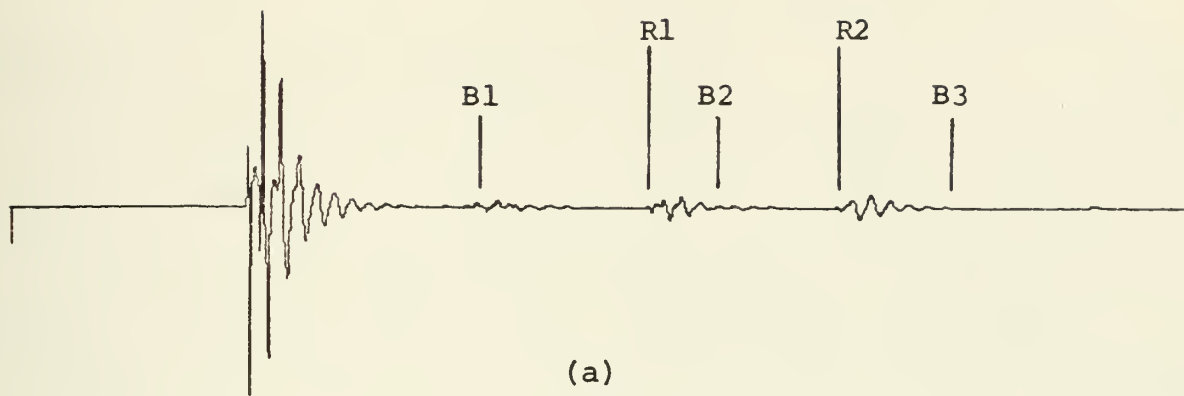


Figure 31 Processed seismograms associated with figure 19c and curve (3) of figure 29. (a) Travel time estimate 40 msec early (b) 40 msec late.

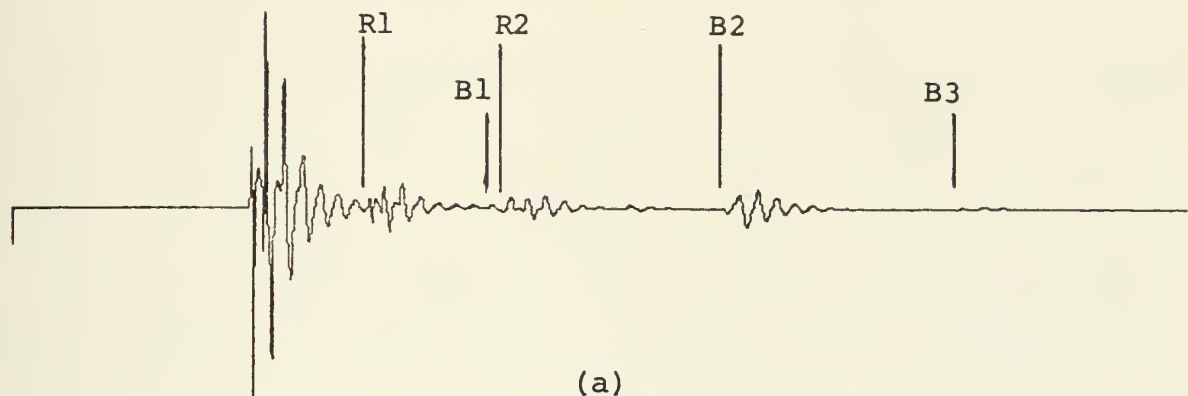
the approximation of the crosscorrelation, R_{mr} , by the correlation, R_{rr} , near the multiple onset is not generally valid. Reflector energy in the multiple regions is usually significant in shallow water seismograms.

It is apparent from the TDL formulation and the discussions of the preceding two sections that the TDL algorithm has some capability to compensate for aperiodicity in which the deviation is of the order of the tapped delay line length. For greater aperiodicities the TDL filter will not be effective on later multiples. Figure 25 indicates that even slight deviations can be very detrimental in later multiple removal. Dynamic corrections can be applied as suggested by Backus [1], however, these are beyond the scope of this study.

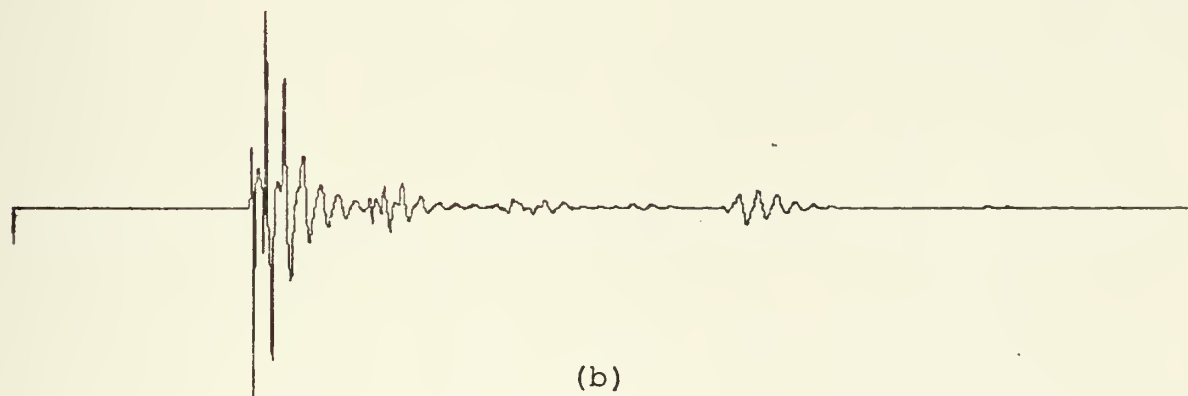
4. Reflector/Multiple Overlap

Figures 32-36 show seismograms before and after processing for several cases in which multiples and reflectors overlap. A brief description of each situation is given here.

The seismogram of figure 32a has reflectors at 1.5, 2.1 and 3.0 seconds, and distorted multiples. Significant energy near 2.0 seconds is removed by processing but a clearly visible response is still present. Other regions of the signal are not visibly affected. The visual resolution is not significantly improved in this case, however, stacking of successive shots after multiple removal could be employed to enhance the reflector



(a)



(b)

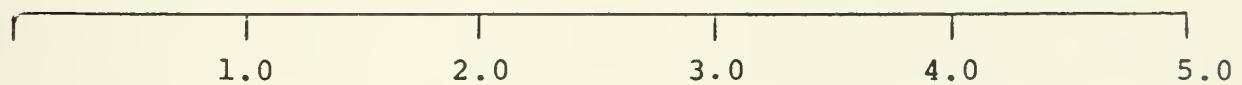
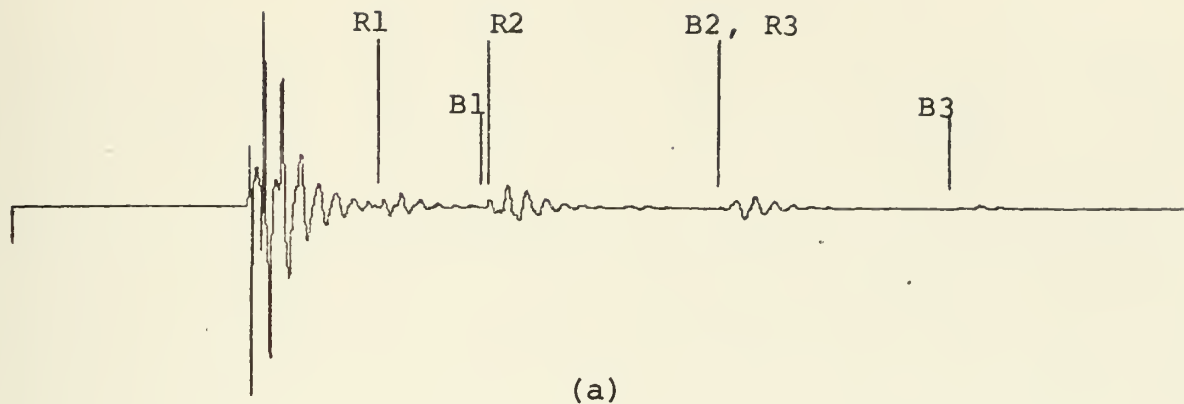


Figure 32 Seismogram with reflectors at 1.5, 2.1 and 3.0 seconds (a) before and (b) after TDL processing.

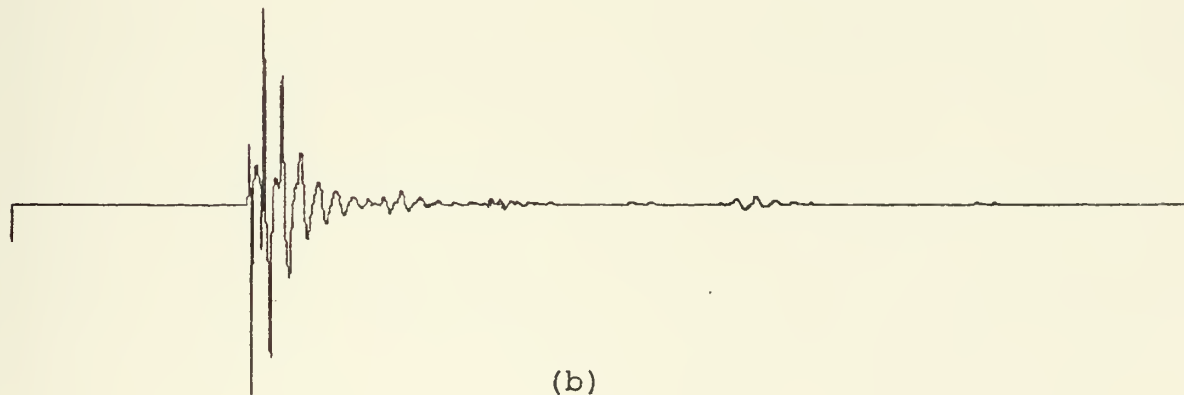
in this situation. The success of stacking would require that the reflector be more coherent than the residual multiple after dereverberation.

In figure 33 reflectors occur at 1.5, 2.02 and 3.0 seconds. Reflectors may be expected to have a strong influence on the crosscorrelation function in this situation of extreme overlap. The result is nearly complete removal of the second reflector with the multiple. The last reflector is clearly visible at 3.0 seconds. In this example the tapped delay line length (.054 second) is greater than the reflector/multiple separation (.02 second). The bottom impulse response is significant for .035 second so that it cannot be estimated accurately with an operator which is shorter than the reflector/multiple separation. Even if the bottom response were much shorter, the effect of the large reflector in the crosscorrelation window would lead to degraded performance. This example shows worse degradation than would be expected in practice because the reflectors are very ccherent in this synthetic data. The less coherent reflections in deep water signals would generally be less susceptable to removal. When reflector energy is significant in the crosscorrelation, however, and TDL length is greater than reflector/multiple separation, the filter design algorithm essentially interprets the reflector as part of the multiple and tries to remove it.

Figure 34 contains reflectors at 1.6, 1.95 and 3.0 seconds.



(a)



(b)

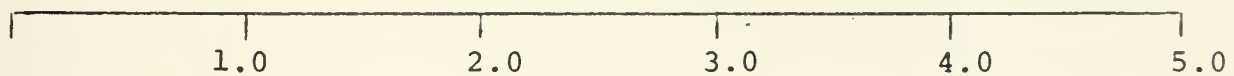


Figure 33 Seismogram with reflectors at 1.5, 2.02 and 3.0 seconds (a) before and (b) after TDL processing.

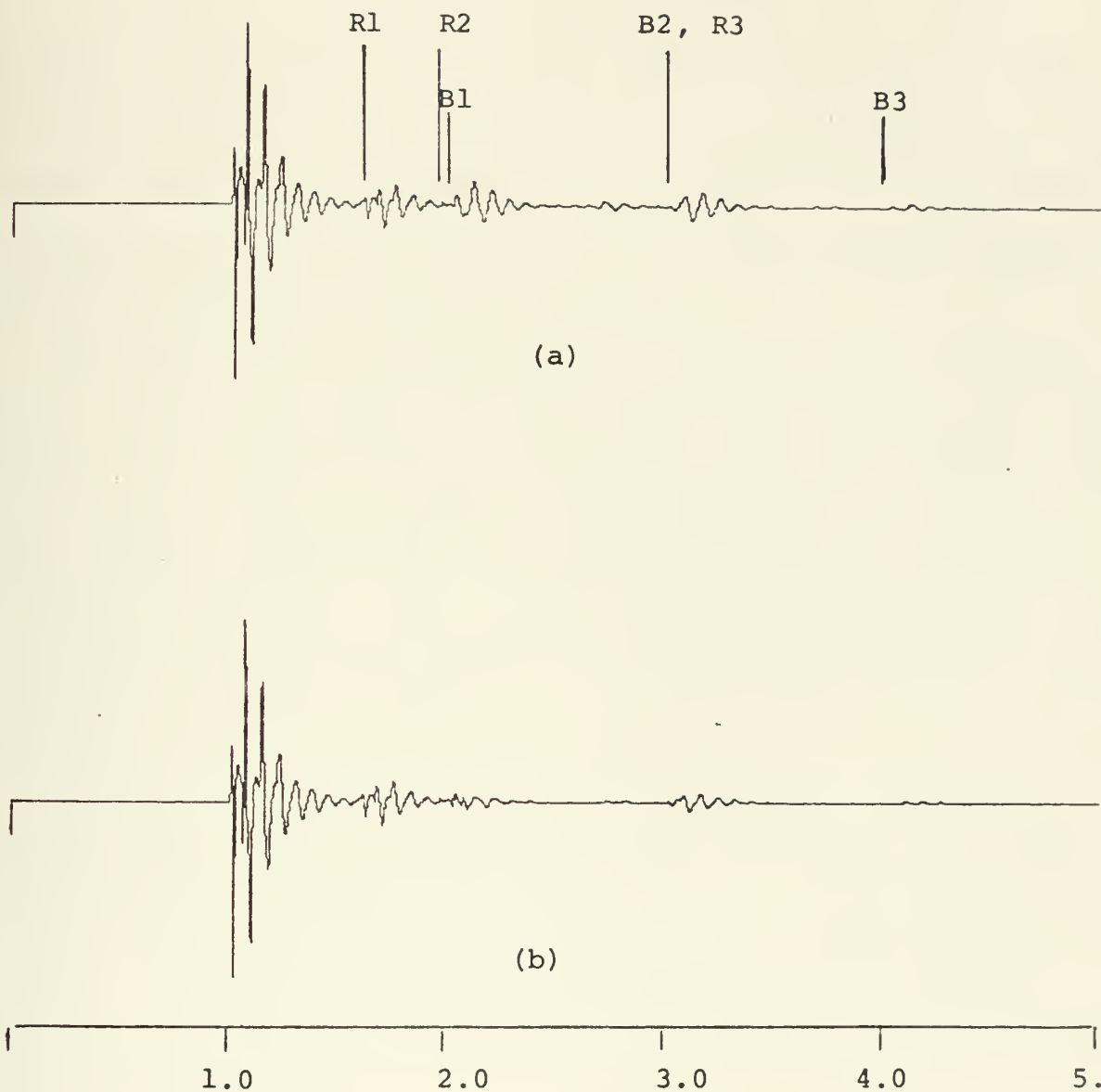


Figure 34 Seismogram with reflectors at 1.6, 1.95 and 3.0 seconds (a) before and (b) after TDL processing.

These locations are slightly different from those of figure 33. Significant energy is present at the second reflector location after processing. Since the reflector precedes the first multiple in this case it has a less significant effect on the crosscorrelation function than the 2.02 second reflector in the previous example. The variability of performance on individual seismograms (of similar structure) with overlap again suggests the use of stacking to enhance reflectors.

The reflectors of figure 35 are situated as in figure 34; however, the first reflector and multiple are significantly larger in this case. This seismogram is more typical of a shallow water return. The processing is quite effective on the first and second multiples. The aperiodicity of reverberation in most shallow water seismograms would lead to much poorer performance on later multiples, in practice.

Figure 36 illustrates a situation where the overlap is not severe but visual resolution is impaired by the first and second multiples. Reflectors occur at 1.55, 2.4 and 3.25 seconds. Processing results in effective reduction of both multiples and significantly improved resolution in the second and third reflectors.

We conclude from these examples of reflector/multiple overlap that visual improvement due to dereverberation varies widely, depending upon several aspects of the individual signal structure. The bottom impulse response, the extent of reflector/

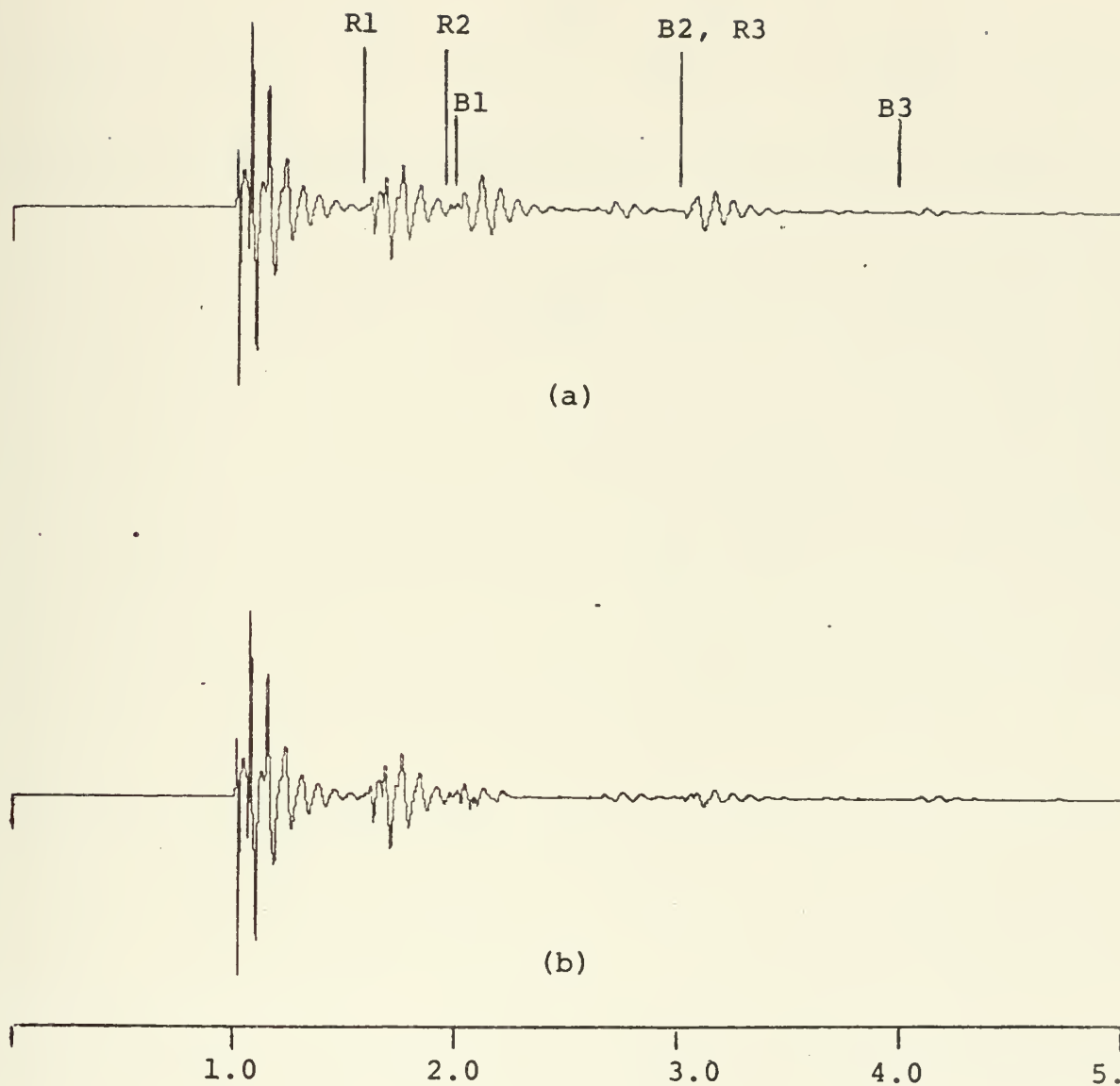


Figure 35 Seismogram with reflectors at 1.6, 1.95 and 3.0 seconds (a) before and (b) after TDL processing.

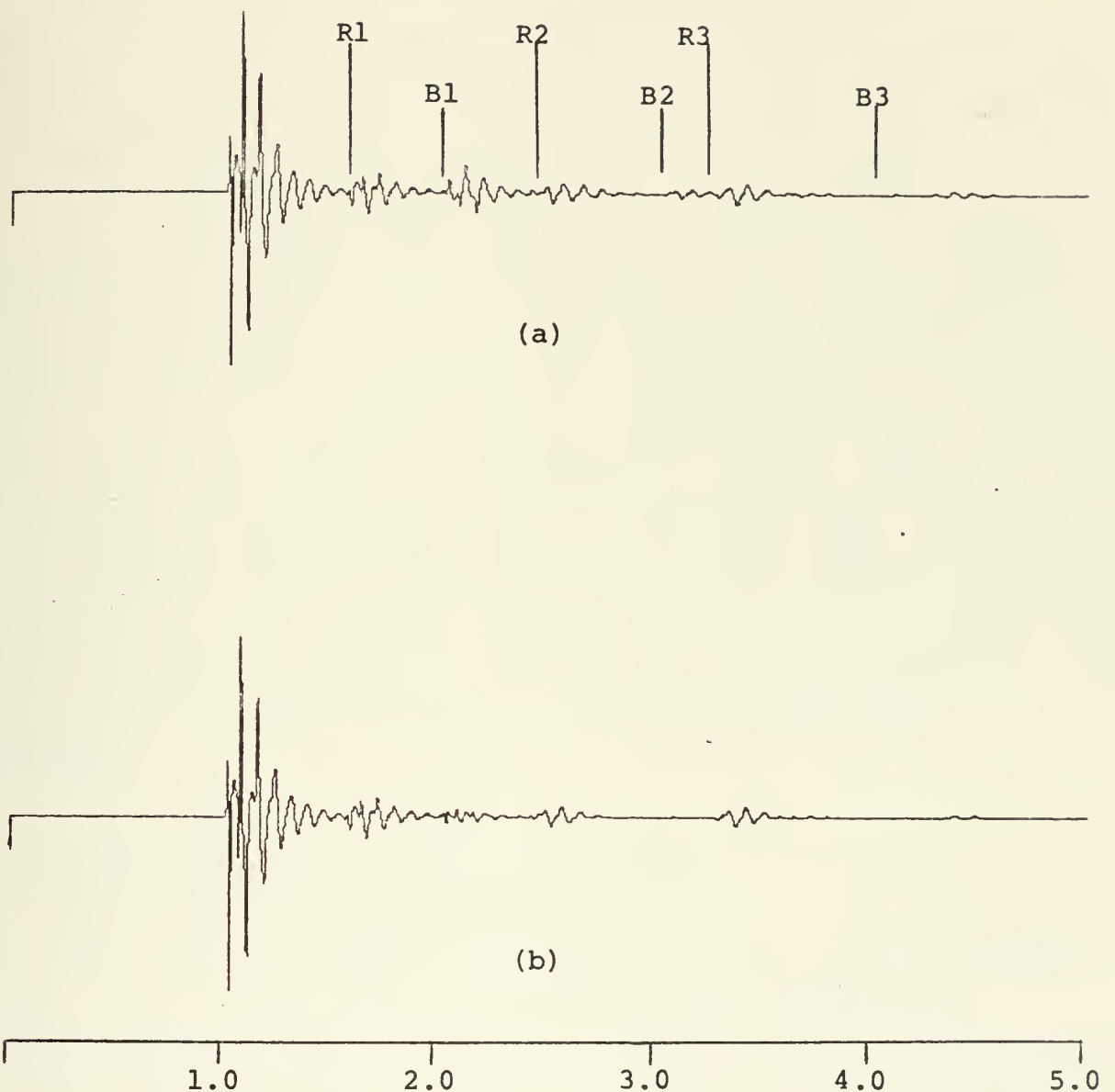


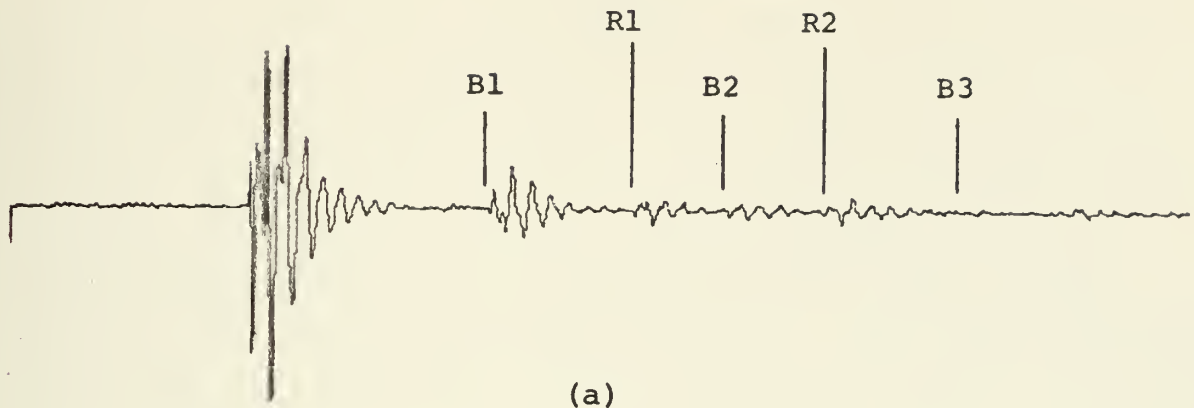
Figure 36 Seismogram with reflectors at 1.55, 2.4 and 3.25 seconds (a) before and (b) after TDL processing.

multiple separation, the relative coherence of reflector and multiples, and the relative sizes of signal components all appear to affect performance. Each of these factors influences the effectiveness of the crosscorrelation operation in identifying energy which is specifically due to the multiples.

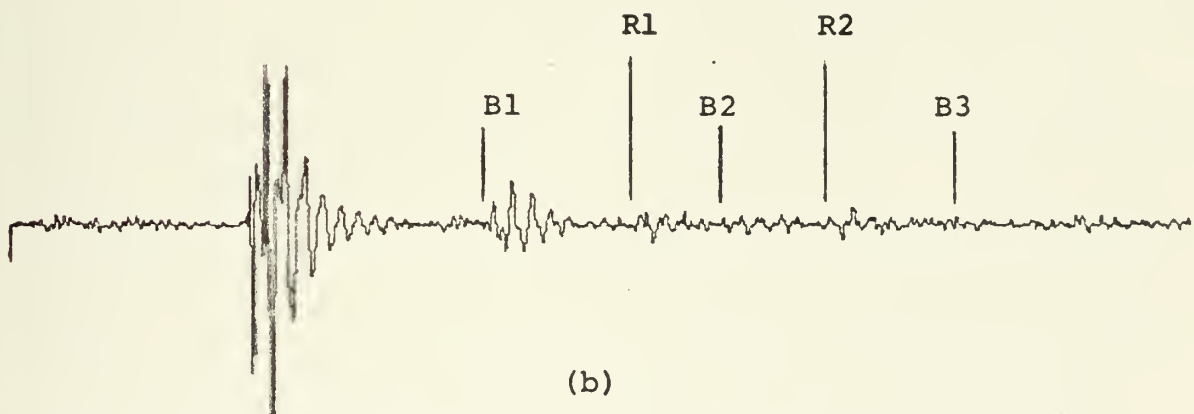
The visual improvement due to dereverberation can best be determined by analysis of continuous seismic profiles (presentations showing many seismograms side-by-side) since coherent residual energy, if present, becomes apparent as visual trends in the data. The effects of stacking can also be observed in this format. It was not practical to generate such a profile with synthetic data but the single-shot results indicate that TDL dereverberation is potentially useful for enhancing the visibility of reflectors which are partially masked by multiples.

5. Additive White Noise and Filtering

White Gaussian noise was generated in the following manner. First, a set of uniformly distributed random numbers was obtained using a standard digital routine. A set of approximately Gaussian numbers was then formed by summing separate groups of twelve of the uniformly distributed numbers. The resulting set was weighted to obtain the desired standard deviation. Figure 37 shows a seismogram with two different levels of added noise, each lowpass filtered at 50 Hz.



(a)



(b)



Figure 37 Seismograms with added white noise, lowpass at 50 Hz.
(a) $\sigma_n = 50$ (b) $\sigma_n = 100$.

Figure 38 illustrates the performance of the TDL filter for various noise levels on a seismogram having disjoint reflectors and multiples. The maximum noise standard deviation shown corresponds to a SNR of 0.7 dB. No bandpass filtering was done prior to dereverberation. The results presented here are typical of the cases tested. Multiple energy removed decreases monotonically with increasing noise level; almost linearly in the case of the first multiple. The later multiples are more severely affected. As the noise level becomes comparable to their amplitudes, the filter becomes ineffective in removing them. This behavior is due to the effect of increasing incoherent energy in the signal. The correlation-cancellation operation is designed to detect coherent, periodic components. These become increasingly masked as more noise is added. For this reason seismograms with larger multiples exhibit less sensitivity to noise. Seismograms of similar structure (i.e., exactly the same reflector and multiple locations) whose multiple energies differed by a factor of twenty were found to exhibit considerable dereverberation performance differences in high noise. Processing of the signal with the larger multiples resulted in 25% greater removal of first multiple energy.

Lowpass filtering before dereverberation can lead to a significant improvement in TDL filter performance in some signals. The plotted results of lowpass filtering two noisy signals at various frequencies are shown in figure 39.

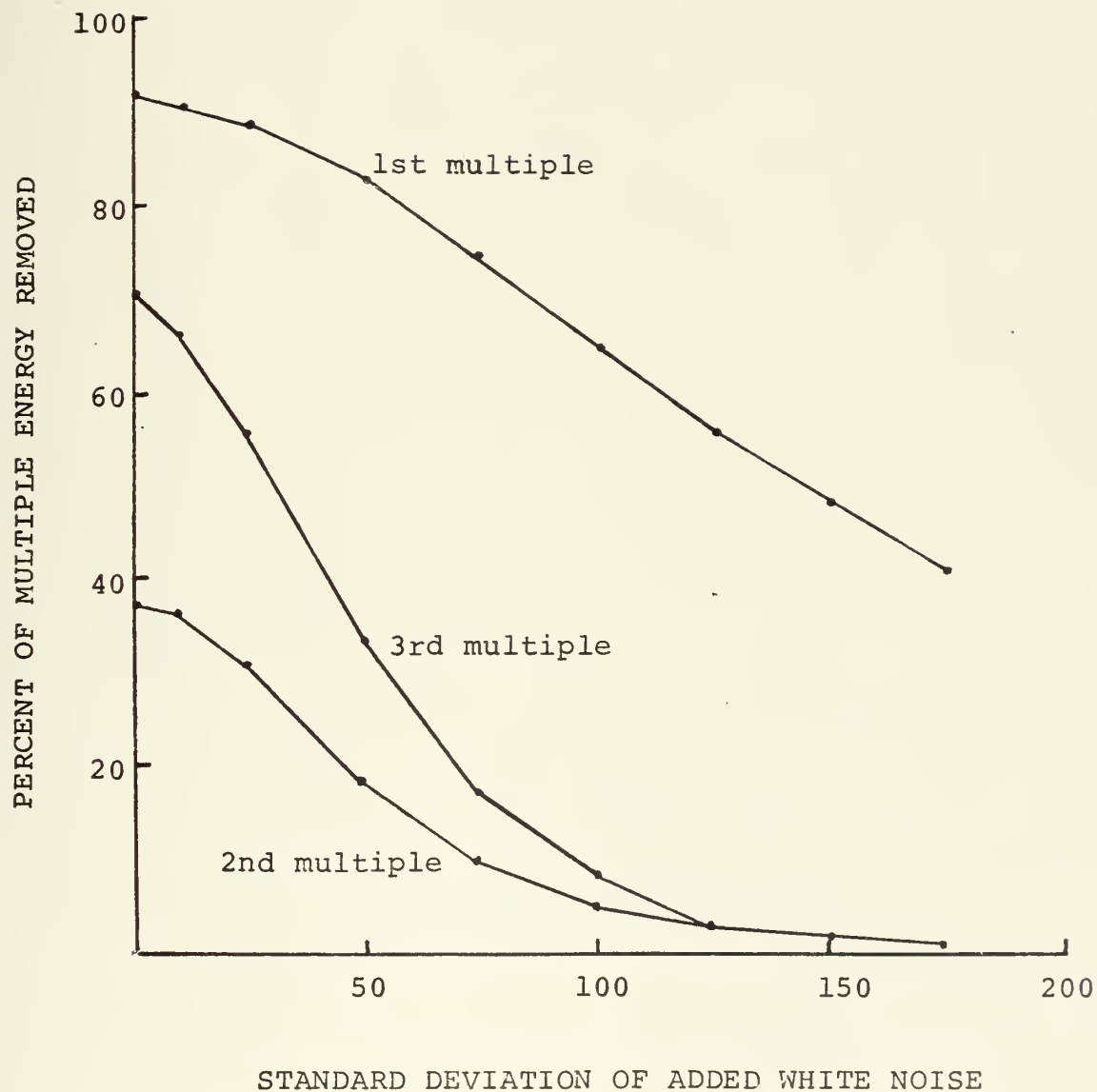


Figure 38 Effects of noise level on TDL performance for a signal with coherent periodic multiples.

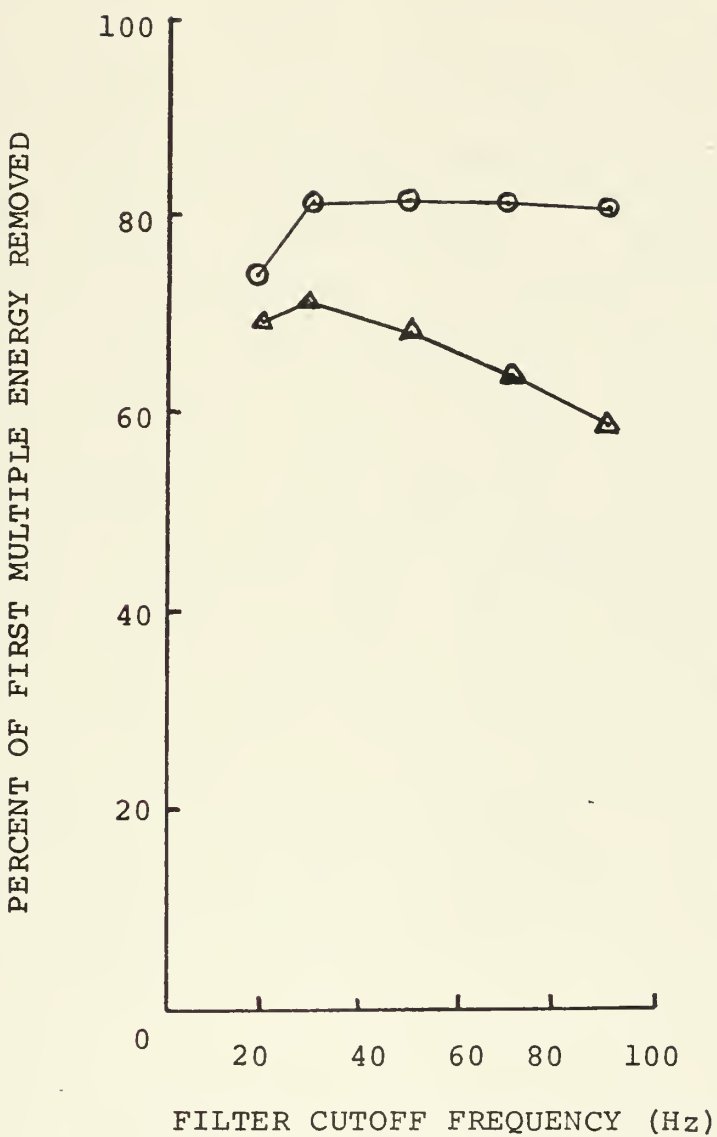


Figure 39 TDL performance vs. lowpass filter cutoff frequency for signals with coherent (lower curve) and distorted (upper curve) multiples.

(A third order Butterworth filter was used throughout. The visual difference in two filtered signals is shown in figure 40. The first is lowpass filtered at 90 Hz and the second at 30 Hz.) The seismogram used to generate the upper curve contains multiples which are considerably distorted while the lower curve is due to a more coherent signal. Decreasing the pass-band from 90 to 30 Hz produces a 12% improvement in performance in the second case but the less coherent signal is relatively insensitive to filtering. Several other signals evaluated were found to exhibit the same behavior. The phenomenon is apparently due to the averaging, or smoothing effect of the operator in the distortion case. Recall that signals of this kind tend to have more extended waveforms in their TDL operators (See figure 20). Convolution of such functions with a noisy signal "smoothes out" the noise because of the significant operator length and the random fluctuation of the noise. This has the twofold result of better overall performance in noise and less sensitivity to removal of higher frequency noise energy.

Performance degenerates for filter cutoff frequencies below 30 Hz because the spectral energy of the signal itself is concentrated in this range. Figure 41 shows the distribution of energy in the frequency domain for the seismogram associated with the upper curve of figure 39. Most of the energy is concentrated between 5 and 30 Hz.

Figures 42-45 illustrate the visual improvement of noisy,

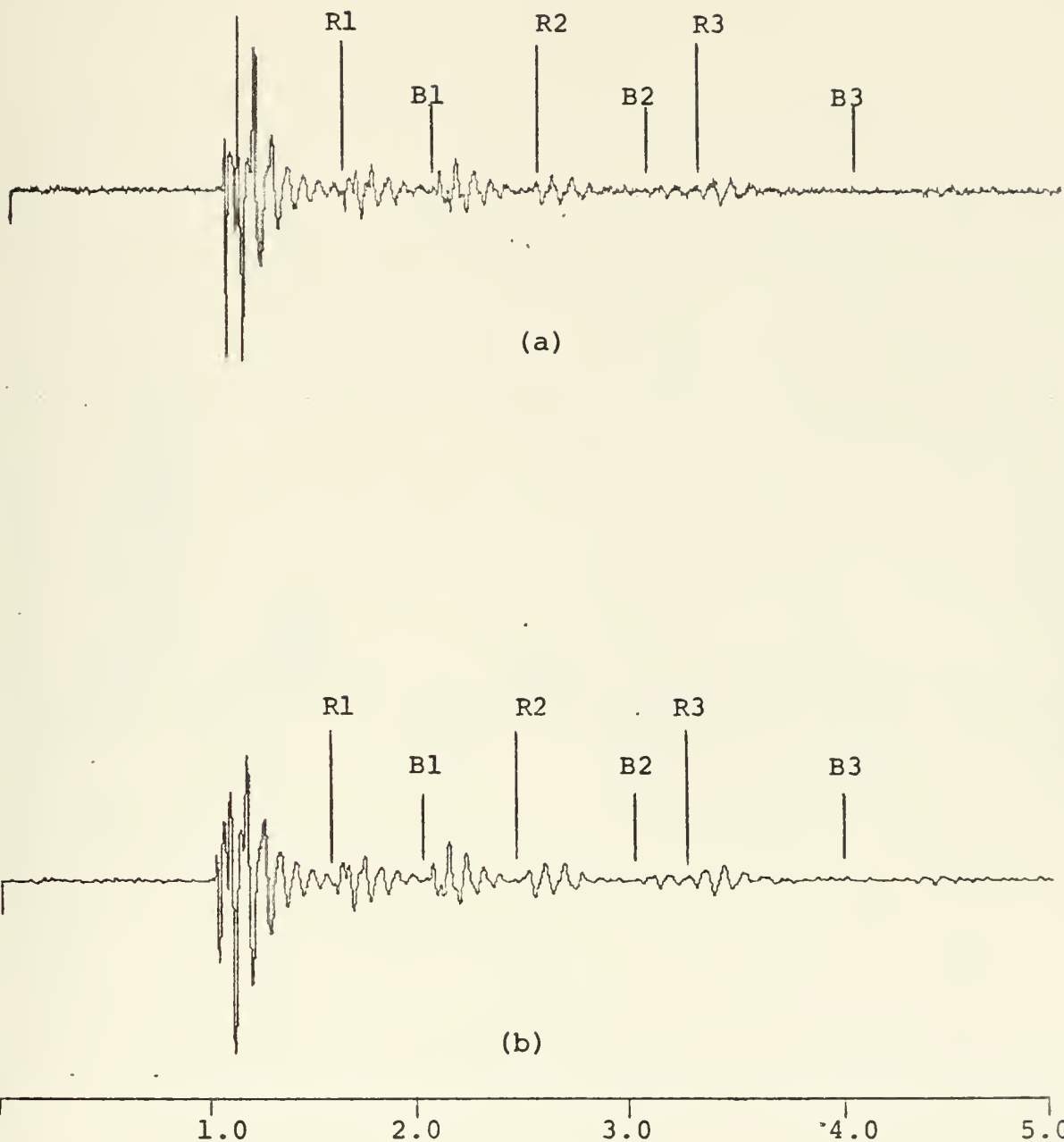


Figure 40 Seismograms with equal white noise levels, lowpass filtered at (a) 90 Hz and (b) 30 Hz.



Figure 41 Squared magnitude of the Fourier transform for the signal associated with the upper curve in figure 39.

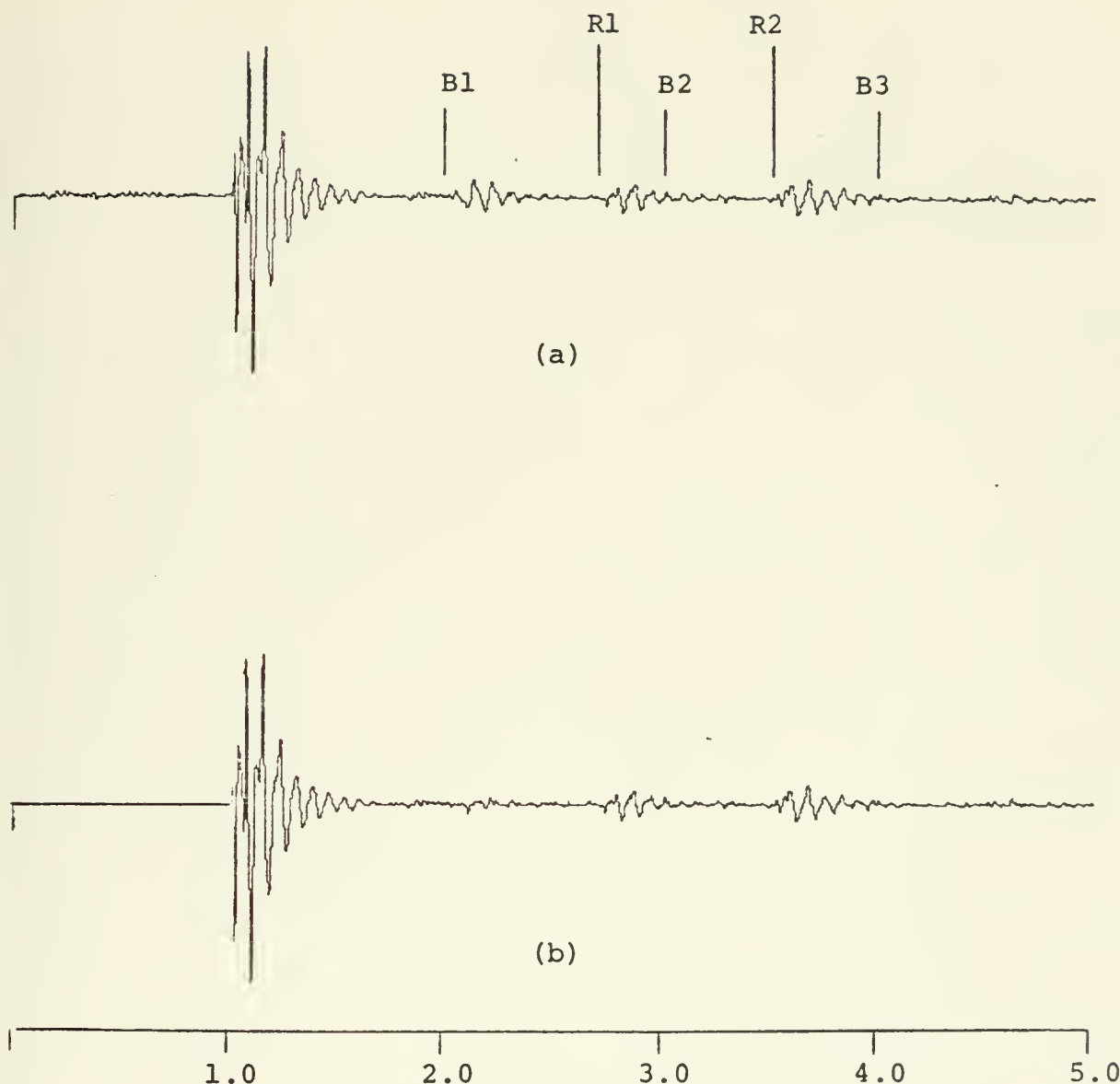
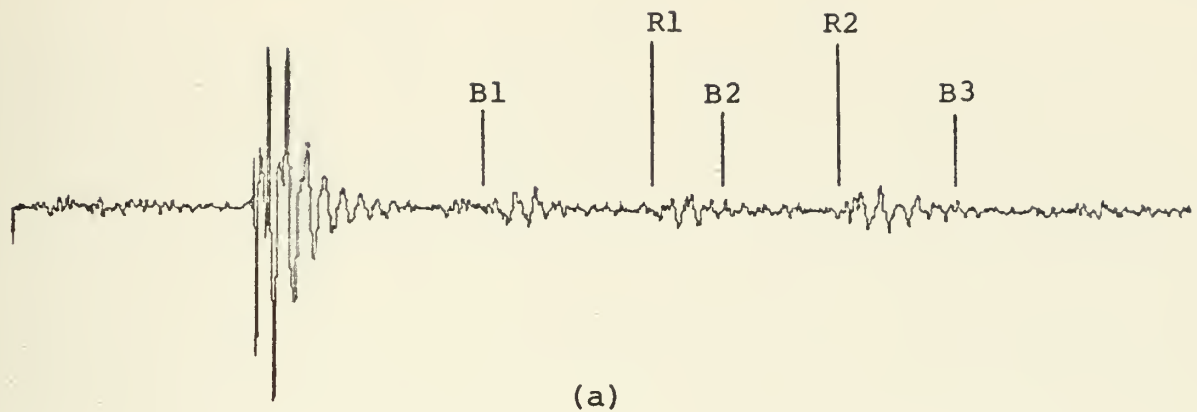
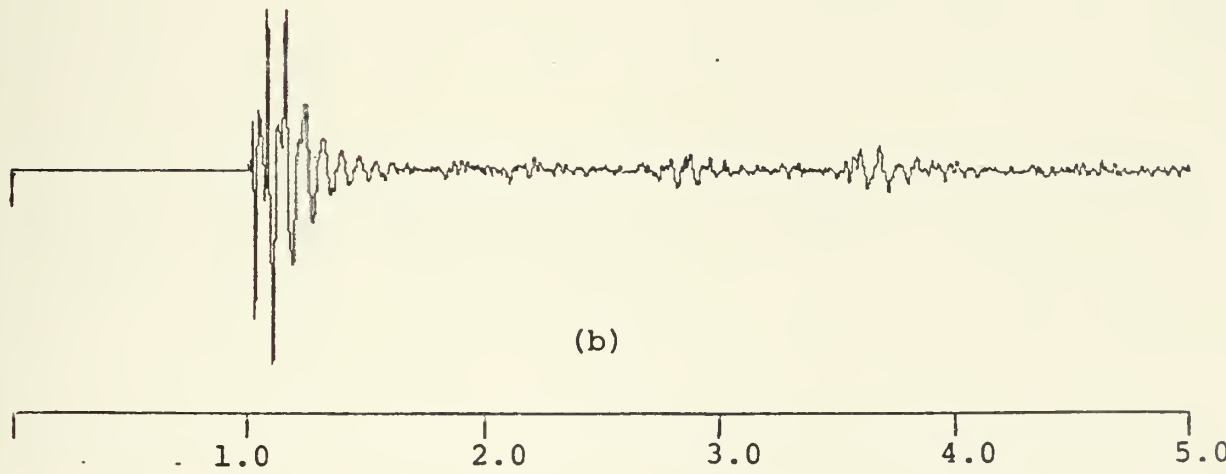


Figure 42 (a) Unprocessed seismogram with added noise, $F_c = 50$ Hz.
(b) Result of TDL processing.



(a)



(b)

1.0 2.0 3.0 4.0 5.0

Figure 43 (a) Seismogram of figure 42a with high noise, $F_C = 50$ Hz.
(b) Result of TDL processing.

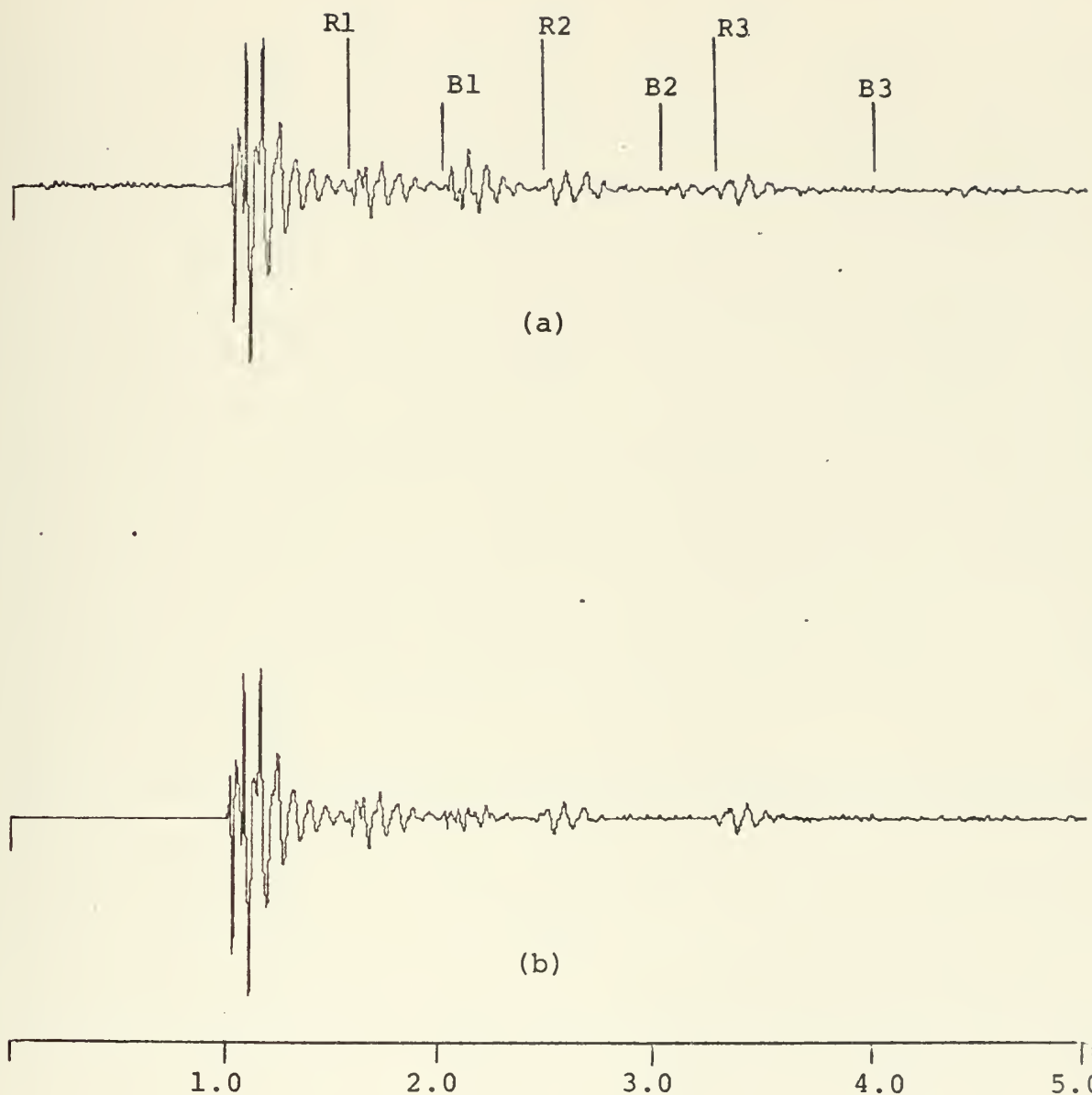
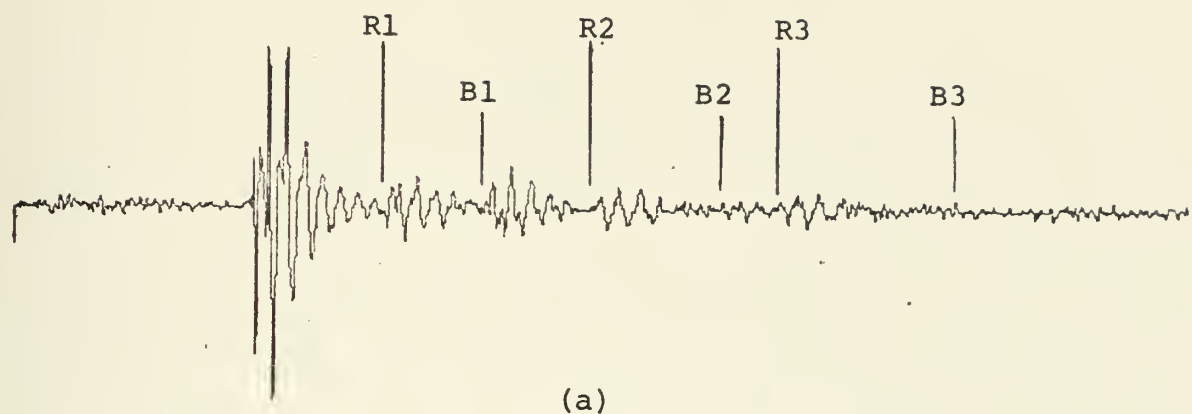
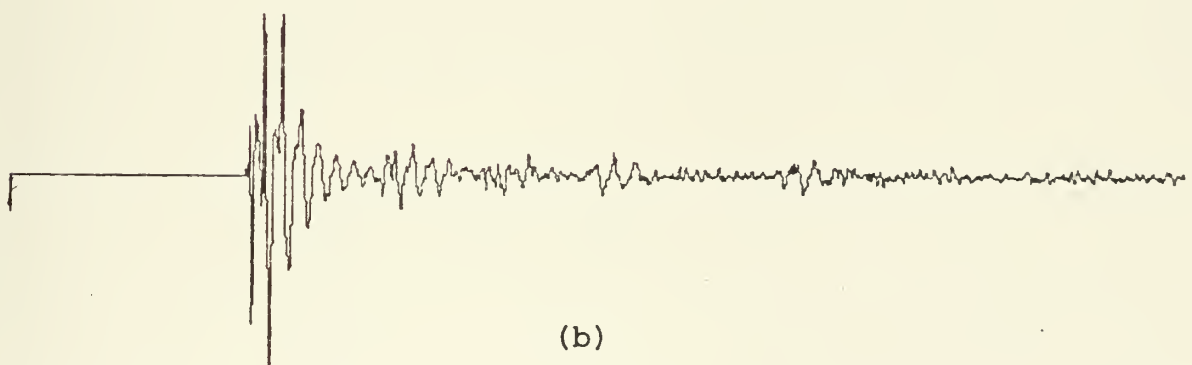


Figure 44 (a) Seismogram with low noise, $F_c = 50$ Hz.
(b) Result of TDL processing.



(a)



(b)

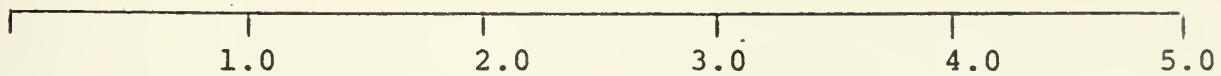


Figure 45 (a) Seismogram of figure 44 with high noise, $F_c = 50$ Hz.
(b) Result of TDL processing.

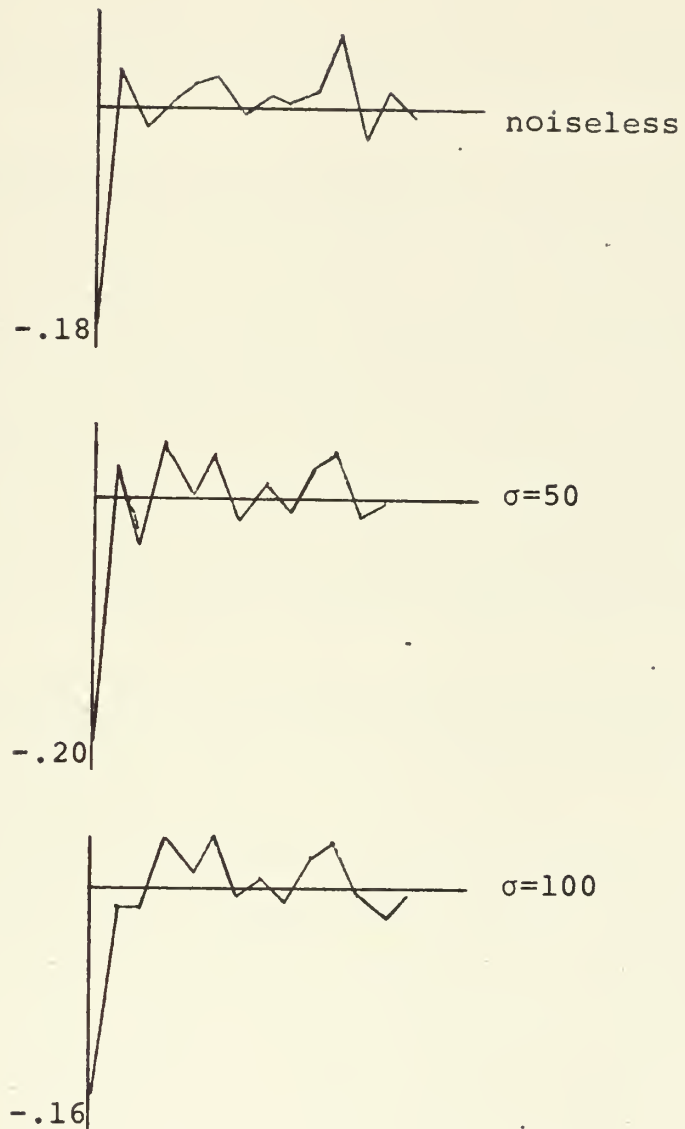


Figure 46 Operator impulse responses for three different noise levels on same signal with coherent multiples.

lowpass filtered (50Hz) signals after processing. Two different seismograms are shown, each at two different noise levels, before and after processing. It can be seen from these figures that no serious reflector distortion occurs due to noise or filtering.

The presence of white noise has a predictable effect on the appearance of the TDL operator. The impulse response itself becomes noisy due to the added incoherent energy and a bias is introduced into the large cancellation peak. An example of this is shown in figure 46 for a signal with coherent multiples. The variation in the first tap gain is significant and the change in appearance of the overall impulse response is apparent.

C. Results of Homomorphic Dereverberation Performance

1. Introduction

The theory of homomorphic dereverberation is based on the properties of periodic minimum phase impulse train cepstra. The incorporation of more realistic effects, such as aperiodicity, distorted multiples, and non-impulsive reflectors, leads to analytical intractability in most cases. Hence, in presenting the experimental results, we view the more complex signal structures in terms of their relation to the ideal signal models of Chapter II. In so doing we hope to provide a basic reference for interpreting observed phenomena, and to provide a stronger intuitive picture of the mechanisms at work in homomorphic dereverberation.

All cepstra used in this analysis are 2048 points in length. Seismograms contain 1024 points except in cases where resampling was required. Zeros have been appended as necessary. The 2048 point length has been used throughout the analysis for uniformity and reduction of aliasing. In most practical seismic processing, shorter cepstrum lengths are adequate.

2. Multiple Periodicity

It was shown in Chapter II that later components of a periodic, minimum phase impulse train can be significantly reduced by removal of the first one or two cepstral contributions. This property is potentially valuable for dereverberation, especially in shallow water cases where several strong multiples may appear in the data. In order for this property to be useful it must be relatively insensitive to (at least) slight aperiodicity since actual reverberation is not exactly periodic. The result of Stoffa, et al. summarized in Chapter II is extended here to rapidly decaying, aperiodic, minimum phase impulse trains.

Consider removing the first j cepstral contributions of $\hat{m}(n)$, the cepstrum of a minimum phase impulse train with contributions $(-R)^i$ at n_i , $i = 1, 2, 3, \dots$, and $|R| < 1$.

We then have

$$\hat{m}_j(n) = \hat{m}(n) - \sum_{\ell=1}^j \frac{(-R)^\ell}{\ell} \delta(n-n_\ell)$$

$$\hat{m}_j(n) = \sum_{\ell=j+1}^{\infty} \frac{(-R)^\ell}{\ell} \delta(n-n_\ell).$$

Transforming,

$$\hat{M}_j(z) = \sum_{\ell=j+1}^{\infty} \frac{(-R)^{\ell}}{\ell} z^{-n_{\ell}}.$$

Exponentiating,

$$M_j(z) = \exp \left[\sum_{\ell=j+1}^{\infty} \frac{(-R)^{\ell}}{\ell} z^{-n_{\ell}} \right]$$

$$M_j(z) = \prod_{\ell=j+1}^{\infty} \exp \left[\frac{(-R)^{\ell}}{\ell} z^{-n_{\ell}} \right]$$

This may be expressed as a power series.

$$M_j(z) = \prod_{\ell=j+1}^{\infty} \sum_{i=0}^{\infty} \frac{(-R)^{\ell i}}{i! \ell^i} z^{-in_{\ell}}$$

$$M_j(z) = \prod_{\ell=j+1}^{\infty} \left[1 + \frac{(-R)^{\ell}}{\ell} z^{-n_{\ell}} + \frac{(-R)^{2\ell}}{2\ell^2} z^{-2n_{\ell}} + \frac{(-R)^{3\ell}}{6\ell^3} z^{-3n_{\ell}} + \dots \right] \quad (10)$$

The rapidly decaying coefficients of $z^{-in_{\ell}}$ combine multiplicatively to yield the time domain impulse coefficients of $m_j(n)$.

If only the first cepstral impulse is removed ($j=1$), the largest value attained by the third coefficient in brackets is

$$\left. \frac{(-R)^{2\ell}}{2\ell^2} \right|_{\ell=2} = \frac{R^4}{8}$$

which is insignificant for reflection coefficients of interest.

All succeeding terms in (10) will be vanishingly small. We

then have the approximate expression

$$M_j(z) = \prod_{\ell=j+1}^{\infty} \left[1 + \frac{(-R)^{\ell}}{\ell} z^{-n_{\ell}} \right].$$

Expanding this product we obtain

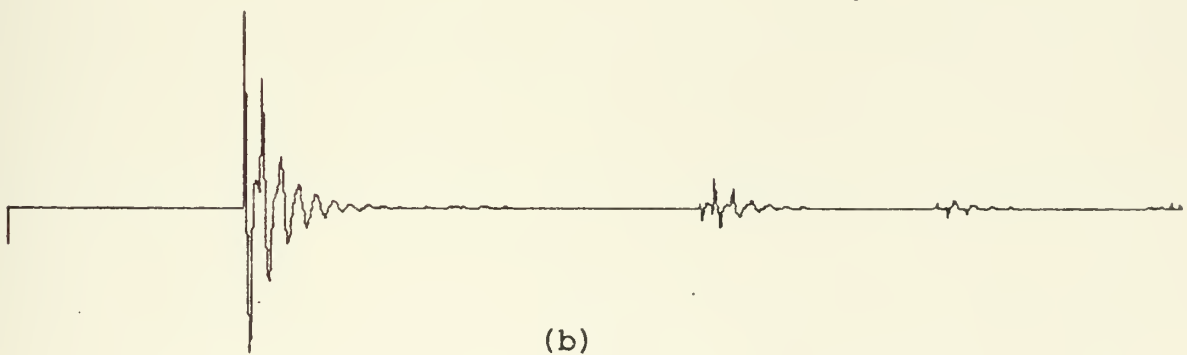
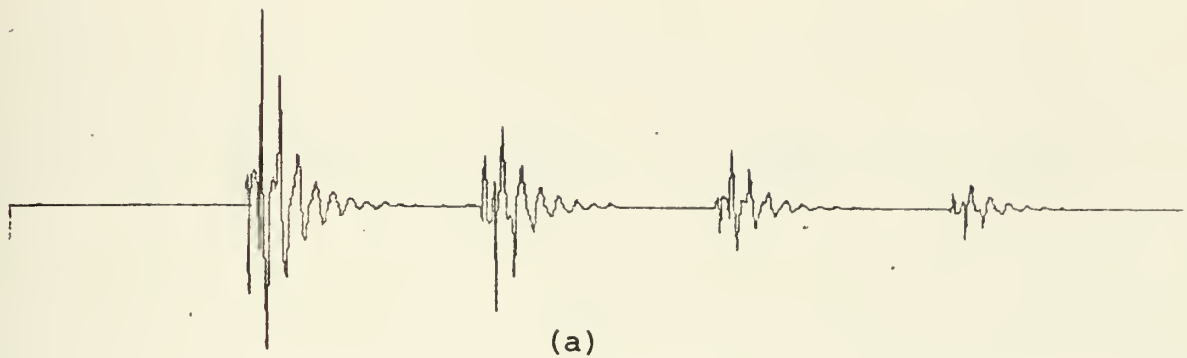
$$M_j(z) = 1 + \sum_{k=1}^{\infty} \frac{(-R)^{(j+k)}}{j+k} z^{-n_{j+k}} + \sum_{k=3}^{\infty} c_k (-R)^{(2j+k)} z^{-n_{2j+k}} + \dots$$

which transforms to

$$m_j(n) = \delta(n) + \frac{(-R)^{j+1}}{j+1} \cdot \delta(n-n_{j+1}) + \frac{(-R)^{j+2}}{j+2} \cdot \delta(n-n_{j+2}) + \dots \quad (11)$$

It is apparent that the remaining terms have been reduced by factors equal to those obtained in the periodic case.

The above result has been verified experimentally by processing a periodic signal containing only a strong bottom reflection ($R=.55$) and multiples (figure 47a). Removal of the first multiple component in the cepstrum results in 75% and 85% energy reductions of the second and third multiples respectively. These correspond exactly to the 50% and 67% amplitude reductions predicted by (11). The periodicity was then disturbed by average deviations of 1%, 5%, 10% and 20% of the original period. In each case the later multiple reductions coincided with (11). Figure 47 shows waveforms before and after processing for the exactly periodic signal and the case of 20% aperiodicity.



1.0 2.0 3.0 4.0 5.0

Figure 47 (a) Signal composed of only periodic multiples of the bottom response.
(b) Result of removing the first multiple cepstrum contribution.

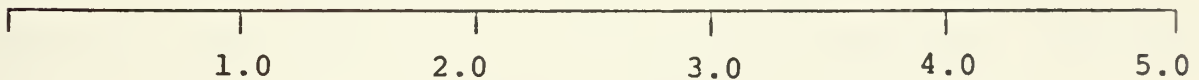
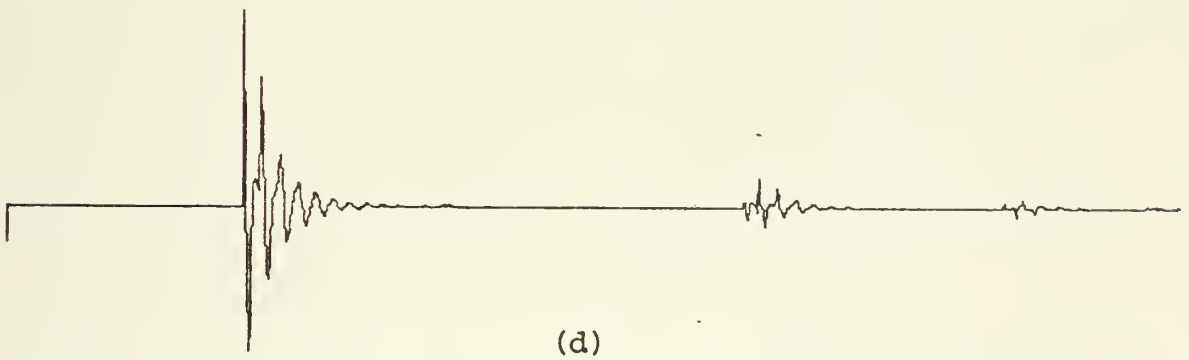
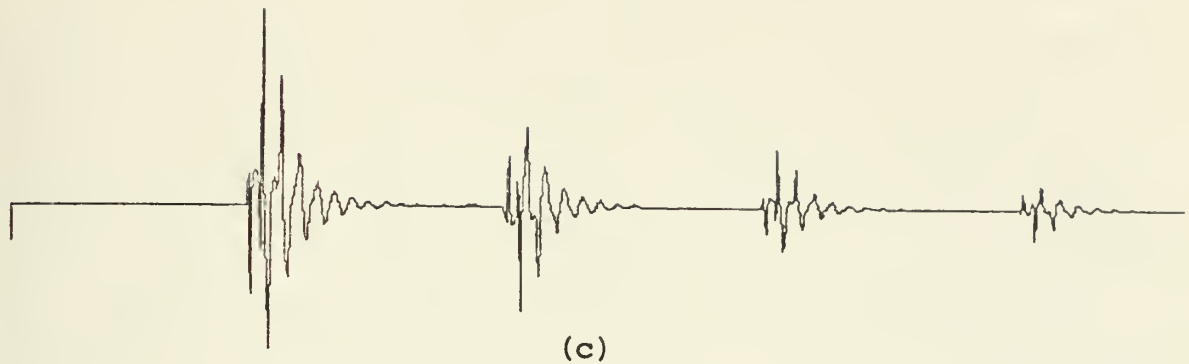


Figure 47 (cont'd) (c) Signal of (a) with periodicity disturbed by average deviations of 20% (.2 sec).
(d) Result of removing the first multiple cepstrum contribution.

3. Multiple-to-Signal Ratio

The results obtained for aperiodic reverberation must be extended to signals containing reflectors as well as multiples if they are to be of practical use. This is not feasible analytically due to the nonlinearity of the homomorphic transformation and the reflector characteristics in the earth model used. Recall that, for this analysis, reflectors have the form $t^2 e^{-bt}$ rather than simply impulses. Each seismogram contains an additive combination of these reflectors with multiples. The logarithmic operation on the Fourier transform of this sum causes the cepstral contributions due to reflectors and multiples to be analytically indistinguishable. Hence, this phenomenon has been investigated empirically for various reflector sizes. It was found that cepstral properties of multiples are essentially preserved in the presence of non-impulsive reflectors although important effects were evident in the cases tested.

Percentage removal of the first multiple was found to be dependent on the width of the cepstral stopband. Figure 48 illustrates this effect for seismograms with different reflector strengths and periodic multiples. Each signal requires a stopband of about 200 msec (41 samples) for complete removal of the first multiple. As notch width is decreased the performance becomes increasingly sensitive to MSR. For the smallest notch width shown (40 msec), performance varies almost 30%

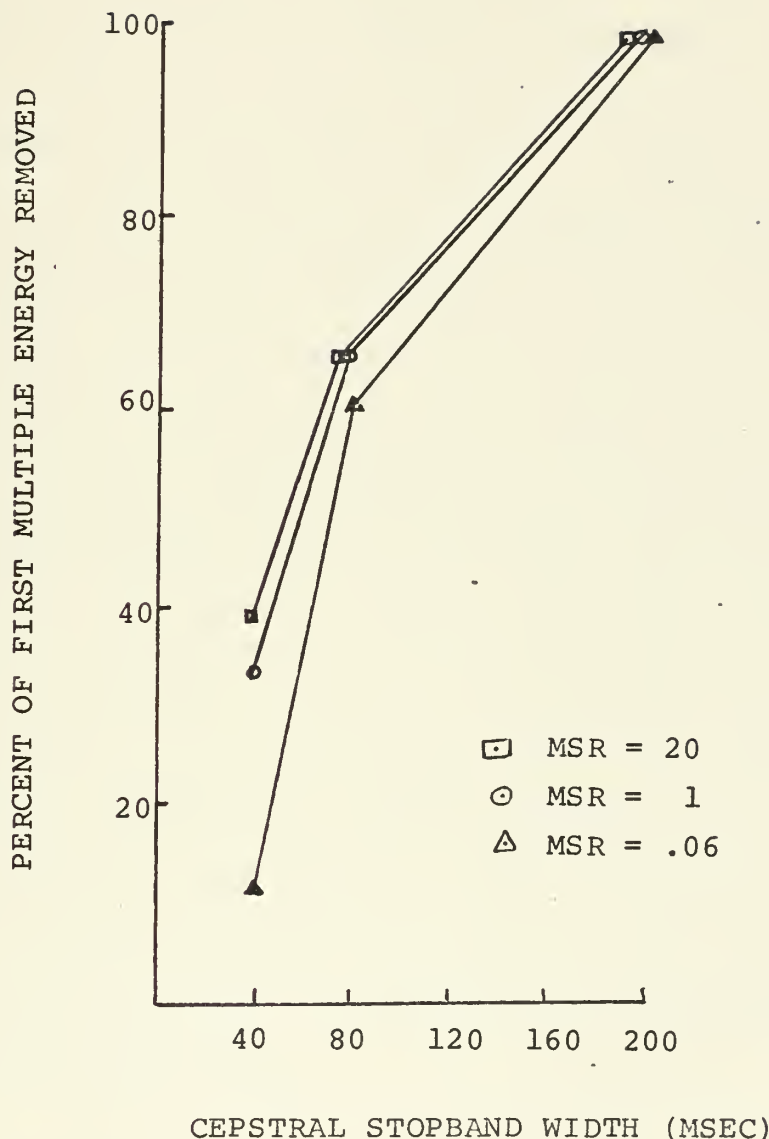
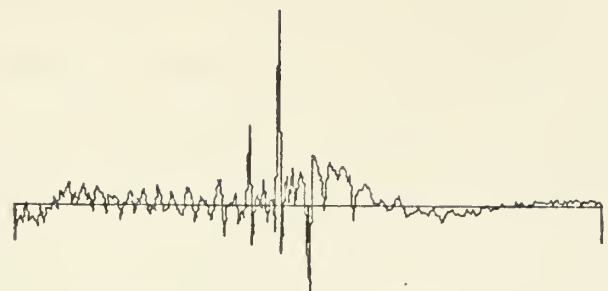


Figure 48 Effect of cepstral stopband width on homomorphic dereverberation performance for signals of varying MSR.

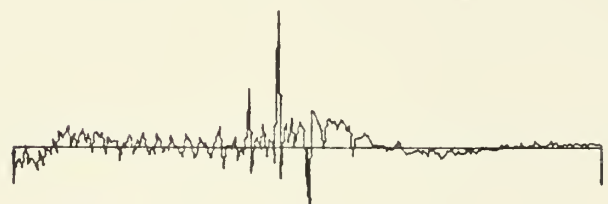
with MSR. In the absence of reflectors the first multiple could be completely removed by zeroing one sample of the cepstrum. It appears that the inclusion of reflectors has the effect of distributing the multiple energy in the quefrency domain, although, in all cases tested the energy remains concentrated near the time domain multiple location. Figure 49 shows the 0.5 second section of the cepstrum centered at the multiple location for each of the seismograms of figure 48. The cepstra are identical in form but the absolute cepstral energy increases with MSR. Three large peaks occur in each cepstrum between .94 and 1.0 second. This similarity in form suggests that equal stopbands should produce equivalent percentage reduction of multiples. We conclude, however, from the experimental results that a greater portion of the multiple energy is concentrated near 1.0 second in the higher MSR cepstra. This effect makes it difficult to select stopband limits by peak detection or visual inspection of the cepstrum. Notch widths which yield the best trade-off between multiple reduction and reflector distortion must be determined by trial-and-error for particular applications.

4. Multiple Distortion

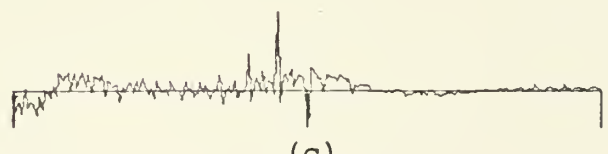
Since homomorphic dereverberation is theoretically based on a model of strictly impulsive multiples, it is important to observe the performance of this technique in the more realistic



(a)



(b)



(c)

.75 1.0 1.25

Figure 49 0.5 second section of cepstra at multiple location.
(a) MSR=20 (b) MSR=1 (c) MSR=.06

case of an extended bottom interaction mechanism. We employ the same bottom response functional form discussed earlier in this chapter. The seismogram of figure 50a contains distorted multiples due to a bottom response of .045 seconds duration. Reflectors are present at 2.7 and 3.5 seconds. Figure 50b shows the region of the cepstrum centered at the first multiple location. The peaks are much broader than those of figure 49. The dominant energy is concentrated near the multiple location as before but it now appears to be more distributed.

Table 1 summarizes the effects of varying the stopband width and location in the cepstrum of figure 50b. First and third multiple energy removed varies widely while the second multiple is not significantly affected by the passband dimensions. In some cases, extending the stopband decreases the amount of multiple energy removed. Zeroing the .94-.98 second region results in greatly increased reduction of the third multiple (74-78%) but first multiple reduction is degraded by 10-12%. This behavior, which has been observed in several cases, is not predicted by the theory and is thought to be a computational effect. The high amplitude oscillations which are dominant in the left side (.75-1.0 second) of figure 50b, or the low frequency "drift" which is apparent throughout the section may be computational noise which contributes to this phenomenon.

Several observations can be made in this case. Although

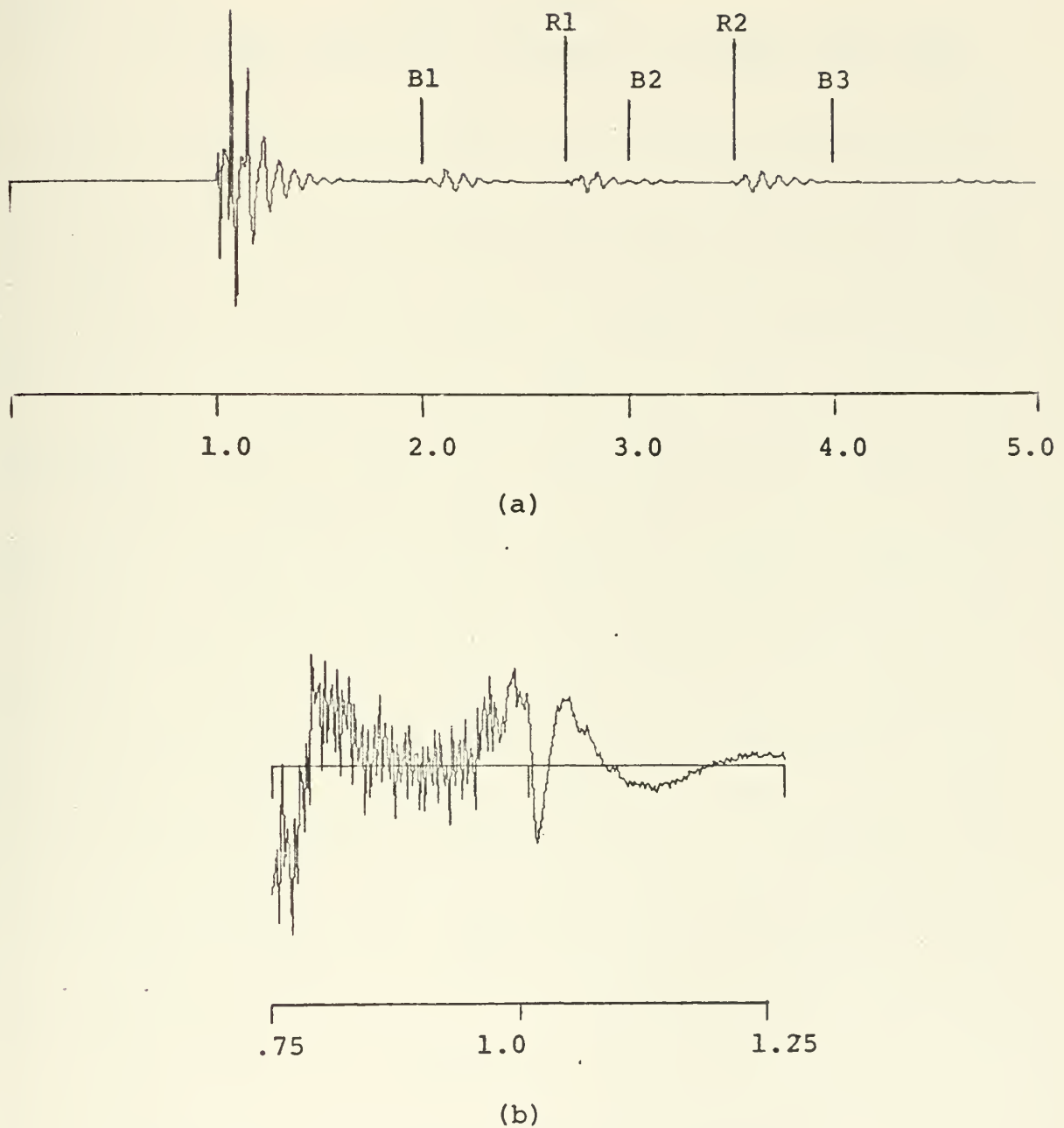


Figure 50 (a) Seismogram with distorted multiples
(b) 0.5 second section of cepstrum centered at
first multiple location.

Stopband Limits
(sec)

ENERGY REMOVED

1st MULT 2nd MULT 3rd MULT 1st REFL. 2nd REFL.

Stopband Limits (sec)	1st MULT	2nd MULT	3rd MULT	1st REFL.	2nd REFL.
.94-1.06	.75	.48	.78	-.13	-.01
.96-1.06	.78	.44	.74	-.13	.01
.96-1.00	.65	.49	.56	-.12	-.03
.98-1.02	.79	.44	.45	-.12	-.03
.98-1.04	.88	.44	.43	-.12	-.03
.98-1.06	.89	.45	.54	-.12	-.02
.99-1.04	.78	.42	.39	-.12	-.05
1.0-1.04	.64	.45	.48	-.13	-.06
1.02-1.06	.50	.45	.50	-.13	-.06

TABLE 1

EFFECTS OF STOPBAND LIMITS ON PERFORMANCE
FOR THE SIGNAL OF FIGURE 50.

performance is somewhat erratic, a stopband of 40-80 msec which straddles the first multiple onset time yields significant multiple reduction. The peak performance in this case is about 10% below that achieved with undistorted multiples but the sensitivity to minor stopband variations is less dramatic. Reflector distortion does not increase significantly due to the presence of distorted multiples.

Figure 51 shows processed seismograms resulting from the application of various stopbands to the cepstrum of figure 50.

Finally, we note that the effects of aperiodicity have not been discussed in the distorted multiple case. Due to limitations of the earth model it was not possible to investigate these effects. Thusfar, however, we have relaxed the theoretical assumptions regarding periodicity and coherence individually, and found that homomorphic dereverberation is not critically sensitive in either case. We surmise that the combination of these effects would not be catastrophic to performance. Further investigation is merited since this topic has an important bearing on the effectiveness of the homomorphic technique in shallow water dereverberation where later multiples are significant.

5. Water Travel Time Estimate

In practice, passband location must be determined by estimation of water column travel time. It is apparent from

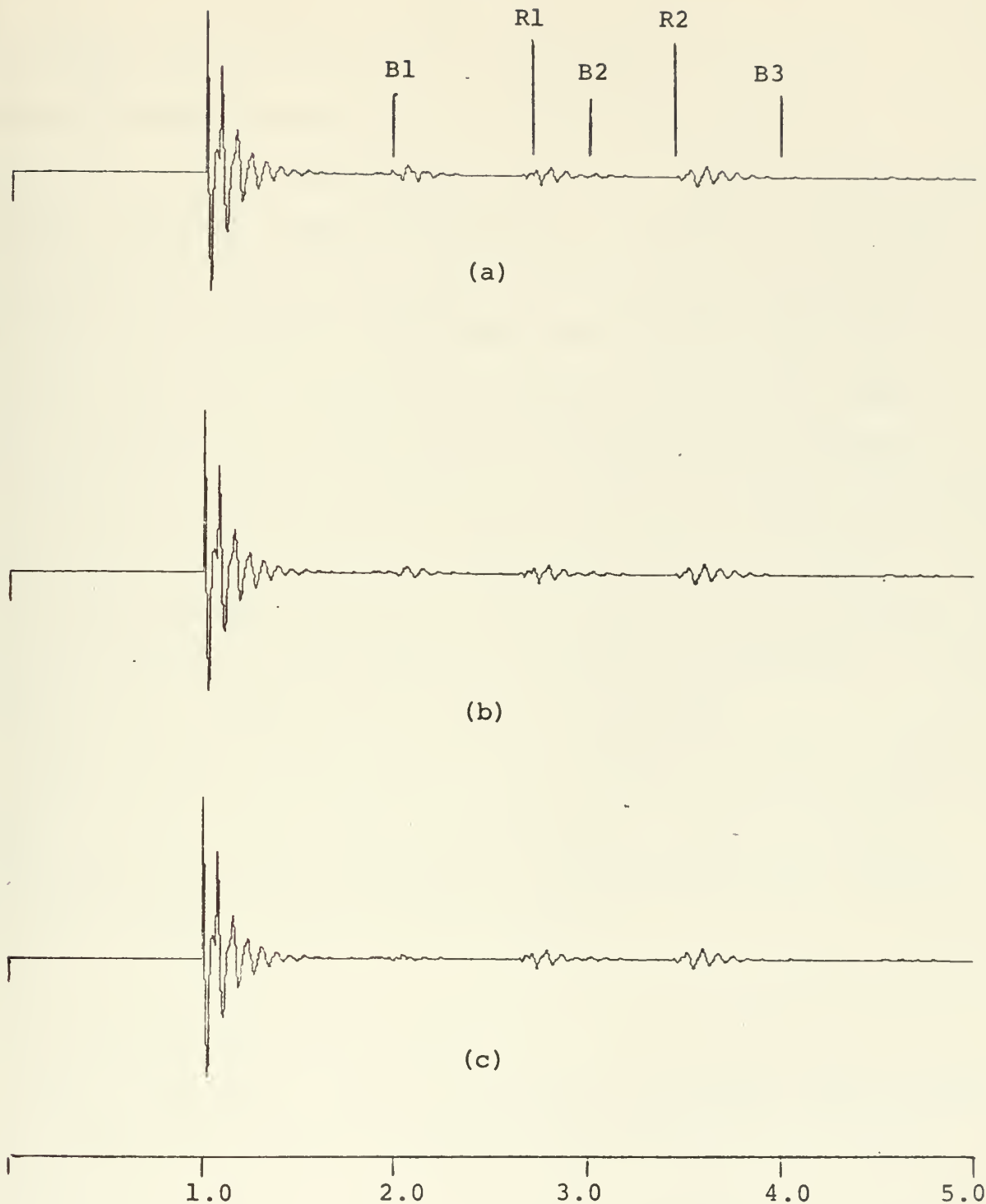


Figure 51 Processed results of the seismogram in figure 50a
for three different cepstral stopbands. (a) 1.02-1.06 sec
(b) 1.0-1.04 sec (c) .98-1.06 sec

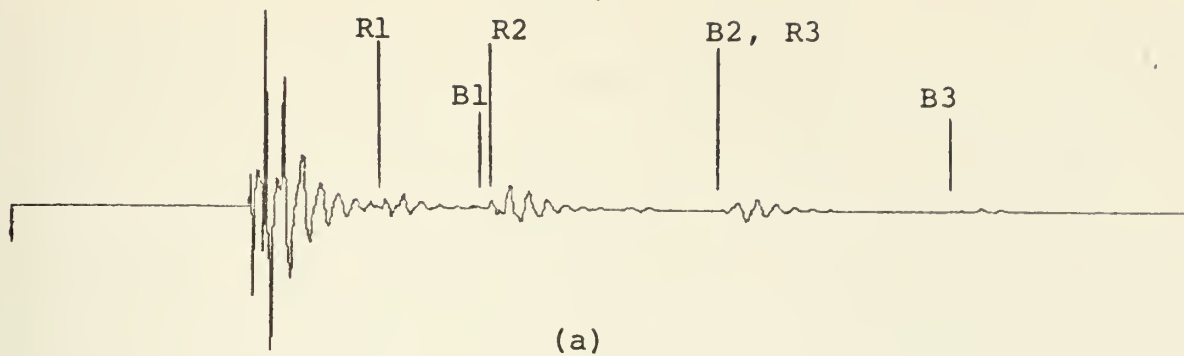
the preceding discussion that the importance of accurate bottom estimation depends on the seismic environment. In particular, we have seen that MSR and bottom characteristics seem to affect cepstral energy distribution. Proximity of multiples to important reflectors also dictates resolution constraints on travel time estimation. For the cases analyzed here the required travel time estimation accuracy would be 20-40 msec since, as determined in the foregoing discussion, a stopband of 40-80 msec is generally required for effective dereverberation. Travel time estimation error of more than half the stopband width causes the major multiple contributions to be excluded from the stopband. This degree of accuracy can easily be attained with existing bottom tracking algorithms.

The reflector/multiple resolution implied by the required stopband widths is also about 40-80 msec for the data tested. A discussion and several examples of reflector/multiple resolution are included in the following section.

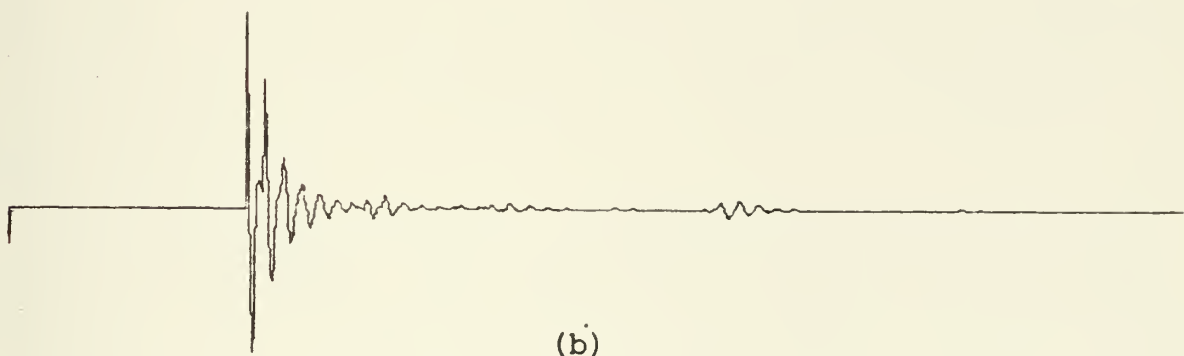
6 Reflector/Multiple Overlap

The following six figures illustrate homomorphic dereverberation of signals in which reflectors and multiples are closely situated.

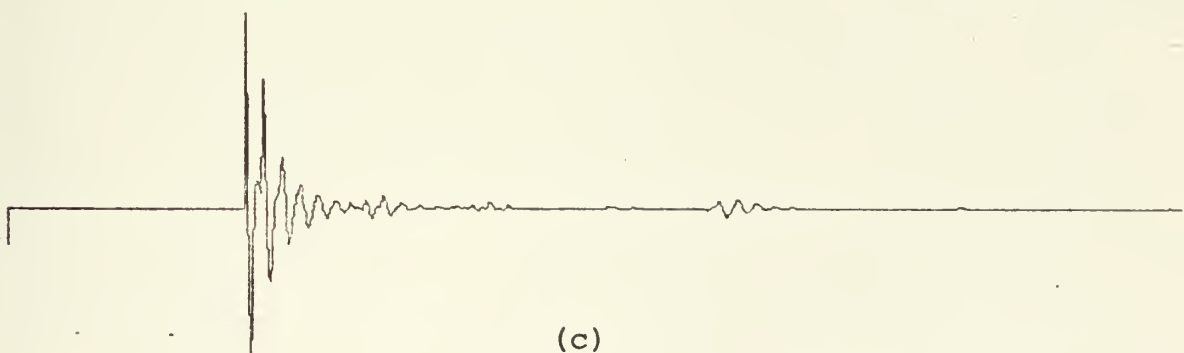
Figure 52a shows a seismogram with reflectors at 1.6, 2.02 and 3.0 seconds. The first and second multiples directly interfere with reflectors and the third multiple is barely visible



(a)



(b)



(c)

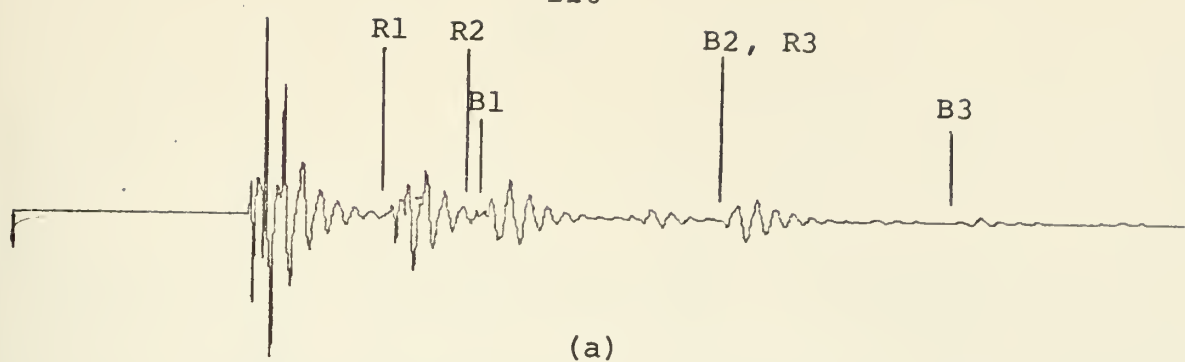
1.0 2.0 3.0 4.0 5.0

Figure 52 (a) Unprocessed seismogram
(b) Result of cepstral notch filtering; .96-1.02 sec
stopband
(c) .98-1.06 sec stopband

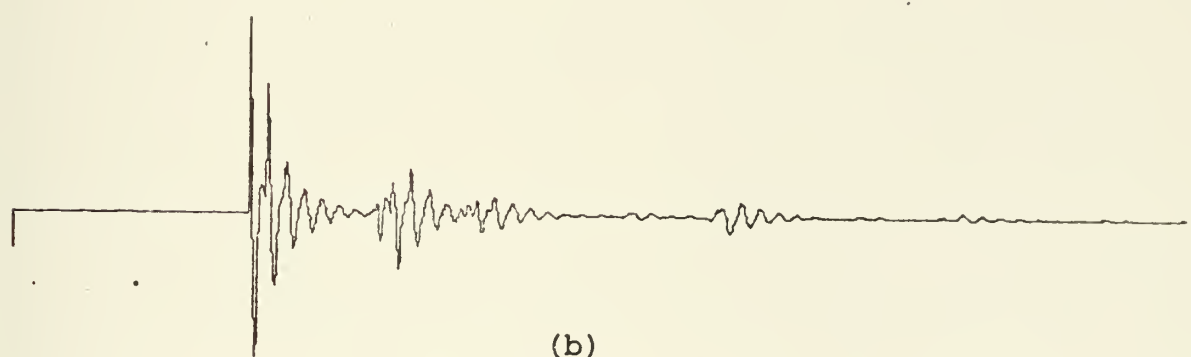
at 4.0 seconds. The result of applying a cepstral stopband at .96-1.02 seconds is seen in figure 52b. Most of the energy near two seconds has been removed but a small reflection is still visible. The signal of figure 52c results from a stopband of .98-1.06 seconds which spans the time domain reflector location as well as the multiple location. Residual energy is still present after this processing which indicates that some of the reflector and first multiple cepstrum contributions are distributed beyond the immediate vicinity of the time domain locations.

The seismogram of figure 53a contains reflectors at 1.6, 1.95 and 3.0 seconds. Each reflector is clearly evident after processing (.98-1.06 second stopband) and first multiple energy has been greatly reduced as shown in figure 53b. Some of the removed energy may be due to the 1.95 second reflector; however, the first multiple in this example is very coherent and its energy is more likely to be localized near 1.0 second in the cepstrum. Extension of the stopband closer to the reflector location (.96-1.06 second) causes complete removal of the reflector as seen in figure 52c. Visible reduction of the second multiple at 3.0 seconds and an internal multiple at 2.7 seconds is apparent in figure 52b.

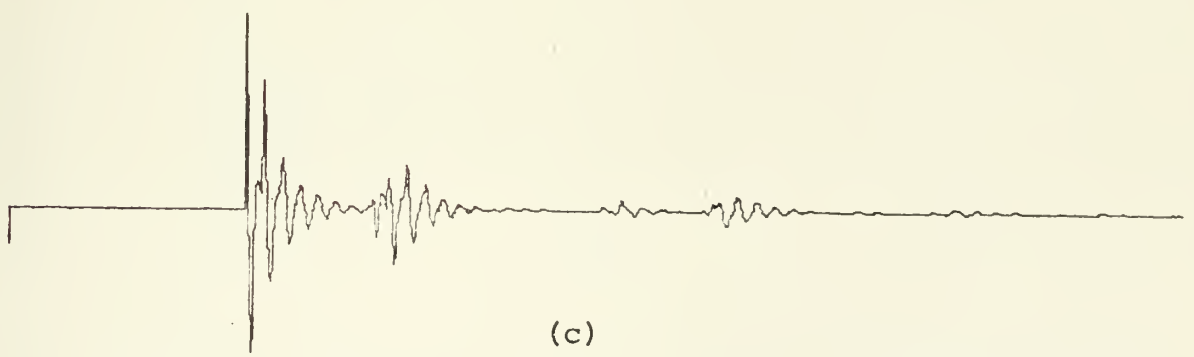
The seismogram of figure 54a has the same reflector placement as that of figure 53a but the multiples in this case are smaller and less coherent. Application of a cepstral stopband



(a)



(b)



(c)

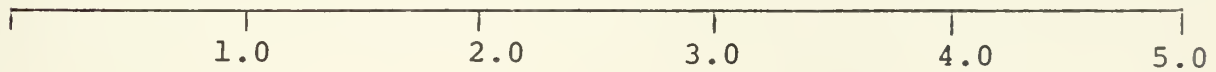
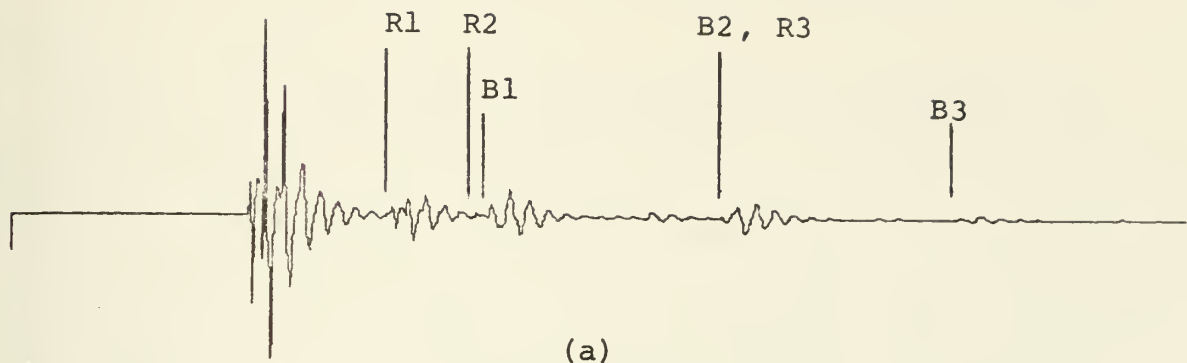
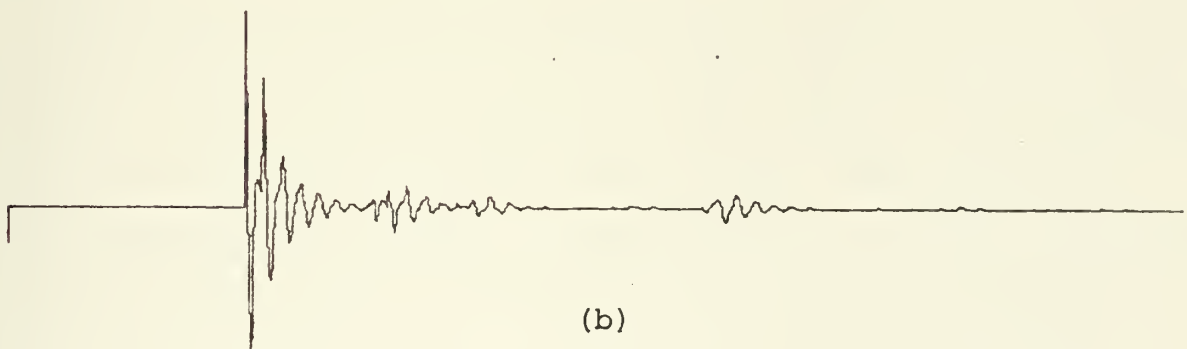


Figure 53 (a) Unprocessed seismogram (b) Result of cepstral notch filtering; stopband .98-1.06 sec. (c) .96-1.06 sec stopband.



(a)



(b)



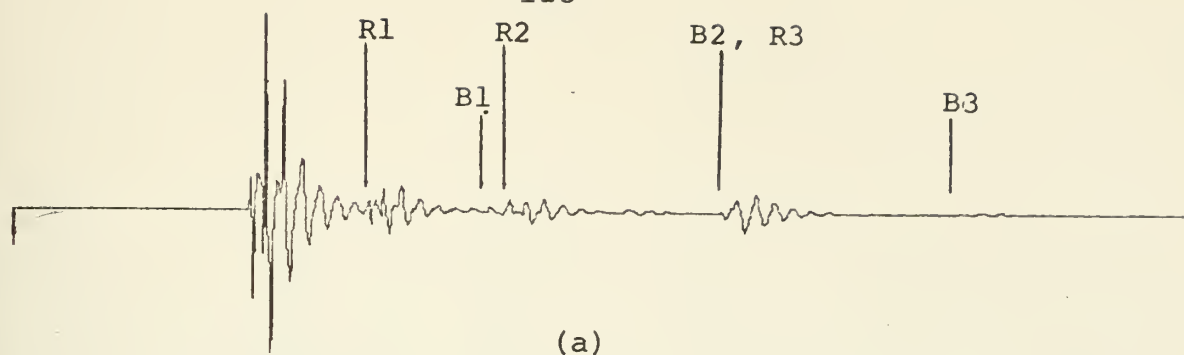
Figure 54 (a) Unprocessed seismogram
(b) Result of cepstral notch filtering; stopband
1.0-1.06 sec.

at 1.00-1.06 second yields (figure 54b) visible reduction of all three multiples and well resolved reflections at the proper locations.

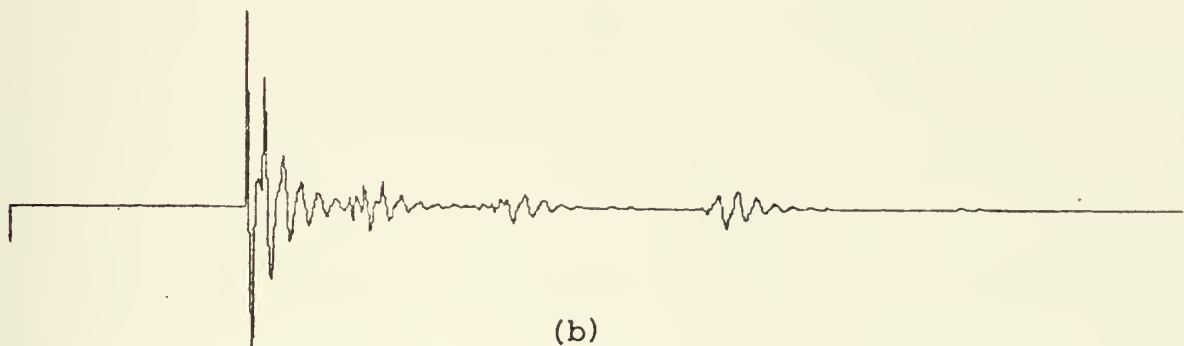
Figure 55a illustrates a seismogram with considerable multiple distortion and reflectors at 1.5, 2.1 and 3.0 seconds. A wide cepstral stopband, .98-1.08 second, has a very minor effect on the first multiple as seen in figure 55b. Extension of the stopband to 1.12 seconds causes removal of virtually all signal energy in the region. The relatively wide (.1 second) reflector/multiple separation cannot be effectively exploited in this case because the very incoherent multiple in a low MSR signal requires a large stopband for effective removal (see figure 48).

The result of longpass filtering the cepstrum of the signal in figure 55a is shown in figure 56. All cepstral contributions prior to 1.02 seconds have been set to zero. The bottom and later reflectors are clearly visible but the 1.5 second reflector has been removed. This illustrates one drawback to longpass dereverberation in deeper water. This effect may be acceptable in some situations, however. For instance, good resolution of closely spaced, deep reflectors may be obtained by longpass filtering whereas the earlier reflectors are frequently obvious before processing.

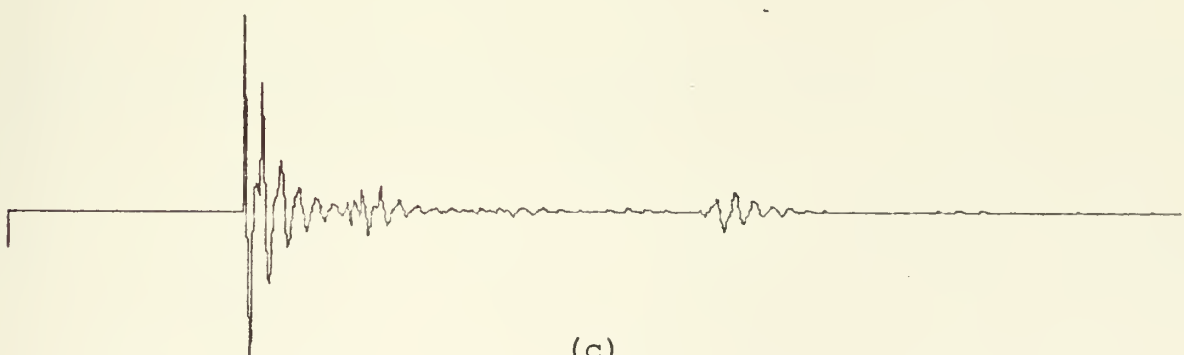
Figure 57 shows longpass results for a signal with impulsive multiples and very sharp reflectors at 2.2 and 3.0 seconds.



(a)



(b)



(c)

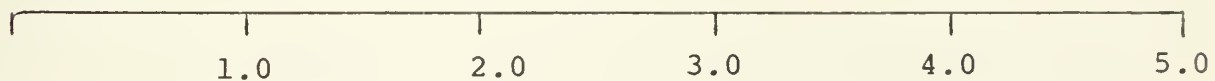


Figure 55 (a) Unprocessed seismogram.
(b) Result of cepstral notch filtering; stopband
0.98-1.08 sec
(c) 0.98-1.12 sec

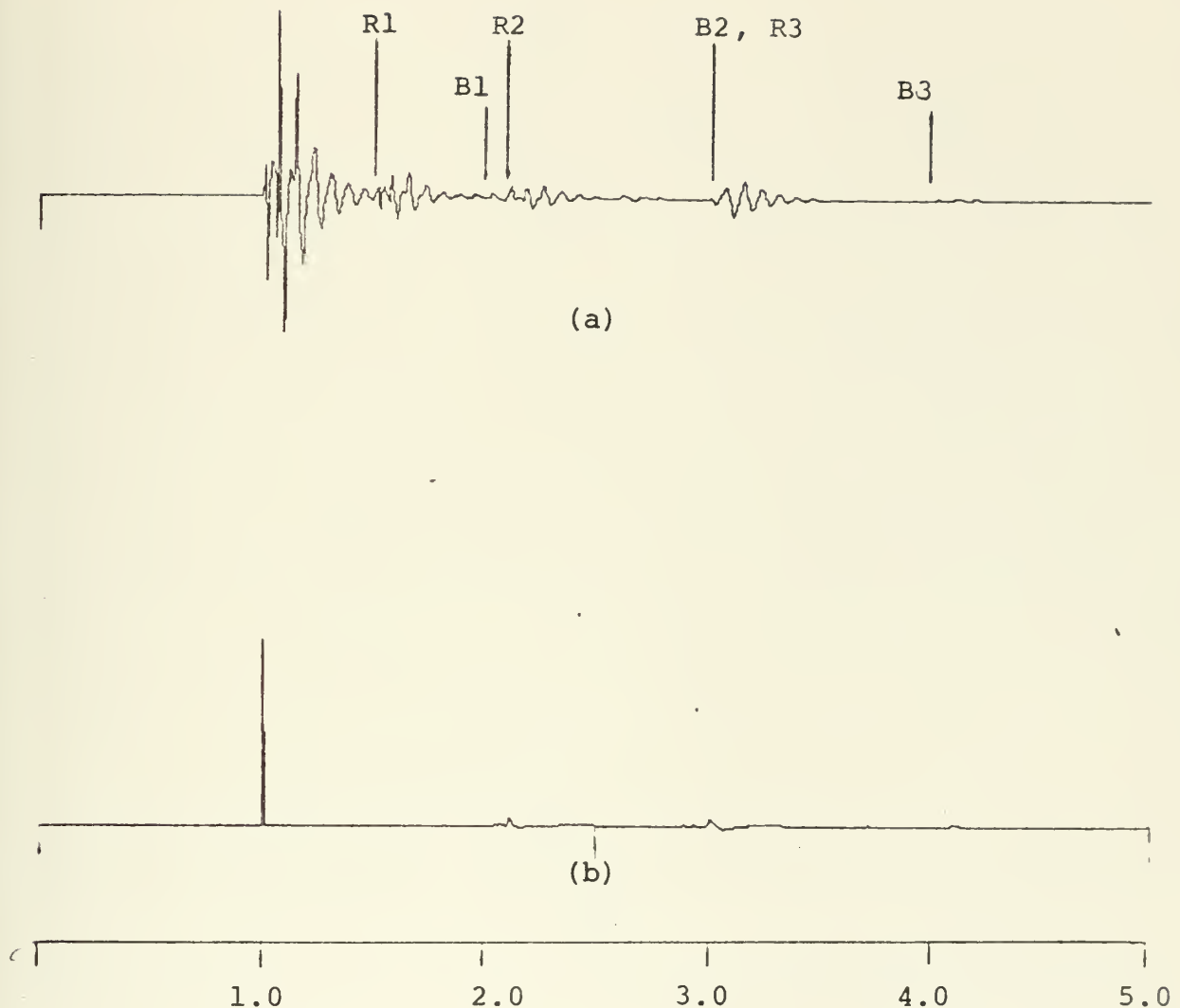


Figure 56 (a) Unprocessed seismogram
(b) Result of longpass filtering cepstrum; cutoff
quefrenency 1.02 sec.

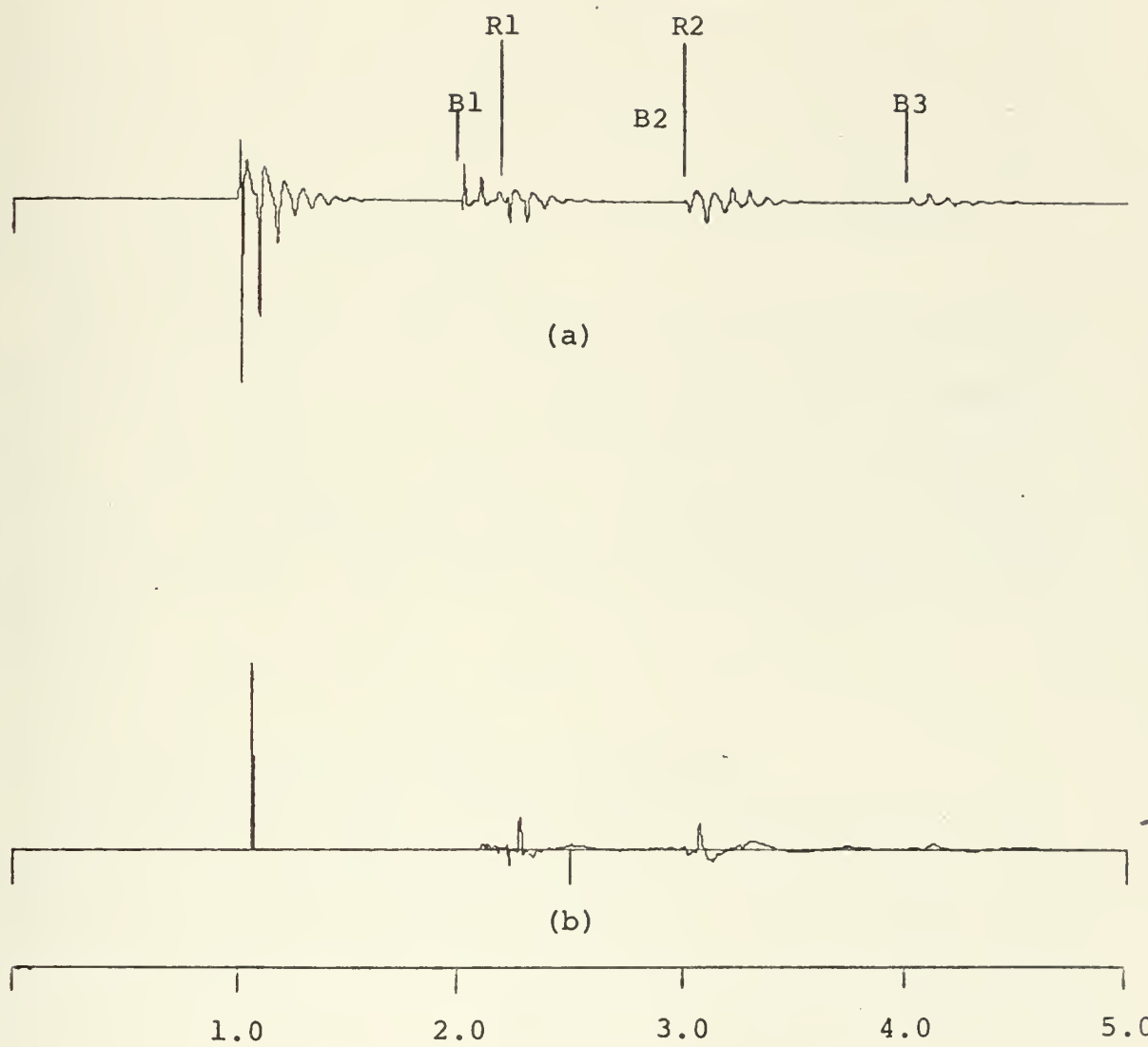


Figure 57 (a) Unprocessed seismogram
(b) Result of longpass filtering; cutoff quefrency
1.01 sec.

The stopband limit is 1.01 seconds in this case. Multiple removal is complete and both reflectors are clearly visible. Longpass filtering was found to be most effective for signals of this type. Very sharp reflectors are more clearly visible than more distorted reflectors of comparable energy, especially in noisy signals. Longpass filtering of noisy signals is discussed later in this chapter.

The low frequency noise present in the reflector region of figure 57 is typical of that observed in several longpass results. The cepstra of figures 49 and 50 contain similar components. No attempt was made in this analysis to remove this type of noise. The reason for its presence has not been determined.

7. Additive White Noise and Filtering

The effects of additive noise are not addressed in the formulation of the homomorphic system for deconvolution since there are no apparent cepstral properties of noise which can be exploited for its removal. Linear filtering is a more suitable way of reducing additive noise in individual signals. This can be performed prior to, or in conjunction with, homomorphic deconvolution. The effects of this combined processing in the special case of Gaussian white noise have been investigated and are discussed here. The data presented represent a relatively small number of experiments performed with synthetic data and

noise generated as previously discussed. These results cannot be generalized categorically due to the relatively narrow scope of the experiments and the lack of precise theoretical characterization of noise properties under homomorphic transformation. The results do indicate performance trends and computational effects due to additive noise and filtering.

Since noisy signals usually undergo linear filtering prior to dereverberation, we begin by discussing an important computational issue which arises when signals are bandpass filtered. Such filtering introduces spectral regions (stopbands) containing little or no spectral energy. Recall that the homomorphic transformation involves computing the logarithm of the Fourier transform of the signal. Since the logarithm of zero is not defined, this computation is not possible in frequency bands where the Fourier transform is zero. In the case of lowpass filtered signals this problem can frequently be overcome by resampling after filtering. Figures 58 a, b and c illustrate this process. If the sampling frequency is decreased to the Nyquist rate implied by the filter cutoff frequency, the resulting discrete Fourier transform will include only the frequency components in the passband region. Figure 58d shows a distribution of spectral energy which is not readily amenable to elimination of the zero region. In this case the baseband region is zero so that resampling would not be effective. Investigation of this problem is currently in progress (Tribolet [11]).

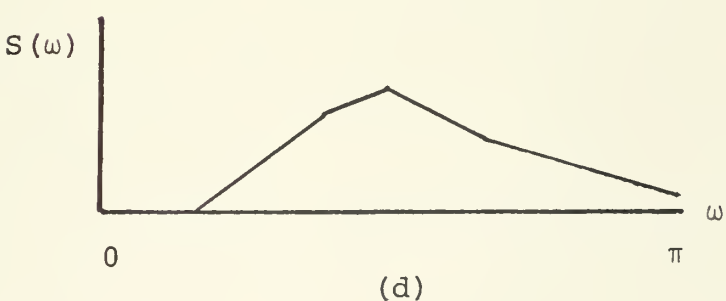
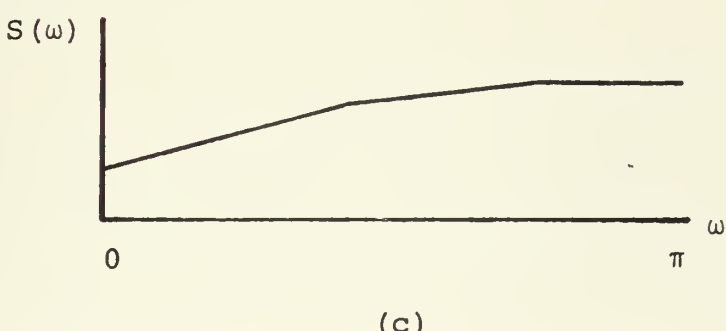
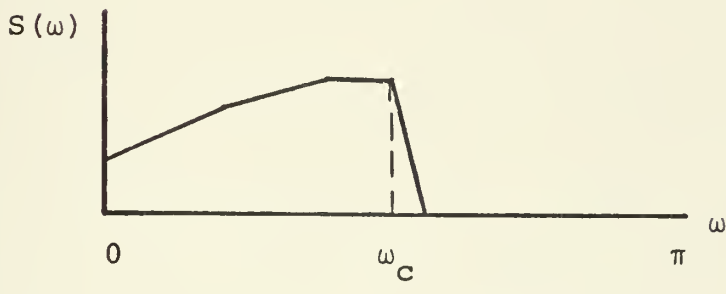
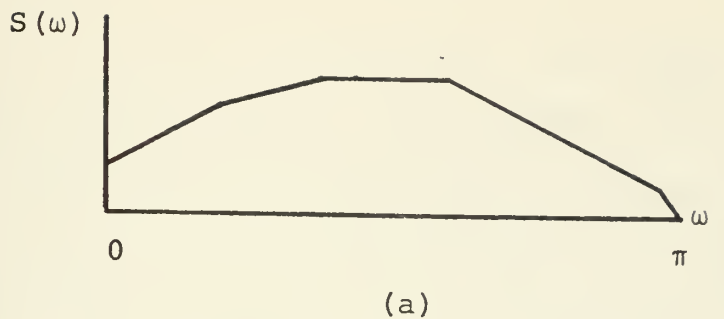


Figure 58 (a) Unfiltered spectrum sampled at the Nyquist rate.
(b) Spectrum of (a) after lowpass filtering at ω_c without resampling.
(c) Filtered spectrum after reampling.
(d) Spectrum with zeros in the baseband region.

It was found in this analysis that computing the cepstrum of an over-sampled signal is an unstable procedure which, at best, requires extensive computation time. The low energy regions of the spectrum lead to spurious phase derivative values. Hence, the phase unwrapping algorithm proceeds at small step sizes, requiring computation of many intermediate values of the discrete Fourier transform. In many cases the computer algorithm could not produce an unwrapped phase which was in acceptable agreement with the principal value. Cepstra of over-sampled signals which were successfully computed, however, generally yielded dereverberation results comparable to those of properly sampled signals (see table 2).

Addition of white noise was found to have a computational effect similar to that described above; phase unwrapping time is significantly increased. Heavy weighting ($w = .98-.99$) was found to reduce computation time considerably for noisy signals, although some signals require small phase integration step sizes in isolated sections even when substantial weighting is applied. Recall from Chapter II that there is no assurance that the log-spectrum is adequately sampled, even after lowpass filtering of the signal. Hence, the integration of the phase derivative cannot be expected to proceed quickly in all cases.

Smoothing of the phase derivative was attempted to compensate for the effects of noise. A three-point moving average was applied prior to integration. The resulting inverse cepstra bore no resemblance to the original seismograms.

SAMPLING INTERVAL (MSEC)	FILTER CUTOFF(Hz)	FRACTION OF ENERGY REMOVED		
		1st MULT	2nd MULT	3rd MULT
4.88	50	.91	.064	.25
9.77	50	-.02	.12	.24
19.53	50	.94	.044	.25
4.88	20	.94	.083	.15
9.77	20	.93	.48	.13
19.53	20	.98	.12	.55

TABLE 2

EFFECT OF RESAMPLING ON MULTIPLE REMOVAL FOR A NOISELESS SEISMOGRAM LOWPASS FILTERED AT 50 and 20 Hz. DEREVERBERATION WAS ACCOMPLISHED BY APPLYING AN 80 MSEC CEPSTRAL STOPBAND AT THE FIRST MULTIPLE LOCATION.

Figure 59 summarizes the observed effects of noise on first multiple removal by homomorphic processing. Each seismogram was lowpass filtered at 50 Hz and resampled by a factor of four prior to multiple removal. Percentage of multiple energy removed shows a consistent decrease with increasing noise level. The rates of decrease and amounts of energy removed are seen to vary widely from one signal to another. Examples of noisy signals before and after processing are shown in figures 60 and 61. Significant reduction of the first multiple is evident in both examples. In the first case, the noise level is moderate and multiple reduction has a marked effect on visual quality of the signal. The noise level in figure 61 is considerably higher, resulting in marginal improvement due to dereverberation.

Second and third multiple energy removed was found to decrease generally with decreasing noise also, and in some high noise cases the later multiples were actually enhanced. Data for a typical signal are tabulated below.

STANDARD DEVIATION OF NOISE	ENERGY REMOVED	
	2nd MULT.	3rd MULT.
0	.29	.32
25	.19	.15
50	.04	.02
100	-.21	-.17

TABLE 3

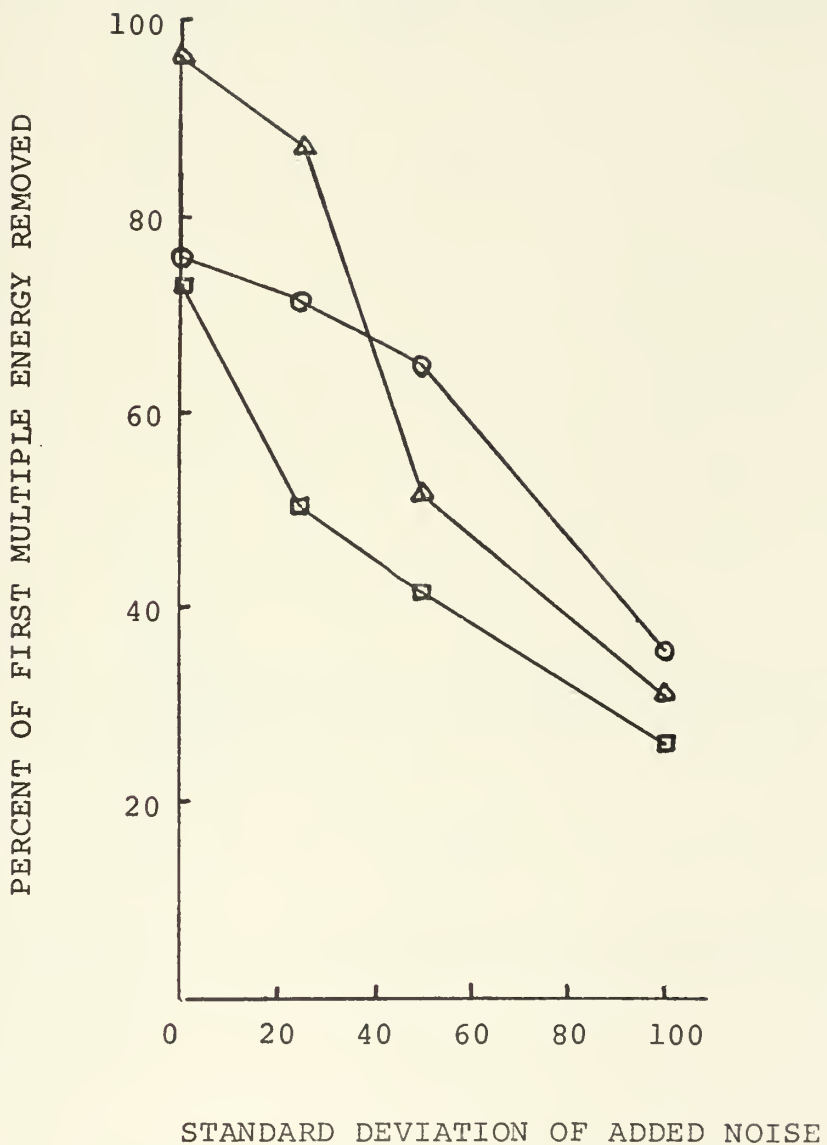


Figure 59 Effect of added noise on homomorphic dereverberation.
All signals are lowpass filtered at 50 Hz and resampled.

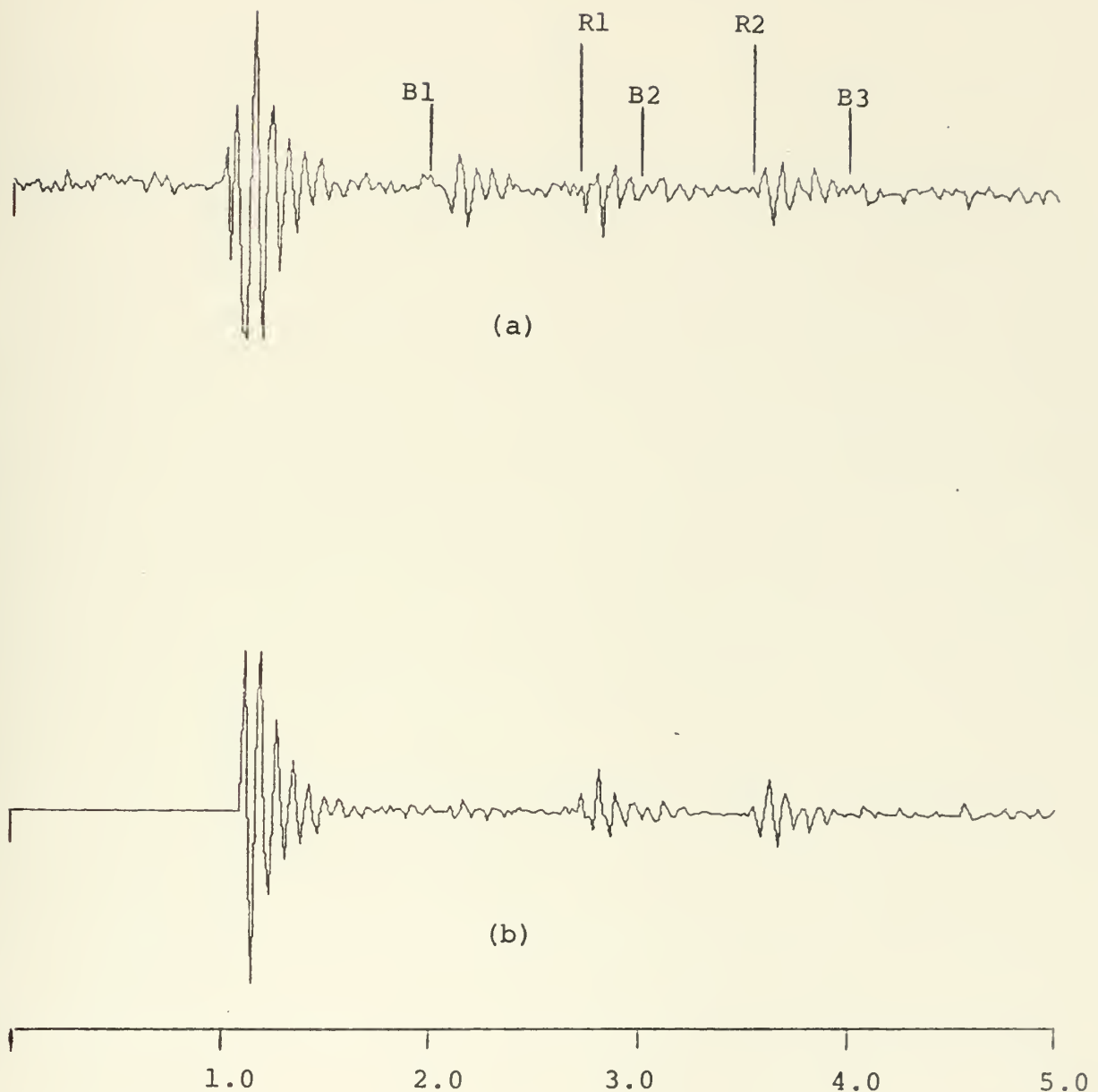


Figure 60 (a) Seismogram with moderately high noise, $F = 50$ Hz.
(b) Result of cepstral notch filtering (.8-1.8 sec).

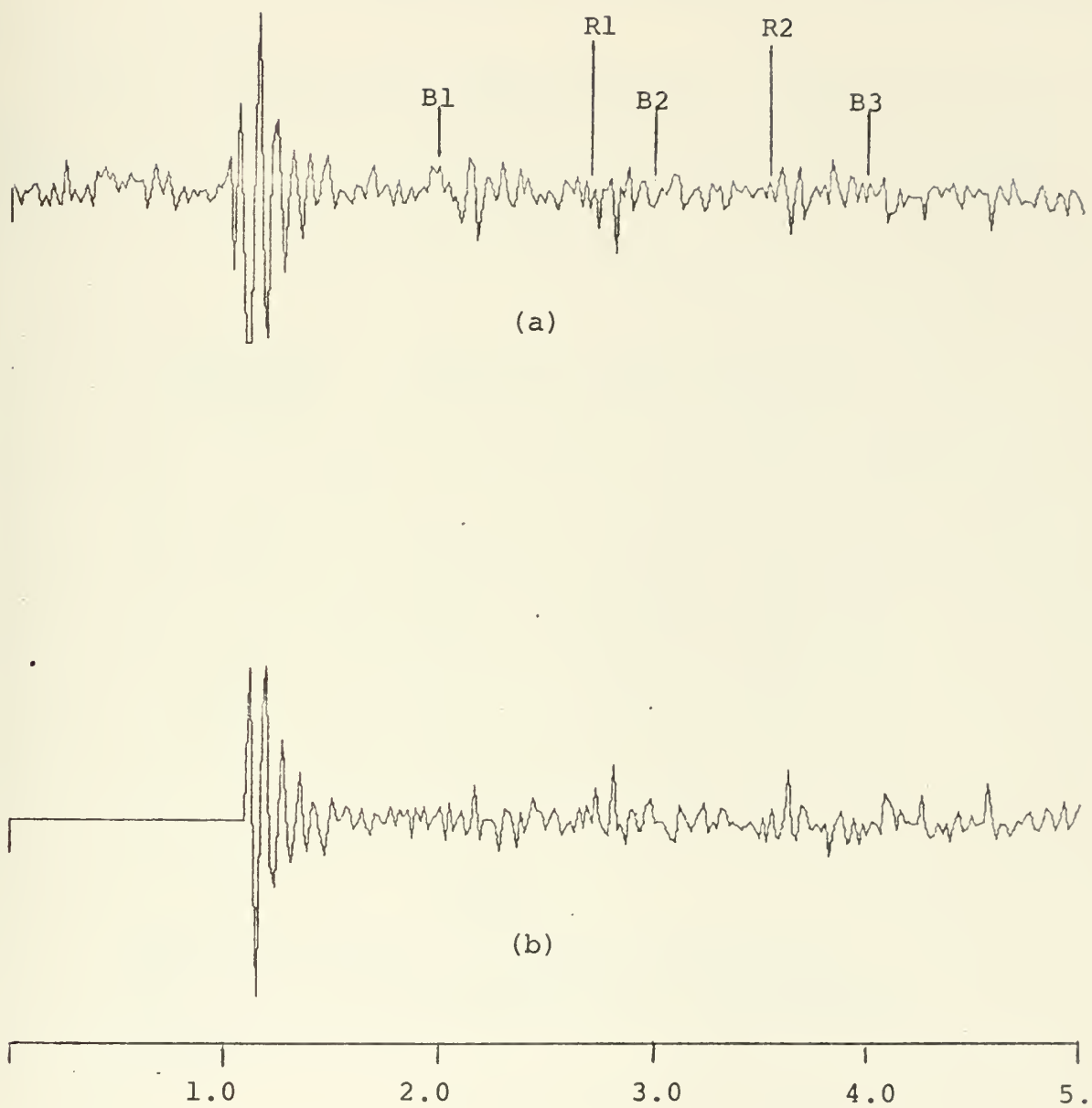


Figure 61 (a) Seismogram with very high noise, $F_c = 50$ Hz.
(b) Result of cepstral notch filtering ($.80-1.04$ sec).

Reference to figure 61 reveals that for the higher noise amplitudes the later multiples are buried so that their removal is not important.

Reflector distortion, summarized for a typical case in table 4, was found to be generally more severe than in noiseless signals but rarely more than 25%.

STANDARD DEVIATION OF NOISE	REFLECTOR ENERGY REMOVED		
	1	2	3
0	-.18	.02	.06
25	-.22	-.25	-.22
50	-.07	-.14	-.05
100	.14	-.12	-.09

TABLE 4

EFFECT OF NOISE ON REFLECTOR DISTORTION
FOR A TYPICAL SEISMOGRAM WITH 3 REFLECTORS,
FILTERED AT 50 Hz.

The above results indicate that the addition of noise leads to decreasing performance with respect to all three criteria. The behavior is somewhat spurious and frequently exhibits wide variation from signal to signal.

Several lowpass filter bandwidths (20, 30, 50, 70, and 90 Hz) were applied to the signals evaluated in figure 59. The results are shown in figure 62. In each case, first multiple removal is least effective when the signals are prefiltered at 50 Hz. Figures 63 and 64 illustrate this behavior. The same seismogram is shown in figures 63a and 64a, lowpass filtered at 50 and 20 Hz respectively. The difference in appearance is dramatic. Resolution of the reflectors on either side of the first multiple (at 1.55 and 2.4 sec) is greatly improved by dereverberation in the latter case while figure 63 shows very little visual improvement.

The behavior illustrated in these figures cannot be fully explained on the basis of the data available. The signals tested have dissimilar reflector locations and varying amounts of multiple distortion which implies that the similar performance dips are not due to similarities in signal configuration. The observed behavior may be due to the properties of the source signature (which is common to all three seismograms) or the characteristics of the recursive third order Butterworth filter employed. More data using different filter routines and a wide range of signal characteristics is needed to completely characterize this behavior. The results obtained here suggest that a filter bandwidth very close to the bandwidth of the noiseless signal leads to the best dereverberation performance. The same result was obtained for the TDL algorithm.

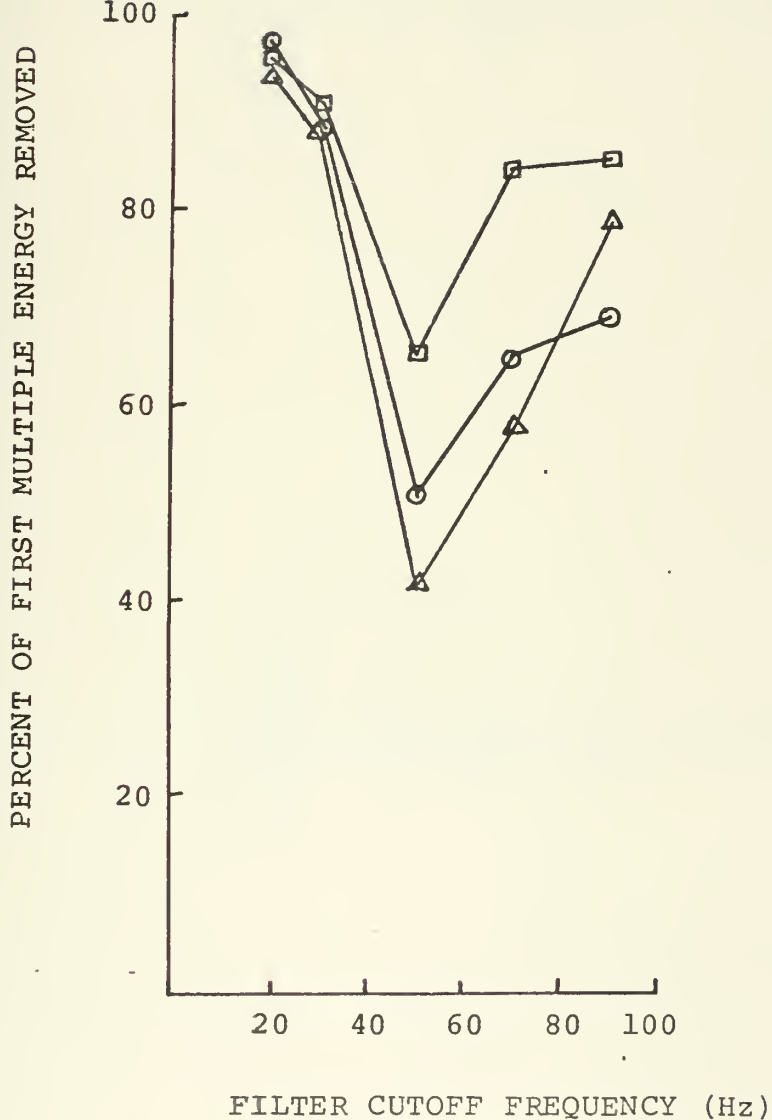
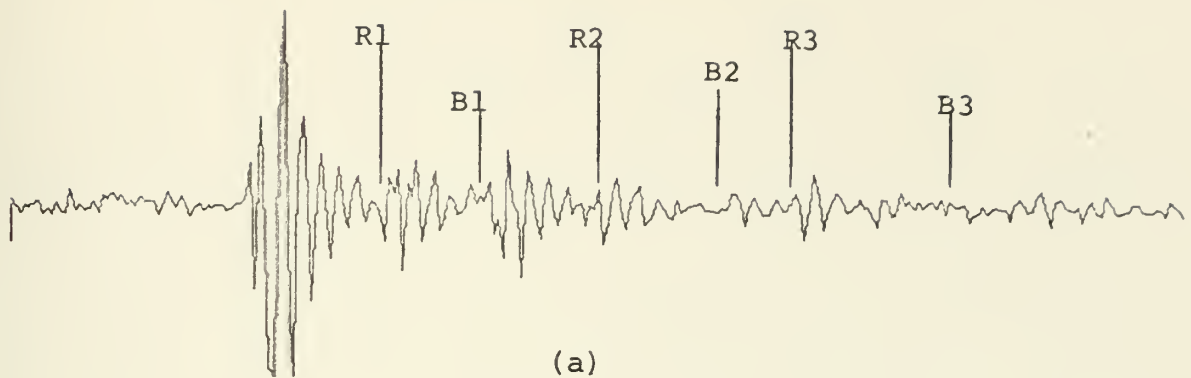
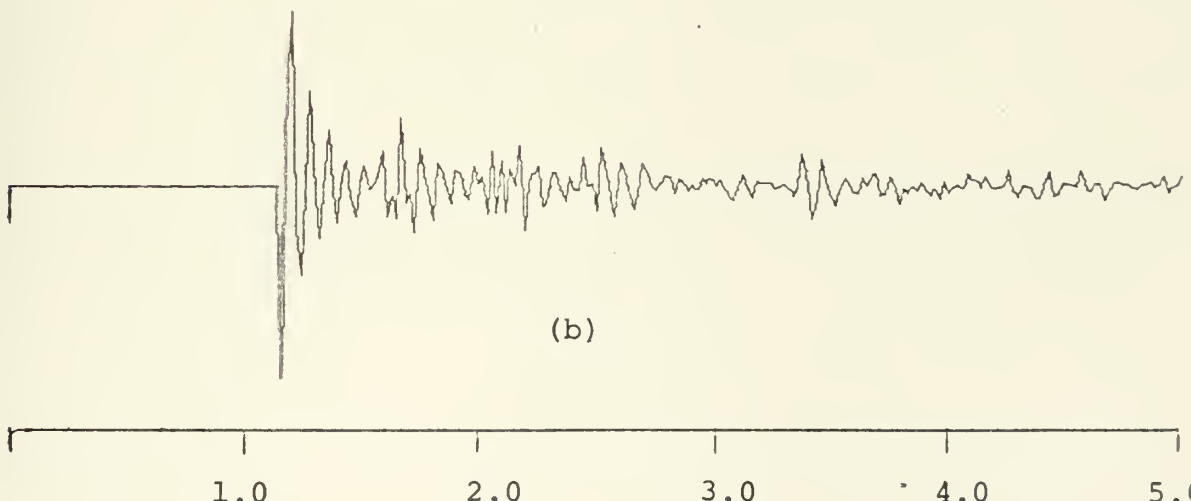


Figure 62 Effects of lowpass filtering signals with added white noise prior to homomorphic dereverberation.



(a)



(b)

1 1.0 2.0 3.0 4.0 5.0

Figure 63 (a) Noisy seismogram lowpass filtered at 50 Hz. and resampled at 51 Hz.
(b) Result of cepstral notch filtering; stopband .8-1.04 sec.

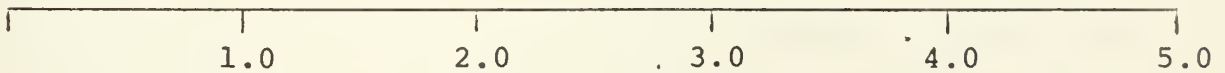
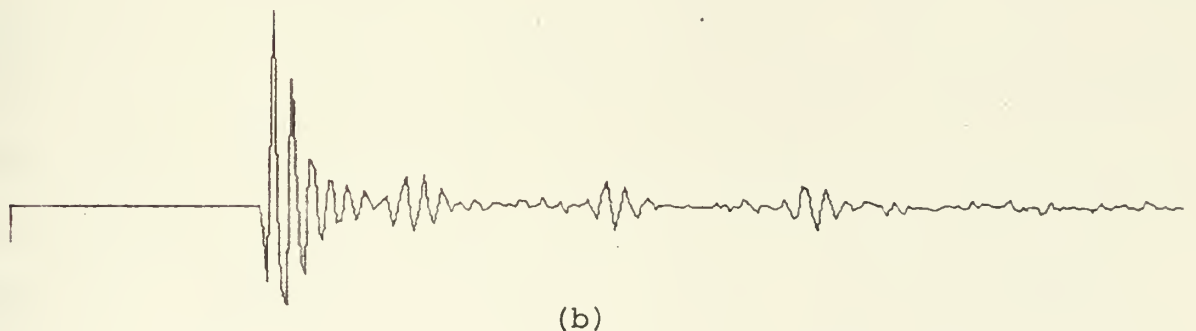
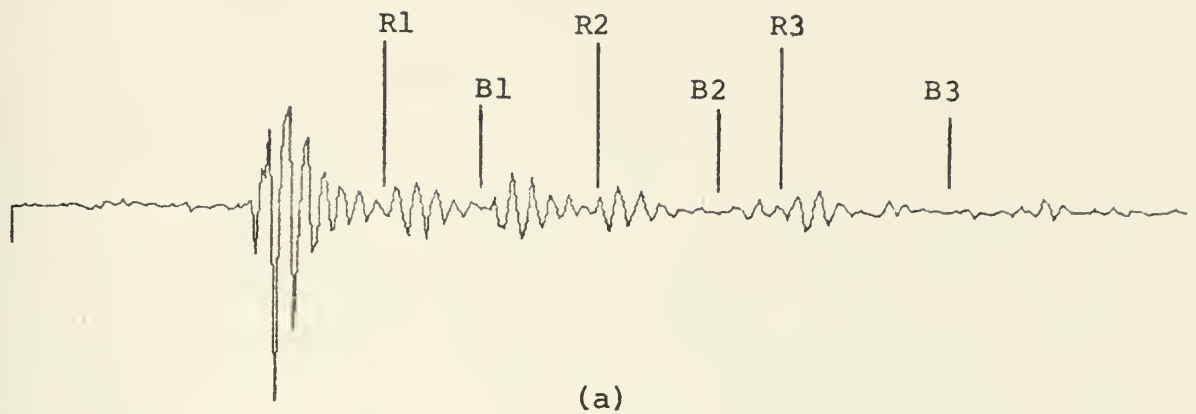


Figure 64 Noisy seismogram lowpass filtered at 20 Hz and resampled at 51 Hz. (b) Result of cepstral filtering; stopband .8-1.04 sec.

Additive noise was found to have a particularly adverse effect on longpass filtered signals. Noise, which may be relatively low in the received signal, tends to be amplified with respect to reflectors in the process of longpass filtering, especially in the later portion of the signal. Although longpass filtering removes a large part of the noise energy with the source, the overall effect is usually a decrease in SNR. The advantage of longpass filtering, which includes source deconvolution, is that greater resolution of close reflectors can be achieved. It was found that this approach is worthwhile in low noise signals but not effective when the white noise level is significant with respect to reflector amplitudes.

Proper resampling after prefiltering was found to be very important for successful longpass filtering. Figure 65a illustrates the effect of longpass filtering the cepstrum of a noisy signal which was first lowpass filtered at 20 Hz but not resampled. The filtered signal contains relatively low noise and the sampling frequency is 205 Hz. The processed result of figure 65b is useless due to the high sampling rate. Reduction of the sampling frequency to 102.5 Hz leads to the processed signal of figure 66a. The 3.5 second reflector is clear but the high background noise almost obscures the 2.7 second reflector. Multiple removal is complete. Resampling to 51 Hz, which is approximately the Nyquist rate in this case, leads to some improvement (figure 66b) but the SNR is much lower

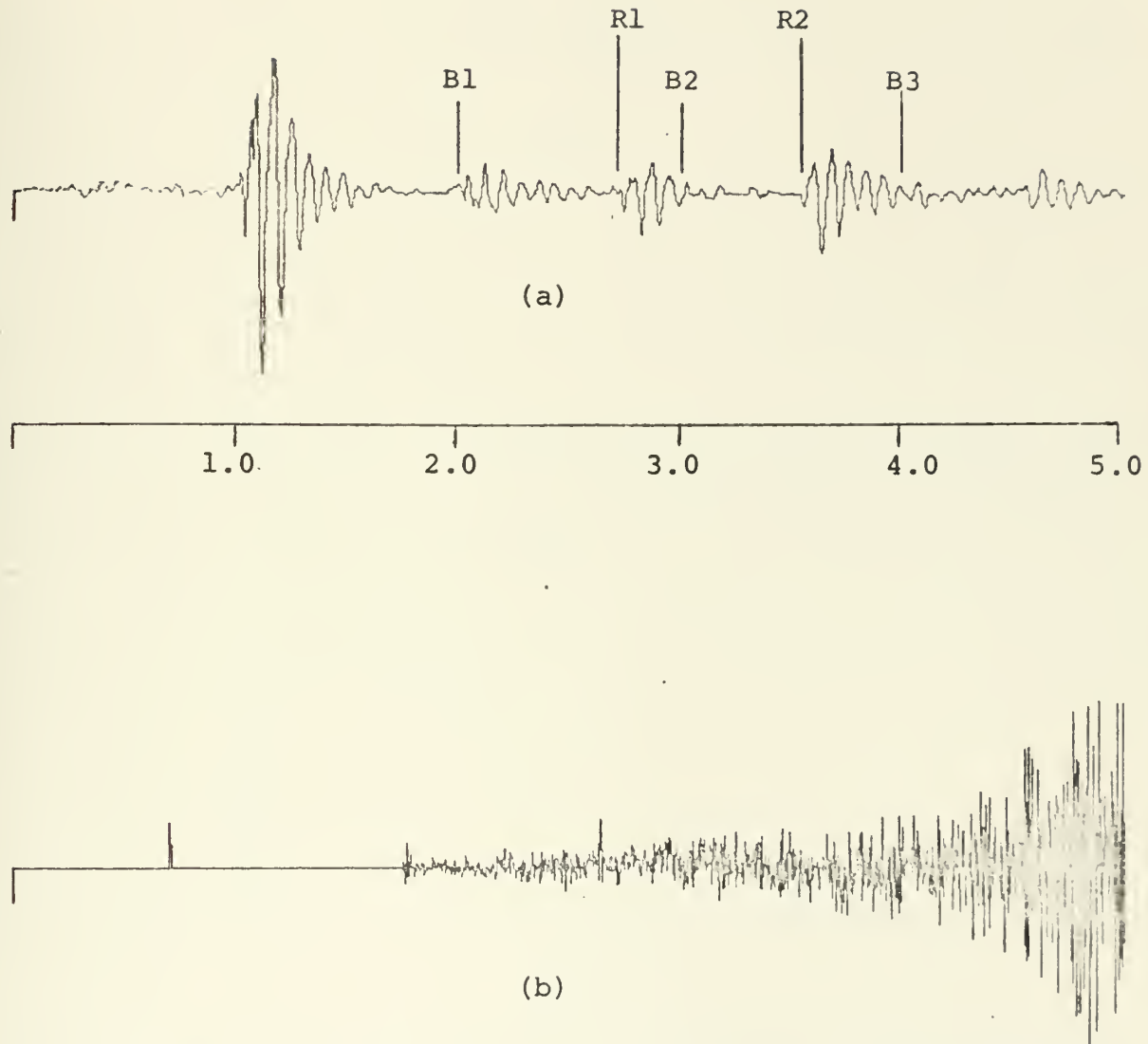


Figure 65 (a) Noisy seismogram lowpass filtered at 20 Hz but not resampled.
(b) Result of longpass filtering the cepstrum of (a).

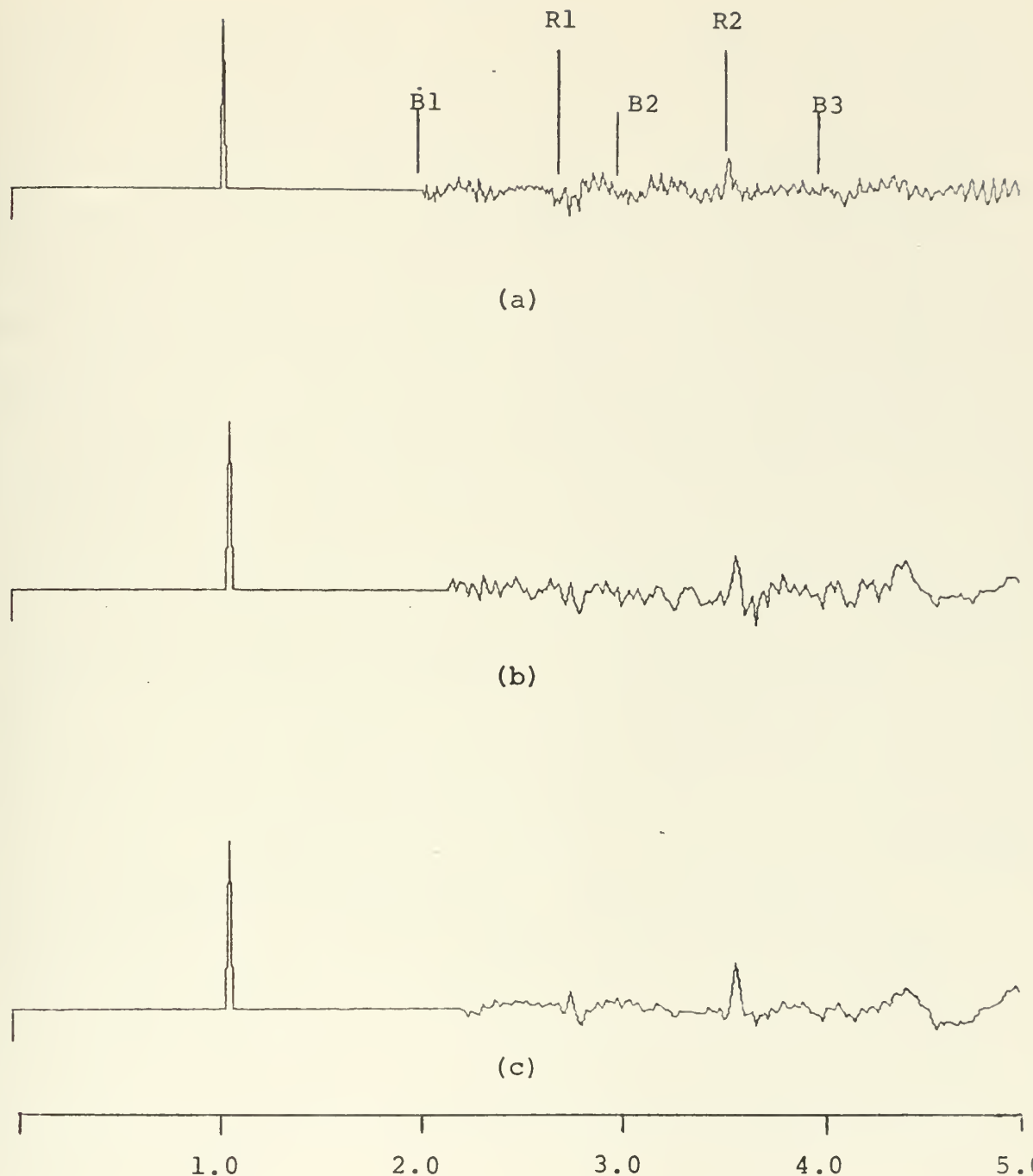


Figure 66 Longpass processing results (a) for the signal of figure 65a, resampled at 102.5 Hz before processing. (b) for the signal of figure 65a, resampled at 51 Hz before processing (c) for a signal identical to figure 65a with one half the white noise level, resampled at 51 Hz.

than before dereverberation (figure 65a), Figure 66c results from processing identical to that of figure 66b, on the same signal, with the noise amplitude halved. Both reflectors are clear and the multiples have been removed but the background noise is much higher even than in the signal of figure 65a. Thus, longpass filtering of noisy signals is seen to involve a trade-off between effective dereverberation and decrease in SNR. For signals with moderate to heavy noise the reduction in SNR was found to be unacceptable in the cases tested.

Although this subject was not extensively investigated there is some indication that lowpass filtering can be employed to improve the results of subsequent longpass processing. Figures 67 and 68 illustrate the longpass processing of a noisy signal after lowpass prefiltering at (a) 70 Hz, (b) 50 Hz and (c) 30 Hz. In each of the signals in figure 68 the multiples have been removed but the reflector resolution improves considerably from (a) to (c). These results are reasonable in that improvement of performance coincides with increasing rejection of out-of-band noise; however, the filter and signal characteristics must be studied more closely to explain this behavior accurately.

D. Comparative Examples of Processing Results

The foregoing results and discussion illustrate the performance of the TDL and homomorphic dereverberation algorithms

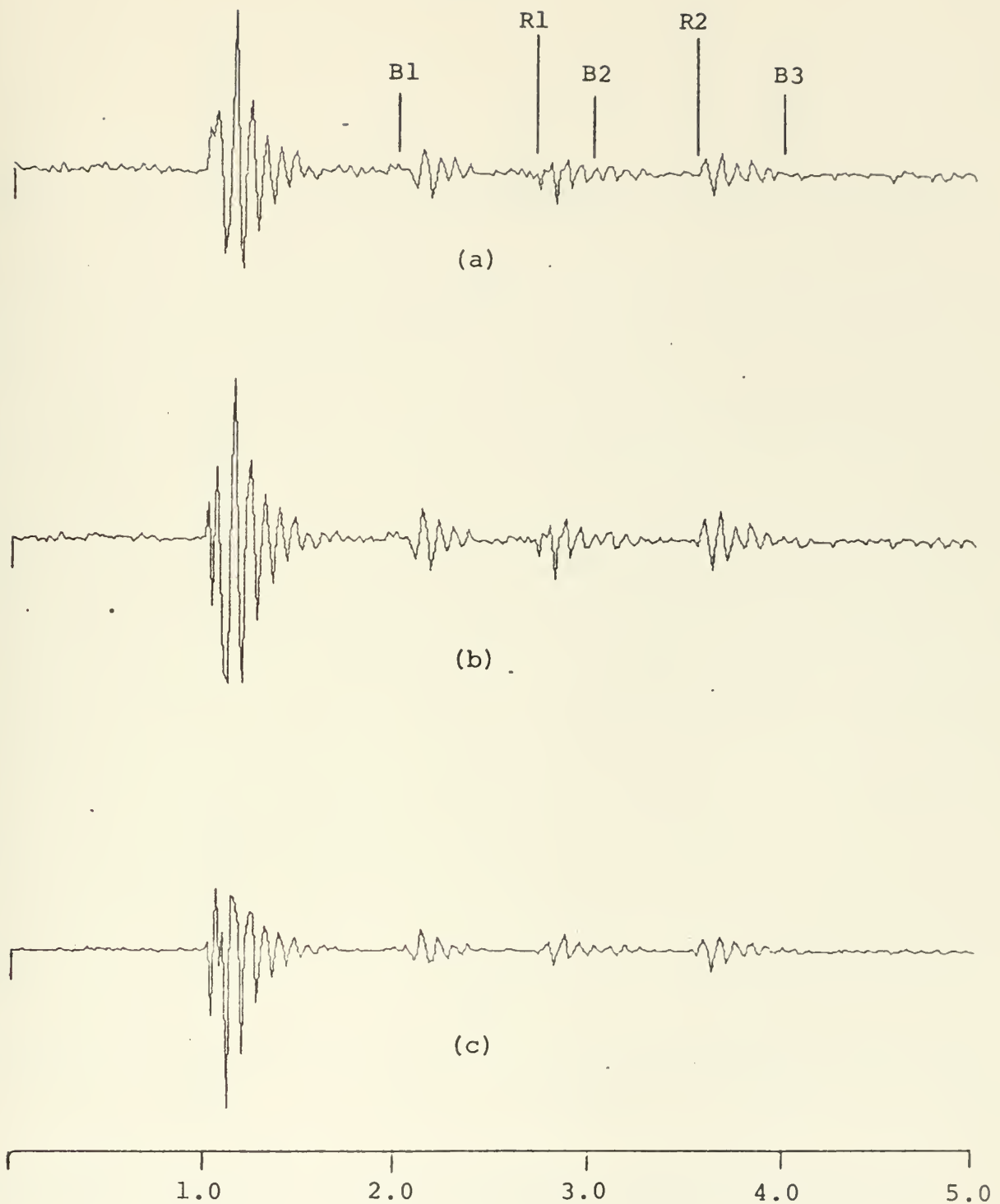


Figure 67 Noisy seismogram lowpass filtered at three different frequencies (a) 70 Hz (b) 50 Hz (c) 30 Hz. Each has been resampled at 51 Hz which is the approximate Nyquist rate for the signal without noise.

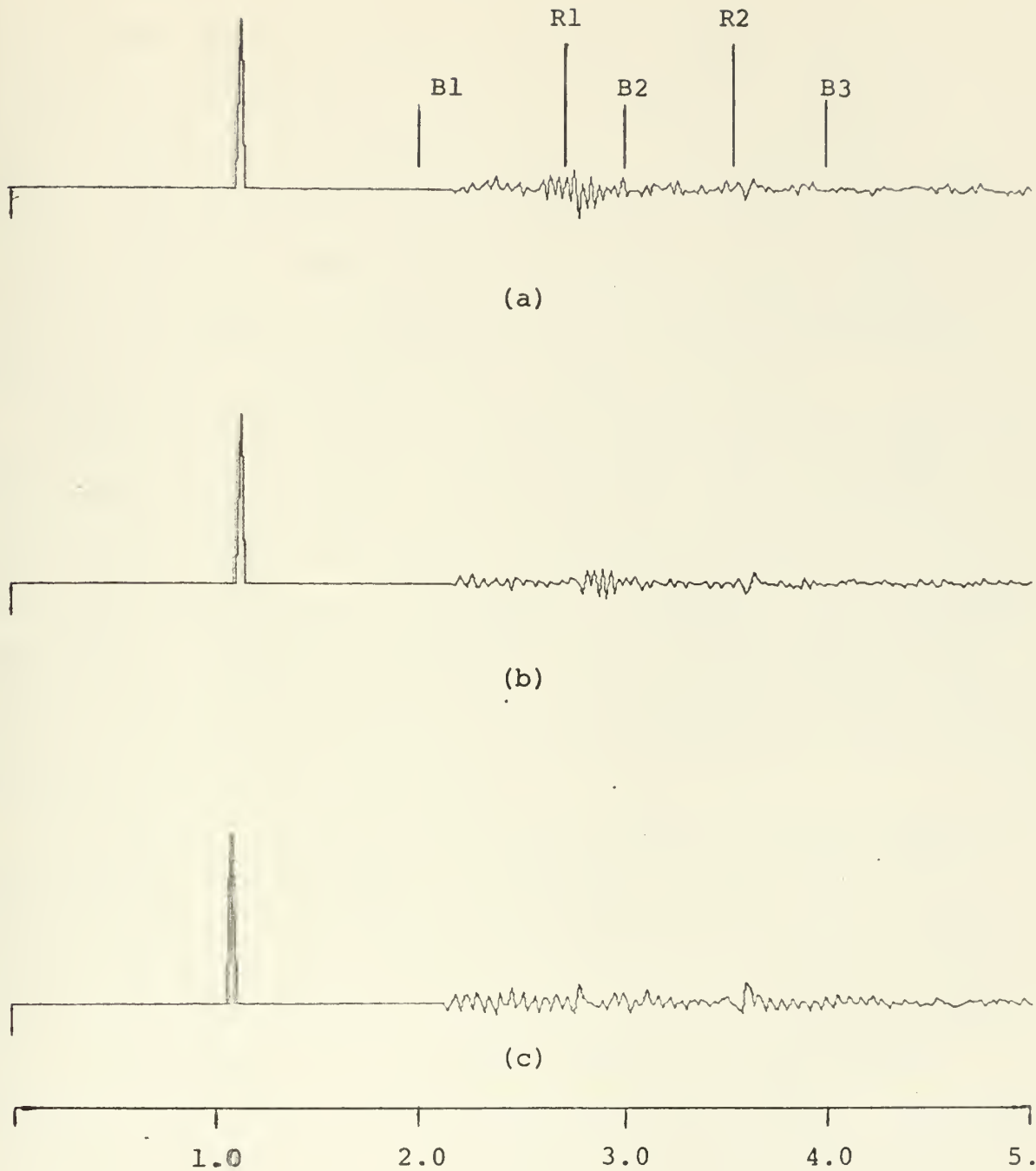


Figure 68 Results of longpass filtering the seismograms of figure 65 a, b and c, respectively.

for a variety of processing conditions. Several trends in performance are apparent. Before proceeding to a summary and discussion of the relative strengths and weaknesses, we present several examples which allow direct visual comparison of the techniques. Each of the following figures contains (a) an unprocessed seismogram and the two processed results obtained by (b) homomorphic and (c) TDL filtering.

Figure 69 illustrates a noiseless seismogram with multiple/reflector overlap at both 2 and 3 seconds. Both algorithms leave a small amount of energy at the first location and effect only slight reduction at the second. In general, both methods were found to eradicate reflectors which are extremely close to the first multiple and retain signal components which closely coincide with later multiples.

In figure 70 the multiple onset occurs .1 second before the reflector and the MSR is considerably lower than in the previous figure. In this case the separation is great enough that both methods retain a significant amount of signal energy near 2.1 seconds. The homomorphic result is considerably sharper although very little energy has been removed. Multiple/reflector separation of .1 second was found to be the approximate resolution limit of both techniques when reflector onset is later than multiple onset and travel time is estimated accurately.

Figure 71 shows a reflector at 1.95 seconds, slightly

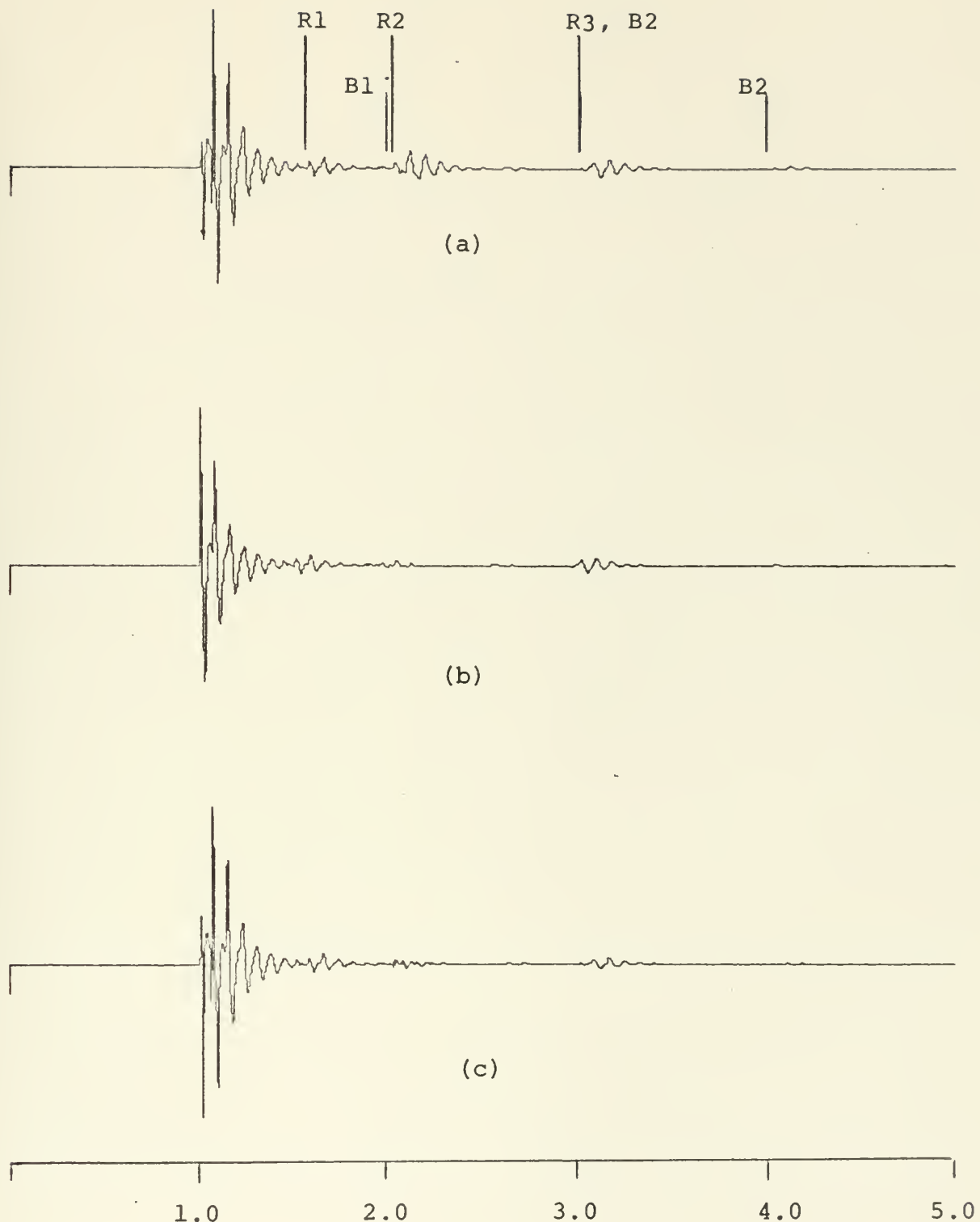
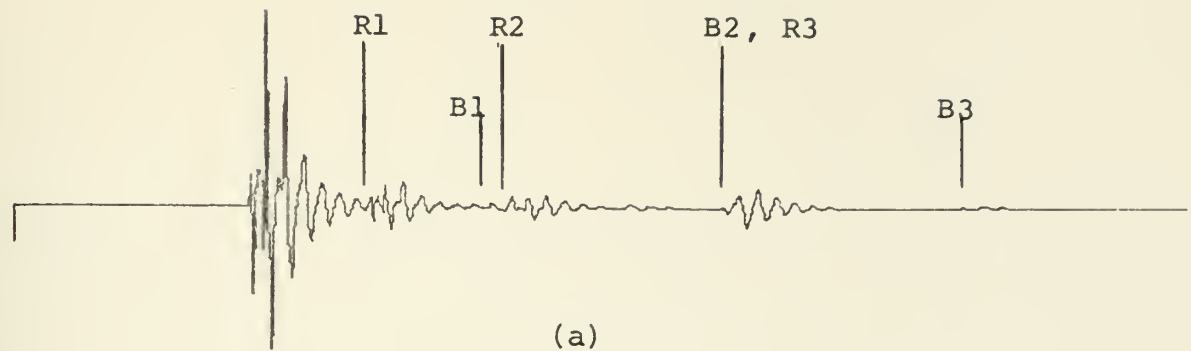
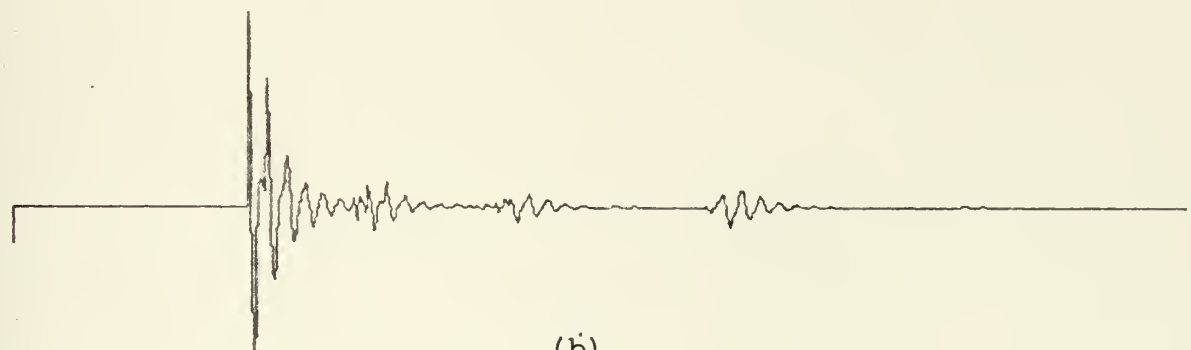


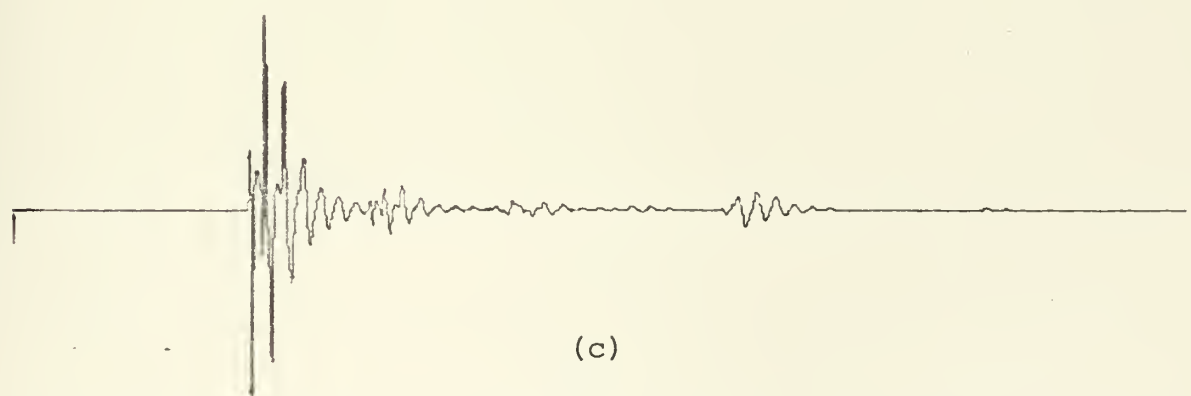
Figure 69 (a) Unprocessed seismogram with reflectors at 1.5, 2.02 and 3.0 seconds.
(b) Result of homomorphic processing.
(c) Result of TDL processing.



(a)



(b)



(c)

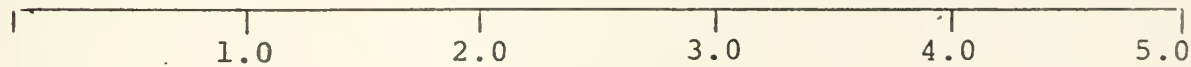


Figure 70 (a) Unprocessed seismogram with reflectors at 1.5, 2.1 and 3.0 sec.
(b) Result of homomorphic processing
(c) Result of TDL processing.

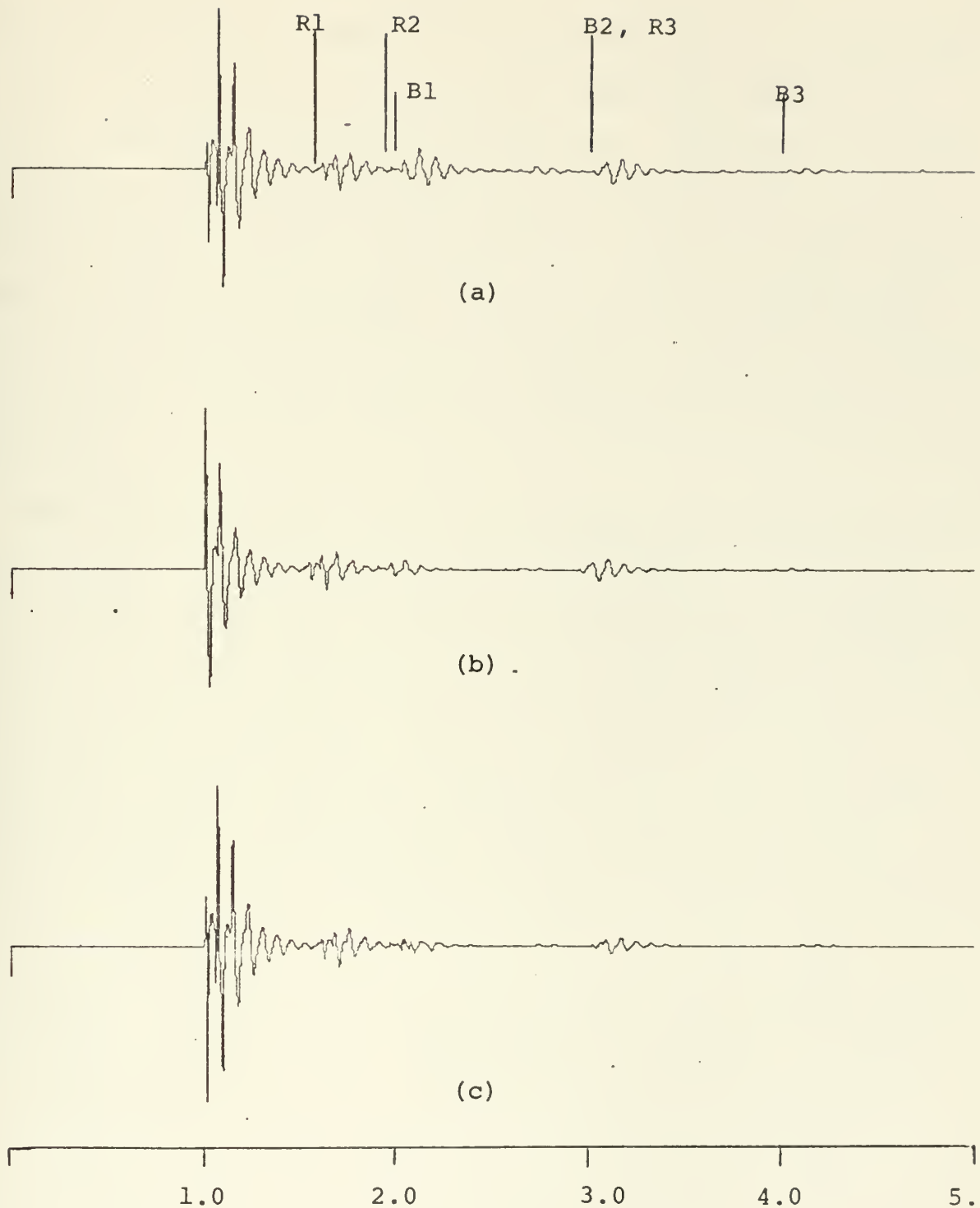


Figure 71 (a) Unprocessed seismogram with reflectors at 1.6, 1.95 and 3.0 sec.
(b) Result of homomorphic processing.
(c) Result of TDL processing.

before the multiple. Effective dereverberation is accomplished in both b and c. As in the previous figure the reflector is better resolved by homomorphic processing. Resolution of both techniques was generally observed to be slightly better when reflector onset is earlier than multiple onset, provided travel time is estimated accurately. In such cases of severe interference the homomorphic filtering generally yields more distinct reflections. A further example of this behavior is shown in figure 72.

The following three figures illustrate dereverberation of noisy signals. Each seismogram has been lowpass filtered at 30 Hz and the homomorphic outputs as shown have been resampled at 51 Hz. In this first case (figure 73) the performance of both methods is comparable. The first multiple is almost completely removed while other regions of the signal are not visibly affected. Figure 74 also shows comparable multiple removal, however, the resolution of the reflectors at 2.6 and 3.4 seconds is somewhat better after TDL filtering. The homomorphic algorithm was found to produce higher random noise spikes than the TDL filter. This effect is present in figure 74 and again in figure 75. In both examples the homomorphic method achieves slightly better multiple removal but the overall noise level in the result appears higher.

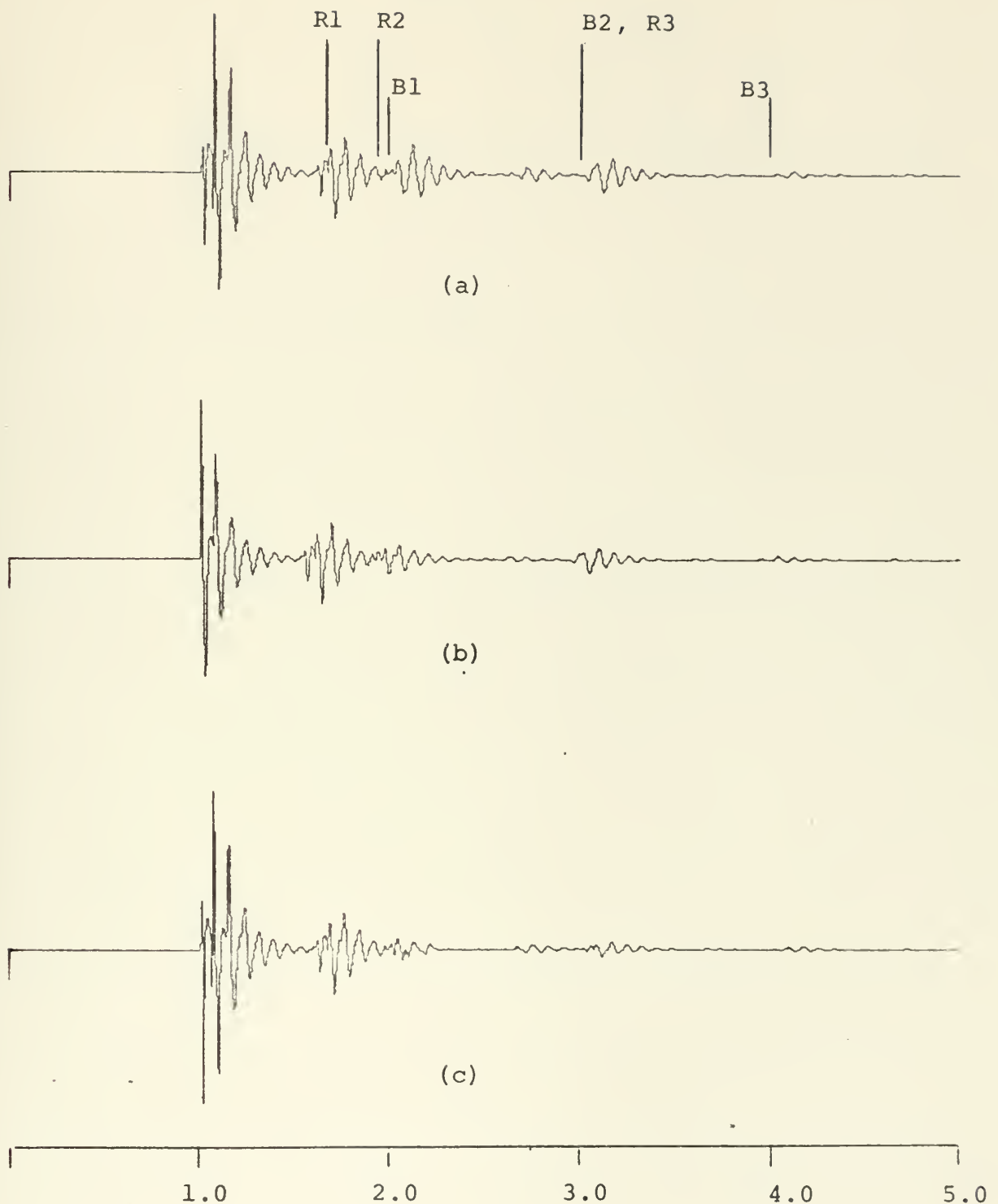
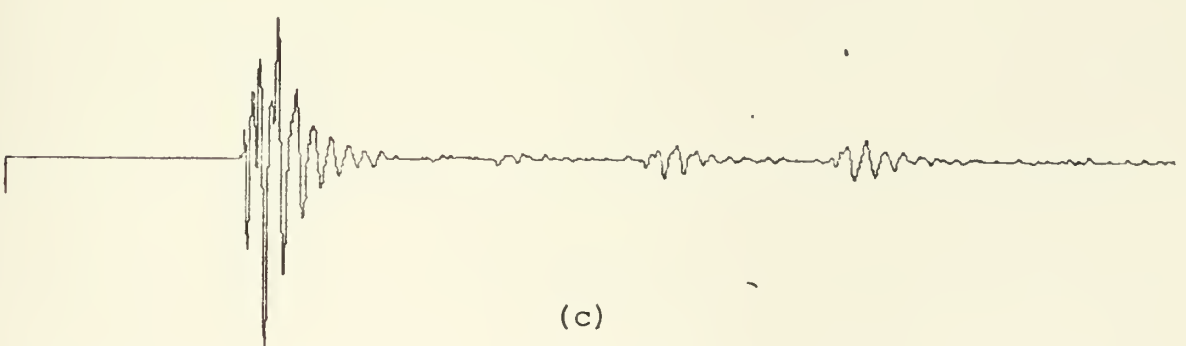
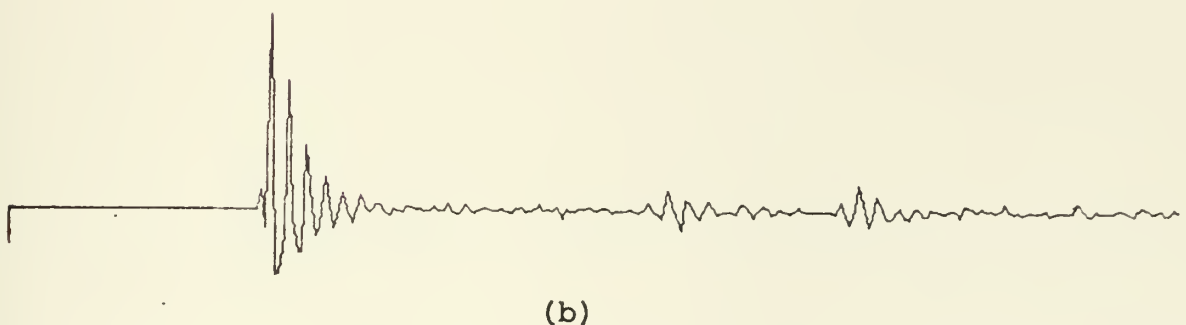
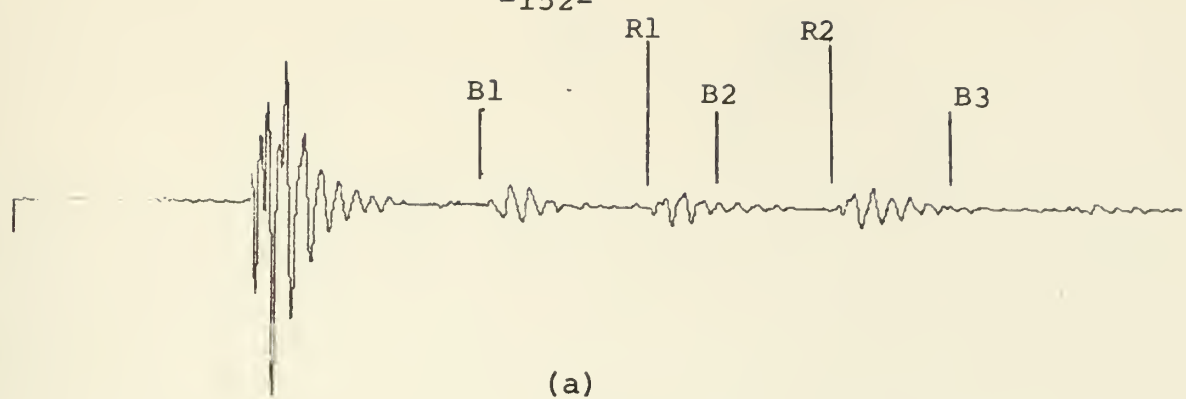


Figure 72 (a) Unprocessed seismogram with reflectors at 1.6, 1.95 and 3.0 sec.
(b) Result of homomorphic processing.
(c) Result of TDL processing.



1.0 2.0 3.0 4.0 5.0

Figure 73 (a) Noisy seismogram with reflectors at 2.7 and 3.5 sec, and lowpass filtered at 30 Hz.
(b) Result of homomorphic processing.
(c) Result of TDL processing.

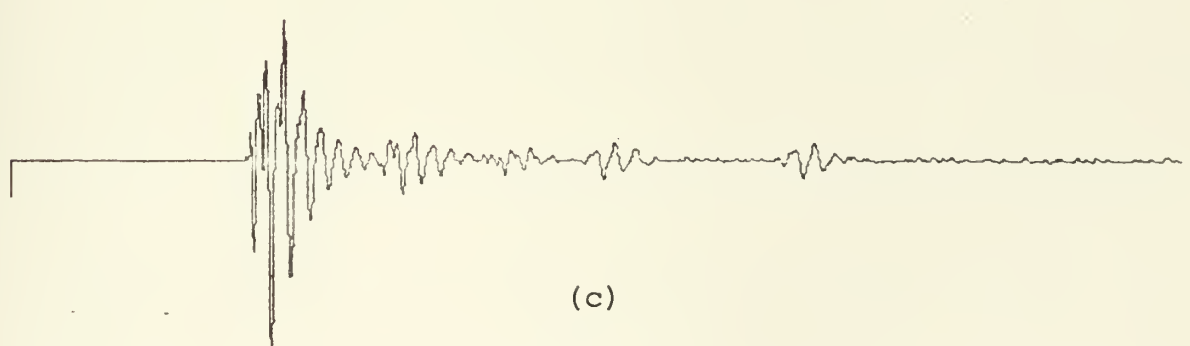
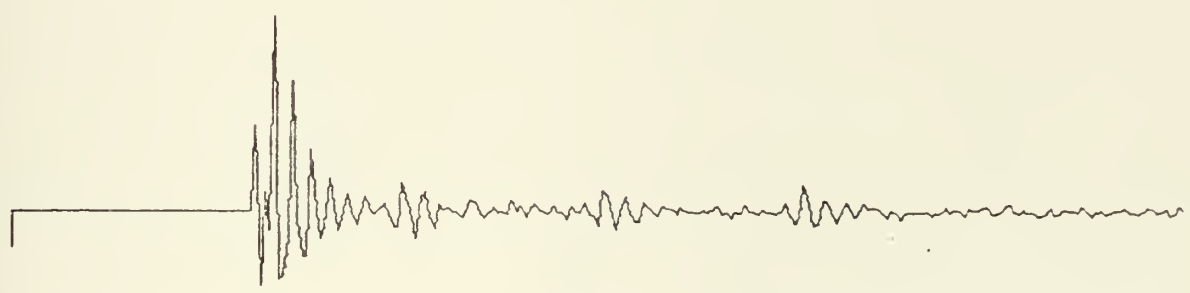
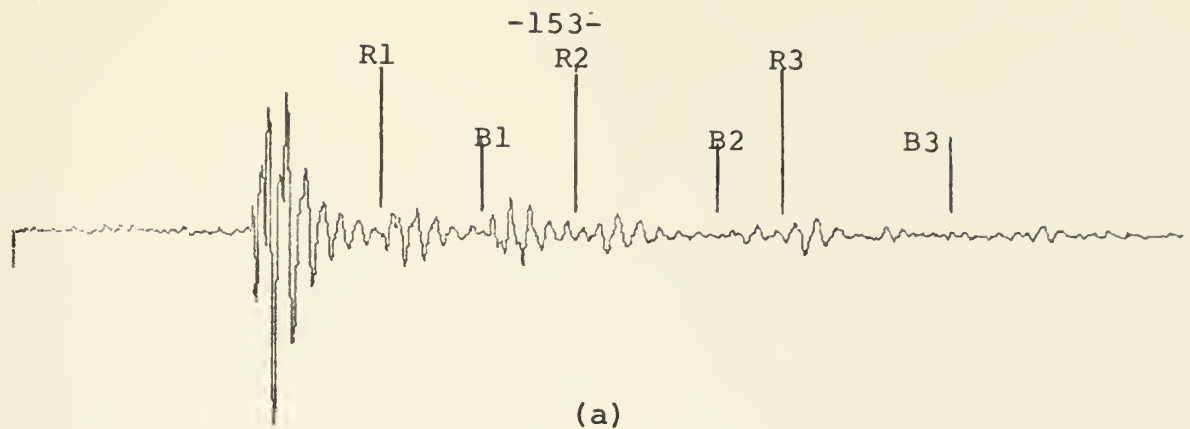


Figure 74 (a) Noisy seismogram with reflectors at 1.55, 2.4 and 3.25 sec, lowpass filtered at 30 Hz.

(b) Result of homomorphic processing.
(c) Result of TDL processing.

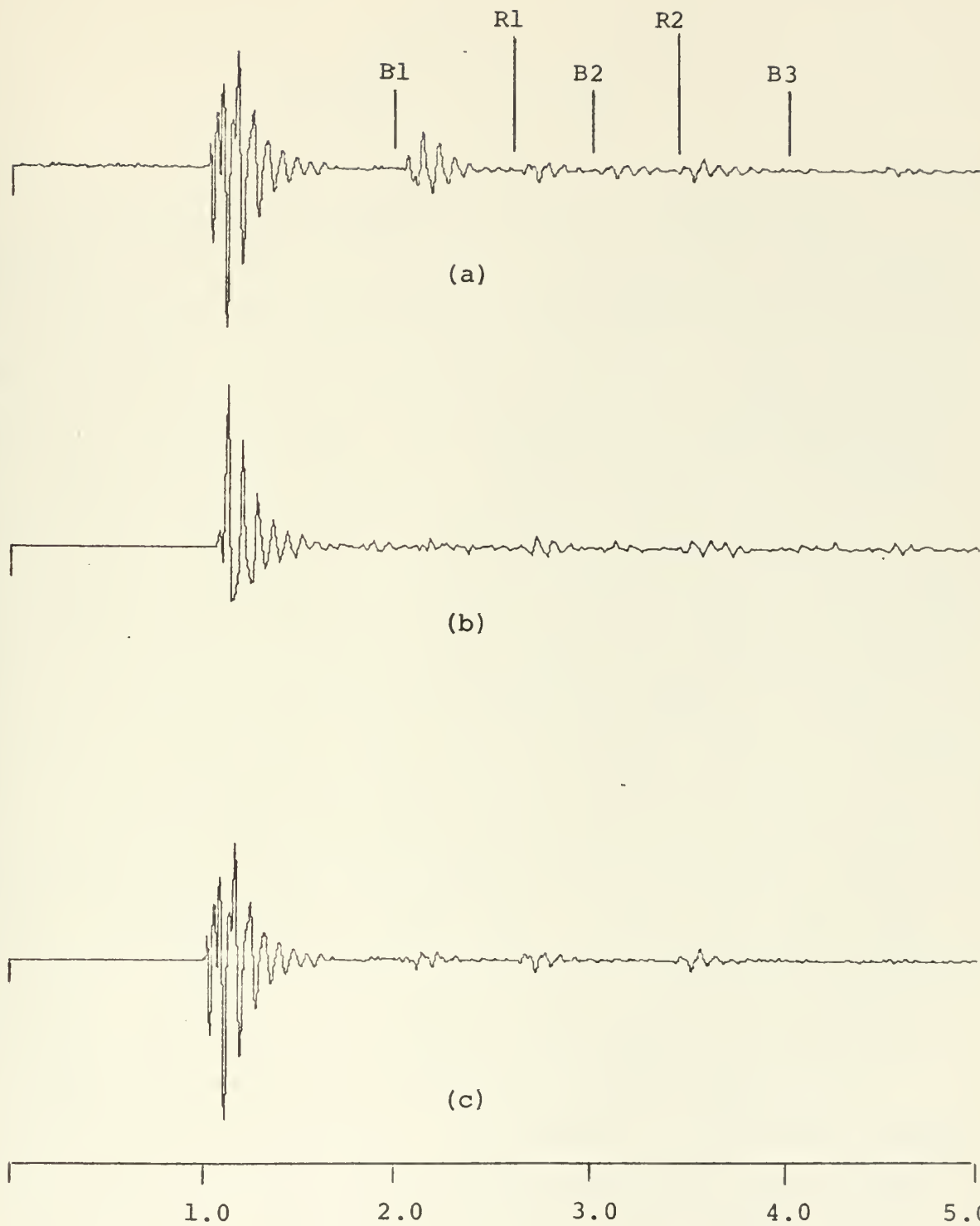


Figure 75 (a) Noisy seismogram with reflectors at 2.6 and 3.4 sec, lowpass filtered at 30 Hz.
(b) Result of homomorphic processing.
(c) Result of TDL processing.

CHAPTER V
DISCUSSION AND SUMMARY

In the preceding chapters we have (1) examined the theoretical structures of the TDL and homomorphic dereverberation techniques, (2) established a comprehensive set of performance criteria, and (3) presented the results of applying both methods to synthetic data. Our approach has been essentially that of perturbation analysis. Through variation of environmental and signal processing parameters we have observed performance trends due to deviations from the ideal theoretical models upon which the methods are based. In a more practical sense the parameter variations simulate a range of seismic processing conditions. Since there are many different environments in which these algorithms may be applied, we have not emphasized the absolute performance figures obtained from the simple, synthetic data utilized here. Rather, we have tried to present a behavior profile of both algorithms which indicates the basic trends and sensitivities with respect to a number of parameters, interpreted in terms of their theoretical structures and assumptions. This approach is intended to give a more general indication of the dereverberation performance to be expected in different situations. We conclude with a summary and discussion of the comparative results presented in Chapter IV.

In low noise, deep water seismograms the methods have been found to be comparable for reducing dominant first multiples (by 75-95% in most cases). The TDL filter requires accurate signal statistics including an estimate of the multiple-reflector crosscorrelation function, which must be approximated. This leads to degraded performance in shallow water situations where significant reflector energy is within the crosscorrelation window. The homomorphic method requires no statistical characterization of the signal and thus has no similar performance degradation in shallow water; however, the three-stage cepstral transformation requires extensive computation which may be an important limitation for at-sea processing systems. (This issue will be discussed in more detail later.)

Although the effects of aperiodicity could not be thoroughly evaluated experimentally the derived result expressed in equation (11) suggests that the homomorphic algorithm has the potential to reduce later, aperiodic multiples. The combination of such processing with source deconvolution by longpass filtering the cepstra of shallow water seismograms appears to be the most promising application of homomorphic dereverberation. More extensive practical evaluation is needed in this area.

Closely spaced, aperiodic multiples destroy the coherence of the approximated crosscorrelation function at shifts near the two-way travel time which, again, limits the effectiveness

of the TDL filter in shallow water signals.

Increasing white noise level causes monotonically decreasing performance in both methods as illustrated in figures 38 and 57. The TDL performance fell off more slowly with noise when both techniques were applied to similar signals. Bandpass filtering leads to a consistently higher percentage of multiple reduction by TDL processing of noisy signals. Filter effects on homomorphic processing are more complex. The cases evaluated indicate that multiple energy removed is not a monotonic function of filter cutoff frequency. Considerably more data are required to determine the precise effects of filter bandwidth and phase characteristics. The resampling which was found to be helpful after bandpass filtering may have a detrimental effect on visual record quality, so that interpolation may be desirable in some cases.

Reflector distortion does not appear to be a problem for either technique except in cases where overlap is severe. In most cases tested less than 10% of the reflector energy was removed. Close proximity of reflectors to the first multiple frequently leads to severe distortion by both methods due to the resulting bias of the crosscorrelation function and the lack of sufficient cepstral separation. Reflectors close to later multiples are usually well preserved. This behavior suggests two applications of the homomorphic algorithm. First, when regions of geological interest occur after the onset of

the first multiple, a wide cepstral stopband can be employed at the first multiple location to reduce later multiples without distorting reflectors. In very shallow water the stopband may be extended to include more than one multiple. A second possibility for avoiding reflector distortion is the use of weighting coefficients greater than 1.0 to exploit the properties of mixed phase sequences. The object of this weighting is to make the reflector train mixed phase while keeping the multiple sequence minimum phase. This appears to be feasible in many situations since the z-plane zero of the multiple sequence is usually well inside the unit circle. Moving some of the reflector train zeros outside of the unit circle (i.e., making it mixed phase) will, in general, cause some of the cepstral energy due to the reflectors to occupy the negative quefrency region. Even if the reflector train has a maximum phase component before weighting the same effect can be expected. Thus, the amount of reflector energy near the first multiple location may be reduced. Although there is no guarantee that the resulting notch filtered cepstrum will transform to a seismogram with less distortion, this technique appears to be worthy of investigation.

We recall one other reflector distortion effect which was seen in Chapter IV. We saw in figure 55 that dereverberation by longpass filtering completely removes reflectors occurring prior to multiple onset. It was noted that this effect may be

acceptable if it leads to better resolution of smaller, deep reflectors.

In terms of our third criterion, visual improvement of the signal, both techniques were seen to have advantages and disadvantages. Homomorphic processing usually resulted in better resolution of interfering signal components in the low noise signals processed. Increasing noise, however, was seen to cause homomorphic results more prone to random noise spikes which degrade the interpretability of the record. The results of TDL filtering had somewhat better visual resolution in the noisier signals processed. As noted previously the visual advantage of the TDL in this case is partially due to the noisier appearance of the resampled signals produced by homomorphic processing.

Longpass filtering was seen to provide the most effective dereverberation, the best reflector resolution and the best overall visual quality in ideal cases. Unfortunately it degenerates quickly with noise and could not be successfully applied to very noisy signals or signals with important geological regions preceding the multiple onset. Further research and experience may well lead to more extensive applicability of this technique.

The relative simplicity of the TDL algorithm makes it much more desirable from a computational standpoint. TDL dereverberation of a 1024 point signal can be accomplished in 3 seconds or less for the operator lengths typically required.

The three major computational steps are the correlation operations, solution of the estimator equations and convolution of the operator with the signal.

The homomorphic computations include weighting, four FFT's computation of the complex logarithm, phase unwrapping, linear filtering, complex exponentiation and unweighting. This algorithm can be expected to take 20 seconds or more for a 1024 point sequence on a small processing computer. In this analysis the phase unwrapping computation took over one minute for some noisy signals. These figures are highly dependent on hardware available and programming efficiency but, in general, homomorphic dereverberation is several times slower than the TDL algorithm. Special purpose hardware could be used to reduce homomorphic computation time significantly, but the method has not been implemented for processing on a large scale thusfar.

Storage requirements for the homomorphic algorithm vary with the FFT routine used, method of cepstrum computation and cepstrum length. The program used for this analysis requires about $12 * N$ bytes of core and $4 * N$ bytes of disc storage, where N is the cepstrum length. N was twice the signal length in the cepstra computed. Shorter cepstrum lengths, as determined by trial-and-error, may produce results with acceptably low aliasing in many cases. The TDL dereverberation program used requires about $6 * L$ bytes of core, where L is

the data sequence length. No disc storage is required in this computation. These storage requirements apply to a floating point processing scheme on a machine (HP-2100) which uses four byte floating point words.

In conclusion, we make some general observations concerning the results of this analysis.

The TDL dereverberation scheme is a simple and efficient technique which has demonstrated effectiveness in removing deep water multiples. The analytical structure is well understood and its performance characteristics have been explained here in terms of that structure. Further refinements in its implementation may be possible but its potential is essentially clear at this point.

Homomorphic dereverberation is complex, relatively untested and requires extensive computation. It has been shown here to be effective on synthetic data. It appears to be particularly promising for shallow water dereverberation. The complexity of the method leads to a number of possible analytic and computational techniques which can be utilized in its application. Certainly, its full potential has not yet been determined and further investigation is warranted.

REFERENCES

- (1) Backus, M., "Water Reverberations - Their Nature and Elimination," Geophysics, v.24, no. 2, pp. 233-261 (April, 1959).
- (2) Mayne, W., "Common Reflection Point Horizontal Data Stacking Technique," Geophysics, v.27, no. 6, pp. 927-938 (December, 1962).
- (3) Baggeroer, A. B., "Tapped Delay Line Models for Dereverberation of Deep Water Multiples," IEEE Trans. on Geophys. Elec., v. G.E. 12, no. 2, pp. 33-54 (April 1974).
- (4) Van Trees, H. L., Detection, Estimation and Modulation Theory, Part III, John Wiley & Sons, Inc.: New York, 1971.
- (5) Stoffa, P. W., Buhl, P., Bryan, E.M., "The Application of Homomorphic Deconvolution to Shallow Water Marine Seismology," Geophysics, v.39, no. 4, pp. 401-426 (August, 1974).
- (6) Oppenheim, A. V., Schafer, R. W., Digital Signal Processing, Prentice Hall, Inc.: Englewood Cliffs, N.J., 1975.
- (7) Schafer, R. W., "Echo Removal by Discrete Generalized Linear Filtering," Research Lab. of Electronics, M.I.T., Tech. Rep. 466 (February, 1969).
- (8) Ulrych, T. J., "Application of Homomorphic Deconvolution to Seismology," Geophysics, v.36, no. 4, pp. 650-660 (August, 1971).
- (9) Tribolet, J. M., "A New Phase Unwrapping Algorithm," submitted to IEEE Trans. on Acoustics, Speech and Signal Processing, (March, 1976).
- (10) Theriault, K. B., "Optimum Arrival-Time Estimation in Exploration Seismology," Ocean '74 IEEE International Conference on Engineering in the Ocean Environment, IEEE, Inc., New York (1974).
- (11) Tribolet, J. M., personal communication, April 1976.

APPENDIX A

COMPUTATION OF THE PHASE DERIVATIVE OF THE Z-TRANSFORM

When computing the complex cepstrum of a sequence, $x(n)$, it is necessary to determine the unique, continuous phase of $X(z)$. One way of obtaining the continuous phase is to first compute its derivative and then integrate numerically. The computation of the phase derivative from $x(n)$ is discussed in detail here.

We begin with the z-transform of $x(n)$,

$$X(z) = \sum_{n=-\infty}^{\infty} x(n) z^{-n} = X_R(z) + jX_I(z).$$

Taking the complex natural logarithm

$$\log X(z) \equiv \hat{X}(z) = \log |X(z)| + j \arg X(z)$$

We see that the phase of $X(z)$ is equal to the imaginary part of its natural logarithm. The derivative of $\hat{X}_I(z)$ can be expressed in terms of easily computable quantities.

$$\frac{d\hat{X}(z)}{dz} = \frac{d}{dz} \log [X(z)] = \frac{X'(z)}{X(z)} \quad (1)$$

where the prime indicates differentiation with respect to z .

Expanding (1) and solving for $\hat{X}'_I(z)$,

$$X'_R(z) + jX'_I(z) = \frac{X'_R(z) + jX'_I(z)}{X_R(z) + jX_I(z)}$$

$$\hat{X}'_I(z) = \frac{X'_I(z) - jX'_R(z)}{X_R(z) + jX_I(z)} + j \hat{X}'_R(z)$$

Separating the RHS into real and imaginary parts,

$$\begin{aligned} \hat{X}'_I(z) &= \frac{X_R(z) X'_I(z) - X_I(z) X'_R(z)}{X_R^2(z) + X_I^2(z)} \\ &\quad + j \left(\hat{X}'_R(z) - \frac{(X_R(z) X'_R(z) + X_I(z) X'_I(z))}{X_R^2(z) + X_I^2(z)} \right). \end{aligned}$$

The real part yields an expression for the phase derivative,

$$\hat{X}'_I(z) = \frac{X_R(z) X'_I(z) - X_I(z) X'_R(z)}{X_R^2(z) + X_I^2(z)}. \quad (2)$$

Since the z-transform is actually evaluated on the unit circle using the discrete Fourier transform (DFT) we set $z = e^{j\omega}$.

$$\hat{X}'_I(e^{j\omega}) = \frac{X_R(e^{j\omega}) X'_I(e^{j\omega}) - X_I(e^{j\omega}) X'_R(e^{j\omega})}{X_R^2(e^{j\omega}) + X_I^2(e^{j\omega})} \quad (3)$$

Derivatives with respect to $e^{j\omega}$ may be replaced by $\frac{d}{d\omega}$ since

$$\left[\frac{dX(e^{j\omega})}{d\omega} \right] = j e^{j\omega} \left[\frac{dX(e^{j\omega})}{de^{j\omega}} \right]$$

and we thus have a common factor of $j e^{j\omega}$ in each term of (3).

Hence, we need only compute the real and imaginary parts of $X(e^{j\omega})$ and $\frac{d}{d\omega}(X(e^{j\omega}))$ and combine them as indicated in (3). The derivative of $X(e^{j\omega})$ is easily obtained from the sequence $n x(n)$ as follows:

$$x_n(e^{j\omega}) = \sum_{n=-\infty}^{\infty} n x(n) e^{-j\omega n} = j d \frac{X(e^{j\omega})}{d\omega}$$

$$\text{Re}[x_n(e^{j\omega})] = -x_I'(e^{j\omega})$$

$$\text{Im}[x_n(e^{j\omega})] = x_R'(e^{j\omega}).$$

The required computation in terms of the DFT is then

$$\hat{x}_I'(k) = \frac{-(x_R(k)x_{nR}(k) + x_I(k)x_{nI}(k))}{x_R^2(k) + x_I^2(k)}.$$

165497

Thesis
G14053 Gallemore

A comparative eval-
uation of two acoustic
signal dereverberation
techniques.

3 SEP 76

DISPLAY

Thesis
G14053 Gallemore

165497

A comparative eval-
uation of two acoustic
signal dereverberation
techniques.

thesG14053

A comparative evaluation of two acoustic



3 2768 001 00568 9

DUDLEY KNOX LIBRARY